2018

Self-healing in 4g/5g networks

Mohamed Youssef Selim
Iowa State University

Self-healing in 4g/5g networks

by

Mohamed Selim

A dissertation submitted to the graduate faculty

in partial fulfillment of the requirements for the degree of

DOCTOR OF PHILOSOPHY

Major: Co-majors: Electrical Engineering; Computer Engineering

Program of Study Committee:
Ahmed E. Kamal, Major Professor
Ashfaq Khokhar
Daji Qiao
Lu Ruan
Phillip Jones

The student author, whose presentation of the scholarship herein was approved by the program of study committee, is solely responsible for the content of this dissertation. The Graduate College will ensure this dissertation is globally accessible and will not permit alterations after a degree is conferred.

Iowa State University

Ames, Iowa

2018

DEDICATION

I would like to dedicate this thesis to my biggest source of my strength, my family; My father, Youssef Selim, my mother, Elsayeda Rashid, my wife Hebatallah Mahmoud, and my kids, Mohab and Mazen. Each one of them was an important source of courage to me to continue this work.

My father, Youssef Selim, who always dreamed to see his son as a Ph.D. holder, who inspired me with his thoughts and wisdom, who gave me a good example on how to live with respect in this life.

My mother, Elsayeda Rashid, whose prayers for me have resulted in this achievement and without her loving upbringing and nurturing; I would not have been where I am today and what I am today. From her I learned the principles of modesty, tolerance, and kindness to all people.

My wife, Hebatallah Mahmoud, who has made this arduous journey much more pleasant. Her love and helpful spirit have motivated me to achievements beyond my own expectations.

My sons, Mohab and Mazen, you have made me stronger and more fulfilled than I could have ever imagined.

TABLE OF CONTENTS

LIST OF TABLES

LIST OF FIGURES

LIST OF ABBREVIATIONS

4G	Fourth Generation
5G	Fifth Generation
5G NR	5G New Radio
AF	Amplify-and-Forward
AWGN	Additive White Gaussian Noise
BB	Branch and Bound
BBU	Base Band Unit
BOC	Backhaul Outage Compensation
BONMIN	Basic Open-source Nonlinear Mixed Integer Programming
BS	Base Station
C-RAN	Cloud-Radio Access Network
CA	Carrier Aggregation
COC	Cell Outage Compensation
COD	Cell Outage Detection
CQI	Channel Quality Indicator
CR	Cognitive Radio
CSI	Channel State Information
CU	Cognitive User
D2D	Device-to-Device
DBS	Drone Base Station
DF	Decode-and-Forward
DoR	Degree of Recovery
EaaS	Energy-as-a-Service

EH	Energy Harvesting
eMBB	enhanced Mobile Broadband
eNB	evolved Node B
EPC	Evolved Packet Core
FSO	Free Space Optics
GAMS	General Algebraic Moceling System
GBS	Ground Base Station
gNB	next generation Node B
HetNets	Heterogeneous Networks
IAB	Integrated Access and Backhaul
i.i.d	Independent and identical distribution
IoT	Internet of Things
IPOPT	Interior Point OPTimizer
ISP	Internet Service Provider
KKT	Karush-Kuhn-Tucker
LoS	Line of Sight
MBS	Macro Base Station
MDT	Minimization of Drive Test
MIMO	Multi-Input Multi-Output
MINLP	Mixed-Integer Non-linear Programming
MIP	Mixed Integer Programming
mMTC	massive Machine Type Communications
mmW	milli-meter Wave
NLoS	Non-Line of Sight
NLP	Non Linear Programming
NSA	Non Stand-alone
PD	Powering Drone

PF	Pre-planned Femtocell
PL	Path Loss
PTP	Point To Point
PTMP	Point To Multi-Point
PU	Primary User
QoS	Quality of Service
QoE	Quality of Experience
RAN	Radio Access Network
RB	Resource Block
RF	Radio Frequency
RFC	Random Femtocell
RRH	Remote Radio Unit
RSRP	Reference Signal Received Power
RSS	Received Signal Strength
SA	Stand-alone
SBS	Small Base Station
SC	Small Cell
SCA	Successive Convex Approximation
SCIP	Solving Constraint Integer Programs
SDN	Software Defined Networking
SDWNC	Software Defined Wireless Network Controller
SH	Self Healing
SHR	Self Healing Radio
SINR	Signal-to-Interference and Noise Ratio
SON	Self Organizing Networks
SURE	Self-healing of Users equipment by Rf Energy transfer
tBD	Tethered Backhaul Drone

UAV	Unmanned Aerial Vehicle
UE	User Equipment
uRLLC	ultra Reliable and Low Latency Communications

LIST OF SYMBOLS

$\in$	Set membership operator
f_c	carrier frequency
λ_0	Wavelength
$\mathbb{E}[.]$	Expectation function
$(.)^T$	Transpose operator
$(.)^H$	Hermitian operator
$Tr(.)$	Trace function
$(x)^+$	Maximum between x and zero
$\log(.)$	Logarithm function
$\min(x, y)$	Minimum between x and y
$\max(x, y)$	Maximum between x and y
$\min_a(.)$	Minimum of a set or function with respect to a
$\max_a(.)$	Maximum of a set or function with respect to a
argmin(.)	The argument of minimum
argmax(.)	The argument of maximum
$\|.\|$	Absolute value of a function or cardinality of a set
$\mathbb{R}$	Real number
N_0	Noise power density
n	Index for the number of time blocks
m	Index for the number of resource blocks
$\mathcal{D}$	Set of DBSs
$\mathcal{U}$	Set of all UEs
$p_{d,m}$	DBS power over resource block m

$p_{l,m}$	GBS power over resource block m
h	DBS hight (constant)
$\mathbf{J}_d^n$	DBS 2D coordinates
$\mathbf{J}_l$	GBS 2D coordinates
$\mathbf{g}_u$	UE 2D coordinates
$\delta_{u,d}^n$	distance between UE u and DBS d
$\delta_{u,l}$	distance between UE u and GBS l
$\Gamma_{u,d}^n$	the DBS-UE channel power gain during time block n
$\Gamma_{u,l}$	the GBS-UE channel power gain
$R_{u,d,m}^n$	the achievable rate between DBS d and UE u per sub-channel m
$R_{u,l,m}$	the achievable rate between GBS d and UE u per sub-channel m
$P_l^{n(noSH)}$	Power consumed by GBS l to serve its UEs (no self-healing)
$P_{l,m}^{n(SH)}$	Power consumed by GBS l to serve its UEs (self-healing)
α_l	scaling parameter
β_l	a constant power consumed independently of the radiated power of GBS
P_{hov}	DBS hovering power
P_{har}	DBS hardware power
$E_{l,m}^n$	Energy consumed by GBS l using resource block m during time block n
$E_{d,m}^n$	Energy consumed by DBS d using resource block m during time block n
$\mathcal{D}$	Set of DBSs
$\mathcal{L}$	Set of GBSs
$\mathcal{U}$	Set of all UEs
$p_{d,m}$	DBS power over resource block m
$p_{l,m}$	GBS power over resource block m
$E_{l,m}^n$	Total energy consumed by GBS l using resource block m during time block n
$E_{d,m}^n$	Total energy consumed by DBS d using resource block m during time block n
P_s	Drone's static power consumption

P_{full}	Drone's hardware power consumption when the drone is moving at full speed
P_f	Drone's flying power consumption
m_{tot}	Mass of the drone
r_p	Radius of the drones propellers
$v_{\max}$	Maximum drone's speed
v_d	Drone's speed
ρ_a	Air density
T_f	Flying time
$p^c_{a,b}$	Transmit power from Transmitter (Tx) a to Receiver (Rx) b using Resource Block (RB) c
$\Gamma^c_{a,b}$	Channel gain between Tx a and Rx b using RB c
$\gamma^c_{a,b}$	SINR betwwen Tx a and Rx b using RB c
$\Phi^c_{a,b}$	Decision variable indicating association of Rx b with Tx a using RB c
$R^c_{a,b}$	The achievable downlink rate between Rx b and Tx a using RB c
$\hat{R}_{a,b}$	The downlink rate achieved by Rx b served by TX a
R^{th}	The threshold rate for the UEs
$\alpha_{g,\xi}$	Decision variable indicating backhaul link between the gNB g and gNB ξ
$\delta_{g,\xi}$	Decision variable indicating backhaul link between gNB g and gNB ξ
$t_{g,\xi}$	The traffic carried out over the backhaul link between gNB g and gNB ξ
$x_{g,u}$	Decision variable indicating the association of UE u with gNB g
$P^{\max}$	The maximum power for each gNB
$p^{\max}$	The maximum power per each RB
β_{th}	SINR threshold
ρ^a_b	Auxiliary variable to capture the max-min objective
ϱ	scaling factor used to control the degree of failure recovery
Q	Very large number

ACKNOWLEDGEMENTS

First and foremost, I would like to thank God "Allah" Almighty for giving me the strength, knowledge, ability and opportunity to undertake this thesis and to persevere and complete it satisfactorily. Without his blessings, this achievement would not have been possible.

I would like to take this opportunity to express my thanks to those who helped me with various aspects of conducting research and the writing of this thesis.

I would like to express my sincere gratitude to my advisor Prof. **Ahmed Kamal** for the continuous support of my Ph.D study and research, for his patience, motivation, enthusiasm, and immense knowledge. His guidance helped me in all the time of research and writing of this thesis. I could not have imagined having a better advisor and mentor for my Ph.D study. Without his continuous help and support, I would not have been where I am today and what I am today.

Besides my advisor, I would like to thank the rest of my thesis committee: Prof. **Ashfaq Khokhar**, Prof. **Daji Qiao**, Associate Prof. **Phillip Jones** and Associate Prof. **Lu Ruan**, for their encouragement, insightful comments, and useful questions.

I also would like to thank Prof. **Khaled Fouad** from Cairo University and Associate Prof. **Heba Abdel-Atty** from Portsaid University, for their constant help and productive advices during my joint supervision program. In addition, I want to thank Associate Prof. **Hongwei Zhang** and Associate Prof. **Alexander Stoytchev** from Iowa State University for providing me the perfect mentorship to develop my professional skills in teaching and research.

Finally, I would like to thank my fellow labmates in Laboratory for Advanced Networks (LAN) Group: Dr. **Mirzad Mohandespour**, Dr. **Abdulkadir Celik**, Dr. **Ahmad**

Alsharoa, Dr. **Min Song**, Dr. **Yu Jie**, **Abdullah Almasoud**, **Abdullah Alqasir**, and **Ala'Eddin Masadeh**, for the stimulating discussions, for the sleepless nights we were working together before deadlines, and for all the fun we have had in the last four years.

ABSTRACT

Prospective demands of next-generation wireless networks are ambitious and will require cellular networks to support 1000 times higher data rates and 10 times lower round-trip latency. While this data deluge is a natural outcome of the increasing number of mobile devices with data hungry applications and the internet of things (IoT), the low latency demand is required by the future interactive applications such as "tactile internet", virtual and enhanced reality, and online internet gaming, etc.

Self-Organizing Network (SON) is defined as the network that has the capability to dynamically adapt changes in the network in order to optimize its performance. The need for SONs arises from the fact that in future networks, e.g., 5G networks, the number of nodes will be increasing at a rapid rate. Moreover, it is also because of the introduction of a high degree of heterogeneity and complexity, that such SONs could save significant operational expenditure. SON defines three areas: self-configuration (plug and play network elements), self-optimization (automatically optimize network parameters), and self-healing (automatically detect and mitigate failures).

Self-healing is the execution of actions that keep the network operational and/or prevent disruptive problems from arising. It is done in two steps: cell outage detection (COD) and cell outage compensation (COC). COD detects and classifies failures, while minimizing detection time. COC executes actions to mitigate the effect of the failure. Detecting cell outage in 3G and 4G was doable, but it could take up to several hours, thus resulting in salient degradation in network performance. Hence, automatic detection and compensation of failures in 5G networks is mandatory.

The motivation behind this thesis is to meet the need for increasing reliability in wireless communications networks by mitigating, reducing, or alleviating the effect of the network

equipment failures. To achieve these goals, outage compensation models for wireless cellular networks are proposed and analyzed. We are presenting different ways of mitigating the failures that occur in network equipment; 1) the backhaul/fronthaul failures either in traditional or cloud-Radio Access Networks 2) the battery starved users in the network 3) Failures of BSs and using UAVs/Drones in mitigating these failures.

Firstly, a solution for the backhaul/fronthaul failures based on using a new Self-healing Radio (SHR) along with using the concept of Cognitive Radio (CR) and Software Define Networking (SDN) is proposed to mitigate the effect of backhaul/fronthaul failures in 4G/5G networks. We present a novel cell outage compensation approach using new Self-Healing Radios (SHRs) added to each cell site in the 5G network. These SHRs operate only in case of fronthaul/backhaul failure of any cell site in the network. A new software defined controller is introduced to handle the self-healing procedures. We also introduce a high level simulation study that is carried out to assess the proposed approach. The simulation results confirm the advantages of the proposed approach in terms of the degree of recovery from failures.

Secondly, we propose a promising solution for battery starved users in cellular networks. Radio Frequency (RF) Energy Harvesting (EH) holds a promising future for energizing low power mobile devices in next generation wireless networks. Harvesting from a dedicated RF energy source acquires much more energy than simply harvesting from ambient RF sources. A novel Self-healing of Users equipment by Rf Energy transfer (SURE) scheme is introduced between the network operator and battery starved users to heal and extend their battery life time by sending dedicated energy from different sources in order to be aggregated and harvested by starved users. This approach introduces the concept of Energy as a Service (EaaS) where the network operator delivers energy to battery starved users in next generation networks. Simulation results prove that sufficient amounts of energy can be delivered to starved users while minimizing their uplink power requirements and guaranteeing a minimum uplink data rate.

Lastly, three frameworks of cell outage compensation frameworks for 4G/5G network supported by dynamic Drone Base-stations (DBSs) is proposed. Within the first framework, the outage compensation is done with the assistance of sky BSs and Ground BSs (GBSs). An optimization problem is formulated to jointly minimize the energy of the Drone BSs (DBSs) and GBSs involved in the healing process which accordingly will minimize the number of DBSs and determine their optimal 2D positions. Simulation results show that the proposed hybrid approach outperforms the conventional COC approach. Moreover, all users receive the minimum quality of service in addition to minimizing the UAVs consumed energy.

The second framework addresses the way of failure mitigation based on the type and duration of the failure. We propose a framework that uses DBSs or helikites to mitigate GBS failures. Our proposed short-term and long-term cell outage compensation framework aims to mitigate the effect of the failure of any GBS in 5G networks. Within our framework, outage compensation is done with the assistance of sky BSs. An optimization problem is formulated to jointly minimize communication power of the UAVs and maximize the minimum rates of the Users' Equipment (UEs) affected by the failure. Also, the optimal placement of the UAVs is determined. Simulation results show that the proposed framework guarantees the minimum QoS for each UE in addition to minimizing the UAVs' consumed energy.

The third and last framework utilizes a grid of DBSs to provide cellular coverage to disaster-struck regions where the terrestrial infrastructure is totally damaged due to earthquakes, floods, etc. We propose solutions for the most challenging issues facing drone networks which are limited battery energy and limited backhauling. Our proposed solution is based mainly on using three types of drones; tethered backhaul drone (providing high capacity backhauling), untethered powering drone (providing on the fly battery charging) and untethered communication drone (providing cellular connectivity). The simulation results show that we can provide unlimited cellular service to the disaster-affected region under certain conditions with a guaranteed minimum rate for each user.

CHAPTER 1. INTRODUCTION

1.1 Background

The main requirements of 5G are emerging through the efforts of diverse groups such as 4G America in United States, IMT-2020 (5G) promotion group in China and the 5G Private Public Partnership (5G PPP) in Europe. The 5G requirements will tremendously increase the network complexity which requires auto-integration and self-management capabilities that are well beyond todays self-organising network features. Additionally, ultra-reliable communications put very stringent latency and reliability requirements on the architecture [1].

The main challenges for 5G networks are the continued evolution of mobile broadband and the addition of new services and requirements, e.g., anything-to-anything communication, very low latency ($\leq$1 ms), as well as reduced signalling overhead and energy consumption (greener network). Future mobile networks will have significantly increased traffic volumes and data transmissions rates, but also many more use cases. They include not only traffic between humans and between humans and the cloud, but also between humans, sensors, and actuators in their environment, as well as between sensors and actuators themselves [1].

Small access nodes, with low transmission power and no planning requirements, are conceived to be densely deployed, resulting in an Ultra-Dense Network (UDN). UDNs are also called Heterogeneous Networks (HetNets), i.e., multi-layered network with high power macrocells and very dense small cells with low power. This approach improves spectral efficiency per area by reducing the distance between transmitters and receivers, and im-

proves macrocell service by offloading wireless traffic. UDNs are a step forward towards low cost, plug and play, self-configuring and self-optimizing networks. 5G will need to deal with many more base stations, deployed dynamically and in a heterogeneous manner, combining different radio technologies that need to be flexibly integrated. Moreover, a massive deployment of small access nodes introduces several challenges such as additional backhaul and mobility management requirements, which 5G needs to address [CROWD project http://www.ictcrowd.eu/].

The Mobile and Wireless Communications Enablers for the Twenty-Twenty Information Society, METIS, provides a consolidated 5G vision. According to this vision, the most promising requirements of 5G are: 1) total capacity should be increased a 1000 fold, 2) 10-100 times more connected devices, 3) end user data rates expected to increase by 10-100 times, 4) latency should be reduced by five times, 5) all of the above at todays cost or less. The road map towards 5G is gradual. But perhaps, a key 5G qualification that dominates all of the above is network flexibility and reliability. These qualifications can be achieved by integrating Self Organizing Networks (SON) in upcoming 5G networks.

The purpose of this chapter is to cover the topic of self-healing in 4G/5G networks. Self-healing is an important functionality of self-organizing networks (SONs), and it means that networks migrate from manual operation to automated operation (minimize human interaction). SON defines three areas: self-configuration (plug and play network elements), self-optimization (automatically optimize network elements and parameters) and self-healing (automatically detect and mitigate failures in network elements).

This chapter is structured as follows: Section 1 captures SON and address it before 5G and within the 5G networks. Section 2 presents a detailed introduction to self-healing and its two main categories; cell outage detection and compensation and then state-of-the-art of self-healing is discussed. Section 4 presents in details backhaul self-healing case study. Section 5 concludes the chapter.

1.2 Introduction to SONs

The SON is a paradigm defined under the auspices of the Third Generation Partnership Project (3GPP) and the Next Generation Mobile Networks (NGMN) Alliance aiming to automate mobile network operation, administration, and management (OAM). Via SON, operators seek to achieve optimum performance at minimum cost. SON aims to leapfrog the performance of future networks to a higher level of automated operation by self managing the planning, configuration, optimization and healing of networks., which act in three main areas [2]:

Self-configuration: the plug and play capabilities of network elements including self-planning where the selection of the new site location is determined automatically depending on dead coverage zones and/or dense mobile users area. Also, the authentication, verification of each new site are done automatically.

Self-optimization: the adjustment and auto-tuning of parameters during the operational life of the system making use of the measurements and performance indicators collected by the User Equipment (UEs) and the Network Elements (NEs).

Self-healing: failure detection, diagnosis, compensation, and recovery of the network. This is done by execution of certain actions that force the network to work in normal or near normal conditions even in the presence of failures.

1.2.0.1 SON Architecture

There are three different architectures for SON functionality:

(1) Centralized SON: In Centralized SON, optimization algorithms are executed in the OAM System. In such solutions SON functionality resides in a small number of locations, at a high level in the architecture. So all SON functions are located in OAM(s), so it is easy to deploy them. But this architecture adds latency to simple optimization cases due to the centralized processing, and is therefore not suitable for the UDN, hence not suitable for 5G networks.

(2) Distributed SON: In Distributed SON, optimization algorithms are executed in macrocell (eNB in LTE). In such solutions, SON functionalities are found in many locations at a relatively low level in the architecture. So all SON functions are located in macrocells. This adds overhead to deployment. It is also difficult to support complex optimization schemes which require coordination among many BSs. However, it is easy to support quick optimization responses between a small number of BSs.

(3) Hybrid SON: In Hybrid SON, part of the optimization algorithms are executed in the centralized OAM system, while others are executed in macrocells. Thus, simple and quick optimization schemes are implemented in macrocells and complex optimization schemes are implemented in OAM. So it is very flexible to support different kinds of optimization cases.

1.2.1 SON before 5G

1.2.1.1 SON in GSM and UMTS

Deploying and operating conventional cellular networks (GSM and UMTS) was a complex task that comprises many activities, such as planning, dimensioning, deployment, testing, launching and operating optimization, performance monitoring, failure mitigation, failure correction and general maintenance. The GSM network was much simpler than today's networks and had a low degree of automation and operational efficiency. This is why the SON trend was developed parallel to the evolution and increased complexity of cellular networks. When GSM was deployed, it required a large deal of manual operational effort, which was then gradually reduced in the evolved systems, such as UMTS and LTE, which became more sophisticated and needed more automation to operate with high performance.

The NGMN Alliance (reader is referred to www.ngmn.org for more details) identified excessive reliance on manual operational effort as a main problem in conventional mobile networks and defined operational efficiency as a key target. A project started in 2006 by the NGMN with its main focus on SON. The project main objective was to solve the manual operation problem of the conventional mobile networks (GSM and UMTS). The deliverables

of this project were adopted during the development of the Third Generation Partnership Project (3GPP). At that time, the 3GPP implemented some functions for the SON such as minimization of drive test, energy saving, handover optimization and load balancing.

1.2.1.2 SON in 3GPP

The 3GPP mandate is the development of 3G and 4G networks based on the GSM standards. The 3GPP was concerned with technical requirements and specifications for 3G systems and then the maintenance and development of GSM system was added to its responsibility and currently it is responsible of the evolution of LTE and LTE-Advanced. The structure of 3GPP consists of four Technical Specification Groups (TSGs), and each one of them is divided into several Working Groups (WGs). The WGs responsible for the evolution of SON are mainly RAN WG3 and SA WG5.

The SON has been defined by 3GPP in different releases starting from Release 8. In release 9, the main self-configuration functionalities are standardized where a framework was described that covers all necessary steps to put a new eNodeB in operational state (self-configuration). Also manual configuration was still a choice. Self-optimization in Release 9 included the following use cases: neighbor list optimization with 2G and 3G neighbors, mobility load balancing, mobility robustness optimization, and interference control. Finally, self-healing has a few use cases standardized in Release 9 which are: self recovery of network elements software failures, self-healing of board failures, and self-healing of cell outage.

In Release 10, an additional set of SON functions are standardized such as management aspects of interference control, capacity and coverage optimization, interworking and co-ordination between different SON functions, definition of inputs and outputs of self-healing. Also, in 3GPP Release 10, SON for HetNets was recommended for technical requirement study, and the working items related standard. In each of the releases after Release 10, more functions are added to each SON categories. Also, white papers from vendors and deliverables from different projects added new functions and solutions to the SON. The

SOCRATES project was one of the major projects dealing with self-configuration and self-optimization aspects. It started in January 2008 for three years. The project's main objectives were to validate the developed concepts through extensive simulations, and to evaluate the implementation and the impact of the proposed and standardized schemes [3].

1.2.1.3 SON in 4G

As explosive growth in mobile broadband services has stimulated great demands on wireless radio networks, HetNet technology was developed for LTE-Advanced systems in order to overlay low power nodes within a macrocell to improve capacity and extend coverage. In HetNets, SON is a critical technology. On the one hand, the use of SON in HetNets allows operators to streamline their operations, not only reducing the complexity of managing co-channel interference in HetNets, but also saving operational costs for all macro and heterogeneous communication entities, to harmonize the whole network management approach and improve the overall operational efficiency. The availability of SON solutions for HetNets leads to identification of more powerful optimization strategies that are able to suppress interference and improve energy efficiency. Unfortunately, most HetNets still do not offer SON features due to the fact that the architectures of SON specified in 3GPP were designed primarily for a homogeneous network topology.

This latter problem, SON incompatibility with HetNets, stimulated the standardization and research efforts to mainly focus on the extension of the scope of SON paradigm to also include GSM, GPRS, EDGE, UMTS and HSPA radio access technologies besides LTE. The availability of a multi-RAN SON solution enables more complex optimization strategies that deal with several functionalities simultaneously. Such multi-RAN SON is crucial in case there is a cross-layer restriction in the optimization processes. Also the multi-RAN SON will leapfrog the performance of the smart load balancing strategies between different technologies which therefore will increase the overall network grade of service and capacity. However, for implementing the multi-RAN SON, one must take into consideration that SON

is not a native technology in 2G and 3G networks, and an external centralized entity will be needed to provide the SON functionalities to all multi-RAN technologies.

1.2.2 SON for 5G

A candidate future technology of the 5G network is one that requires a major revolution at different layers, starting with migration towards Software Defined Wireless Networking (SDWN), C-RAN and others while equipping network elements with SON capabilities, where required. The SON in 5G networks will be different from that proposed to be implemented in 4G networks because those candidate technologies have new features which will affect directly the application of SON functionalities. Most of the new technologies will facilitate the implementation of the SON such as C-RAN and SDWNC. Both of them will collect a lot of parameters and information, needed by the SON controller, in a centralized entity.

1.2.2.1 C-RAN in 5G

Centralized Radio Access Network (C-RAN) is a cloud computing based new mobile network architecture that supports current and future wireless communication standards. C-RAN is the split of the conventional BS into two parts: 1) the antennas and Radio Frequency (RF) units will be located on site, and 2) all other BS functions will be migrated to the cloud and between them is the high bandwidth and low latency fronthaul links. The focal concept is to redistribute functions, that are traditionally found in BSs, towards a cloud-operated central processor. So the architecture has three main components: 1) Remote Radio Heads (RRHs) 2) Baseband Unit (BBU) pool 3) Fronthaul links (can be wired or wireless).

Such intelligent centralization would consequently enable cooperative operation among cells for more efficient spectrum utilization and for greener communication. A fully centralized RAN consists of taking most of the BSs functionalities to the cloud and leaving the RRHs only for the cells. The main function of the RRHs is to transmit the RF signals to the users in the DL or forward the baseband signals to the BBU pool for further processing in the UL. Consequently, the BBU or the virtual BS, which is traditionally located in the BS equipment, is relocated to the cloud or central processor, hence forming a shared pool to all connected RRHs. The BBU process baseband signals and optimize the network resource allocation. Implementing the C-RAN will leapfrog the performance of data rate boosting radio features such as eICIC, massive Multi-input Multi-output (MIMO) antennas, and Coordinated Multi-point (CoMP) which require tight and fast coordination between various cells, hence SON would benefit from centralized processing in 5G networks [4].

1.2.2.2 Software Defined Wireless Networking (SDWN) in 5G

Software defined networking (SDN), characterized by a clear separation of the control and data planes, is being adopted as a novel paradigm for wired networking. By implementing SDN, network operators can run their infrastructure more efficiently with faster deployment of new services while enabling key features such as virtualization.

The SDN paradigm has many advantages, including a global optimal routing function implementation, simplification of networking, enabling programmability and easy deployment of new functions, applications and protocols which will make the 5G network much more flexible and efficient. All these changes are triggering the need for modification in the way of thinking toward the standardization of 5G networks, as they need to significantly reduce the costs incurred in deploying a new service and operating it.

SDN is currently being considered as an alternative to classic approaches based on highly specialized hardware executing standardized protocols. Until recently, most of the key use cases used to present the benefits of the SDN paradigm have been limited to wired networks

such as google data centers. The adoption of SDN concept for wireless access and backhaul environments can be even more beneficial than wired. Indeed, the control plane of wireless networks is more complex than that of wired networks, and therefore higher gains can be achieved from the increased flexibility provided by SDN. The use of an SDWN architecture would allow the network to offer the service provider an Application Programming Interface (API) to control how the networks behave to serve traffic that matches a certain set of rules. By using SDWN, an API could be offered to external parties (e.g., service providers) so they can participate in the decision of which access technology is used to deliver each type of traffic to a specific mobile user or group of users.

UDN will achieve a significant benefit from the decoupling of the user data and control plane. 5G users cross cell borders frequently, hence generating signalling load from handovers and cell reselections. The concept of decoupling of the user data and control plane between macrocell and small cells is often referred to as soft cell or phantom cell. Fig. 1.1 shows the conventional cellular network versus the 5G network implementing the concept of control/data plane split. As it is shown, the phantom cell sends and receives data from and to the user (data offloading from the macrocell) while the macrocell sends and receives all radio resource control and signalling information to and from the user. The ultra dense small cells/phantom cells in the figure are omitted for clarification and figure simplicity. This split will collect all information needed for SON decisions at the macrocell or the central entity which will result in reducing the complexity of the SON functionalities in the 5G networks.

1.2.2.3 New Path Loss Models in 5G

Due to the use of UDN, the BSs (small cells) will communicate and exchange information between each other. This will introduce new pathloss models for different communication scenarios. The conventional communications scenarios such as outdoor-to-outdoor communications or indoor-to-indoor communications or even outdoor to indoor communications

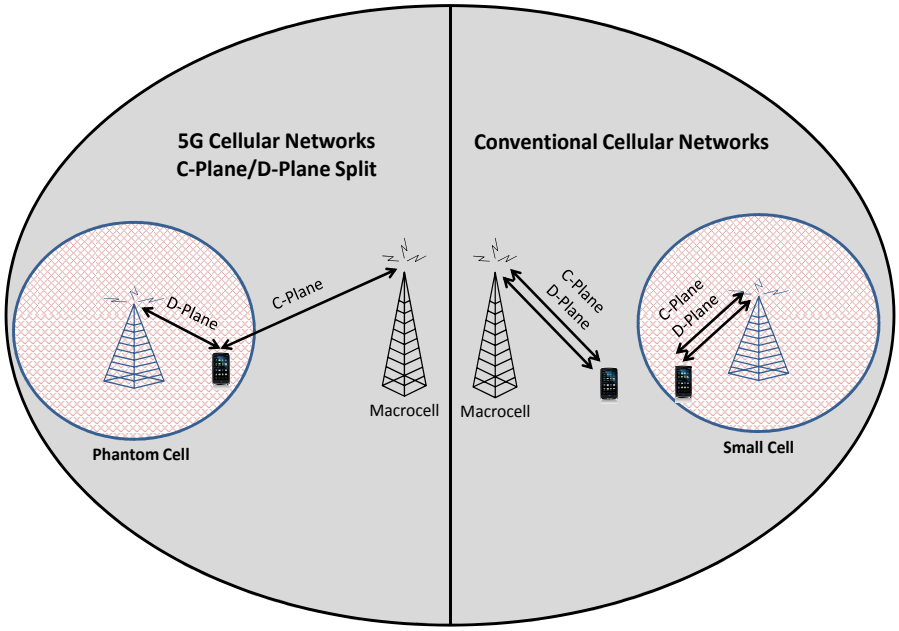

Figure 1.1: Control/data split networks versus conventional networks

will be the same. But a new case that will be introduced due to the implementation of UDN in 5G networks is the indoor-to-outdoor-to-indoor communications.

An example of this scenario is a femtocell in a certain building that communicates with another femtocell in a different building. In this case a new pathloss equation is proposed by modifying the conventional equation of the outdoor-to-indoor communication. PL_{I2O2I} is the path loss from indoor-to-outdoor-to-indoor between two femtocells in two different buildings. Here, there are two outdoor-indoor penetration loss at each side and the indoor distance in the two buildings are considered equal. This is equivalent to dividing the total distance between the two femtocells into $(d_{in_1} + d_{out_1})$ and d_{in_2}. For simplicity, considering $d_{in_1} = d_{in_2} = d_{in}$, $d_{out_1} = d_{out}$ and $L_{\mathrm{ow}_1} = L_{\mathrm{ow}_2} = L_{\mathrm{ow}}$, then the pathloss equation is given by [5]

$$\mathrm{PL}_{I2O2I,\mathrm{dB}} = max(38.46 + 20\log_{10} d_{\mathrm{out}}, \kappa + \nu \log_{10} d_{\mathrm{out}} + 0.3(2d_{\mathrm{in}}) + qL_{\mathrm{iw}} + 2L_{\mathrm{ow}},$$

Here κ and ν correspond to the pathloss constant and pathloss exponent, respectively. d_{out} is the distance traveled outdoor between the two buildings, d_{in} is the indoor traveled distance between the building external wall and femtocell. The maximum in the first term is for considering the worst case. The loss due to internal walls is modeled as a log-linear value equal to 0.3dB per meter, L_{iw} is the penetration loss of the building internal walls, q is the number of walls and L_{ow} is an outdoor-indoor penetration loss (loss incurred by the outdoor signal to penetrate the building). All distances are in meters and it is assumed that all the aforementioned formulas are generalized for the frequency range 2–6 GHz (for more details refer to [5]). This equation can be used to model the millimeter Waves (mmWs) pathloss but after some modifications.

1.3 Self-Healing

Wireless cellular systems are prone to faults and failures due to several reasons. These failures could be software related or hardware oriented. In conventional systems, failures

were mainly detected by the centralized OAM software. When the causes of alarms cannot be cleared remotely, maintenance engineers must visit the failure location. This process could take days before the system returns to normal operation. In some cases, some failures are even undetected by the OAM and cannot be addressed except when an unsatisfied user files a formal complaint, thus resulting in salient degradation in the network performance. In future SON systems, this process needs to be improved by incorporating self healing functionality.

Self-healing is the execution of actions that keep the network operational and/or prevent disruptive problems from arising. In response of failure, self-healing procedures smoothly mitigate the failure and the network works near normal conditions, even in the presence of failure. Self-healing is done in two steps: 1)cell outage detection, and 2)cell outage compensation.

Cell outage detection and compensation provide automatic mitigation of BS failures especially in the case where the BS equipment is unable to recognize being out of service and has therefore failed to notify OAM of the outage. Detection and Compensation are two distinct cases that cooperate to completely mitigate the failure or at least alleviate the failure.

Both detection and compensation provide many benefits to the network operator. Conventional cellular networks have experienced failures of which operators had no knowledge until such time as receiving notification from customer support of problems in the field. Cell outage detection ensures that the operator knows about the fault before the end user does so it detects and classifies failures, while minimizing detection time. Cell outage compensation provides temporary alleviation of the main failure problems such as cell power outage. The cell outage compensation executes actions to solve or, at least, alleviate the effect of the problem. If the failure time exceeds a certain threshold, it is considered as a permanent failure and a site visit by the operator is needed to repair the failure. Hence automatic detection and compensation of failures in 5G networks is strongly recommended.

In Fig. 1.2, the normal operation of the network means that it is operating without any failures in any BS in the network. The system is monitored for detection of any failure. In the case of failure, the self-healing functions are activated and are implemented in the failure region only and the rest of the network operates in the normal mode. The neighboring cells may increase their power and/or change their antenna tilt to overcome the coverage problem in the failure region. When the failure is repaired, the normal operation mode is recovered again and the neighboring cells restore their original power and antenna tilt configuration.

From a timing perspective, Fig. 1.2 shows that normal operation continues for hours or days without any failure or error interruption. In the case of failure, the system will detect and activate the self-healing strategy within a few milliseconds. System repair, which is done by the operator maintenance personnel if the failure is not repaired automatically, can typically be done within 24 hours at most, and in this case the self-healing strategy will provide recovery that satisfies the minimum system requirements in the failure region, even in the worst case (multiple failures). Switching back to normal operation is performed in multiples of milliseconds after system repair.

1.3.1 Sources of Failure

Wireless cellular systems, as most other systems, are prone to failures. The failures can be classified as software or hardware failures. Software failures can be mitigated automatically by restarting or reloading the failed node software while most hardware failures have to be manually repaired through a cell site visit which may take a few hours (up to 24 hours). During the repair time, the network must operate near normal conditions with acceptable quality of experience

1.3.2 Cell Outage Detection

Cell Outage Detection (COD) uses a collection of local and/or global information to determine that a BS is not operating probably. Detection includes active notification to

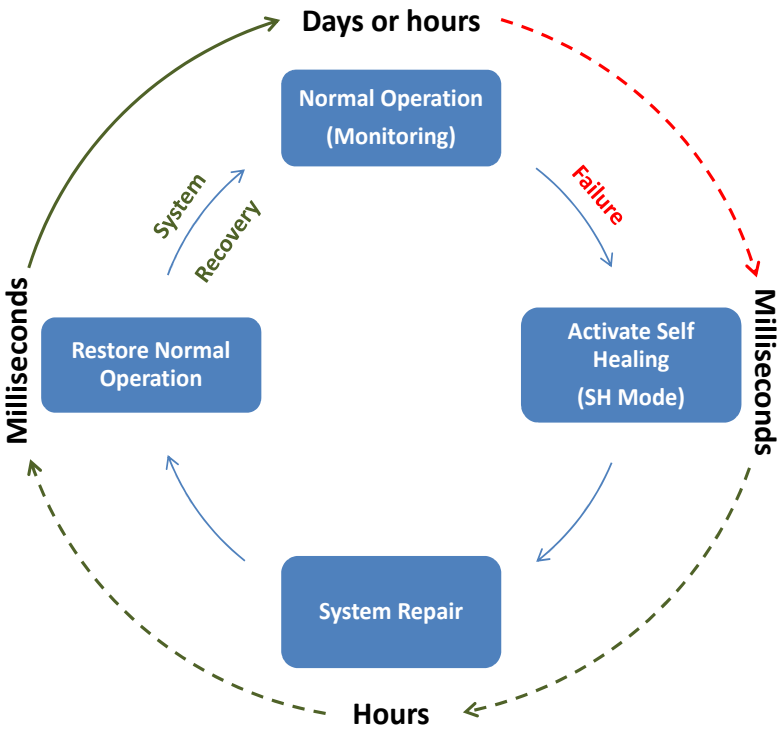

Figure 1.2: Self-healing procedures

cover the generalized case in which OAM is aware of the fault. In the case of complete BS failure, OAM will be unable to communicate with the failed BS to determine if its cell is in service. Lack of communication could be a symptom of failure on the OAM Backhaul rather than an indication that the site is down. In this case, the Network Manager needs to have other evidence to determine the nature of the problem. If the cell is still in service, it will continue to interact with the core network, so the Network Manager should be able to determine from core network metrics whether there is ongoing interaction with a specific BS.

machine learning based algorithms have been the prevailing method for full outage detection in research. Most of the studies on full outage detection that employ learning based algorithms can be split into two categories i.e., supervised learning techniques for full outage detection solutions and unsupervised learning techniques for full outage detection. Supervised algorithms are a popular choice in terms of full outage detection due to their reliance on pre-classified data. On the other hand, The unique ability of unsupervised learning algorithms to cluster data into distinct groups without any pre-classification makes them highly popular in outage detection applications. A major application of unsupervised learning is the detection of cells that are in outage but do not generate any alarms, otherwise known as sleeping cells. Detection of such cells is not immediately possible manually due to the lack of alarms accompanying the outage which makes their detection a highly useful application of unsupervised learning.

1.3.3 Cell Outage Compensation

The Cell Outage Compensation (COC) actions are entirely based on detection done by the COD described in the above subsection. Some software failures can be automatically mitigated while other software and hardware failures have to be manually cleared by network engineering. Compensation actions are triggered immediately after the detection of failure. If the whole BS failed, the compensation action(s) in this case is done by neighboring BSs.

They initiate reconfiguration actions such as changing their antenna tilt and increasing transmission power to extend their cell coverage to cover the failed BS footprint.

Transmit power has an immediate impact on the BS coverage, however, conventional cellular systems makes maximum use of available power, without leaving headroom to enable a BS to increase its coverage in the direction of a neighboring outage. This issue must be considered in planning future networks.

Changing the antenna patterns to achieve the additional coverage for the neighbor is an effective way to cover the footprint of the failed BS. In most cases, changes are achieved with antenna tilt. However, newer antenna technology, such as massive MIMO, enables many complex adjustments of the coverage pattern on demand. The real challenge with use of antenna tilt change in support of any SON functions, is ensuring there is a control loop to guarantee that antenna adjustment to improve coverage in the failure area is not affecting the coverage of the BS itself. SON needs to collect sufficient measurements to profile the impact of antenna pattern adjustment. Increasing the BS power and/or changing the antenna tilt are not the only ways used to do the COC process but they maybe considered as the conventional techniques for failure compensation.

1.4 Thesis Organization

The rest of the thesis is organized as follows:

Chapter 2 includes most recent related works.

Chapter 3 investigates the problem of backhaul/fronthaul failure in 4G/5G networks.

Chapter 4 presents a novel Self-healing of Users equipment by Rf Energy transfer (SURE) scheme is introduced between the network operator and battery starved users to heal and extend their battery life time by sending dedicated energy from different sources in order to be aggregated and harvested by starved users.

Chapter 5 studies the usage of UAVs/Drones to compensate the effect of BS failures in 4G/5G networks. Different frameworks are presented in this chapter.

Chapter 6 proposes to use and quickly deploy a grid of Drone BSs (DBSs) to cover a disaster affected area to provide an alternate connectivity solution. By using the mentioned grid of DBSs, the main technical challenges to solve are the difficulty to charge and backhaul these DBSs.

Chapter 7 concludes the thesis and outlines its main contributions in Section 7.1. Some potential open problems and possible future works are then presented in Section 7.2.

CHAPTER 2. RELATED WORKS

This chapter reviews the stat-of-the-art related to the topic of this thesis.

2.1 State of the art in Self-healing

SON is a rapidly growing area of research and development, and in the last decade a plethora of diverse efforts, from different research bodies, have been exerted in this field. In [6], the authors did a wide survey which covers all three categories of SON including self-healing. They provided a comprehensive survey which aimed to present a clear understanding of this research area. They compared strengths and weaknesses of exiting solutions and highlighted the key research areas for future development. Imran and Zoha [7] explore the challenges in 5G from the SON and big data point of view. They identified what challenges hinder the current SON paradigm from meeting the requirements of 5G networks. They then proposed a framework for empowering SONs with big data to address the requirements of 5G.

Self-healing has been extensively studied in ad-hoc and wireless sensor networks. Recently few researches addressed self-healing in 4G and 5G networks. Most work done in the self-healing field addressed COD and COC. In COD, a cell is said to be in outage if it is still operating but sub optimally, still operating with a major fault or complete outage, i.e., system failure. In [8], the authors presented a novel COD algorithm based on statistic performance metrics which enable a BS to detect a failure of a neighbor cell. Their simulation results indicated that the proposed algorithm can detect the outage problem reliably in real time. The authors in [9] and [10] focused on COD in the emerging femtocell networks.

They proposed a cooperative femtocell outage detection architecture which consists of a trigger stage and a detection stage. They formulated the detection problem as a sequential hypothesis testing problem. They achieved improvements in both communication overhead and detection accuracy.

In [11], the authors employed a classification algorithm, K-nearest neighbor (KNN), in a two-tier macro-pico network to achieve automatic anomaly detection. They proved the efficiency of the proposed algorithm. The authors in [12] considered the software defined networking paradigm where they proposed a data cell outage detection scheme for HetNets with separate control and data planes. Then they categorized their data COD scheme into the trigger phase and detection phase. Their simulation results indicated that the proposed scheme can detect the data cell outage problem in a reliable manner.

COC received a little bit more attention from the researchers than COD. In [13], Amirijoo presented a cell outage management description for LTE systems. Unlike previous works they give a total overview of both COD and COC schemes highlighting the role of the operator policies and performance objectives in design and choice of compensation algorithms. The possibilities of false detection were also highlighted. In another work by the same research group [14], they proposed concrete compensation algorithms and assessed the achieved performance effects in various scenarios. Their simulation results showed that the proposed compensation algorithm is able to serve a significant percentage of the users that would otherwise be dropped, while still providing sufficient service quality in the compensating cells.

In [15], the authors proposed to compensate cells in failure by neighboring cells optimizing their coverage with antenna reconfiguration and power compensation resulting in filling the coverage gap and improving the QoS for users. The right choice of their reconfigured parameters is determined through a process involving fuzzy logic control and reinforcement learning. Results show an improvement in the network performance for the area under outage as perceived by each user in the system. Moysen and Giupponi [16] also used the

reinforcement learning for reconfiguring parameters. They proposed that a COC module is implemented in a distributed manner in eNBs in the scenario and intervenes when a fault is detected and so the associated outage. The eNBs surrounding the outage zone automatically and continually adjust their downlink transmission power levels and find the optimal antenna tilt value, in order to fill the coverage and capacity gap. Their results demonstrated that this approach outperforms state of the art resource allocation schemes in terms of number of users recovered from outage.

In [17], the authors presented a novel cell outage management framework for HetNets with split control and data planes. In their architecture, the control and data functionalities are not necessarily handled by the same node. The control BSs manage the transmission of control information and UE mobility, while the data BSs handle UE data. An implication of this split architecture is that, an outage to a BS in one plane has to be compensated by other BSs in the same plane. Fan and Tian [65] proposed a coalition game based resource allocation algorithm to enable self-healing and compensate abrupt cell outage in small cell networks. In their proposed algorithm, small cells play coalition games to form a set of coalitions which determines the allocation of sub-channels, and each coalition of small cells serves a user cooperatively with optimized power allocation. Their results proved that the proposed algorithm can effectively solve network failure problem.

2.2 Fronthaul/Backhaul Outages in 4G/5G Networks

Wireless backhaul allows densification of mobile networks without incurring additional fiber deployment cost. This, in turn, leads to high spatial reuse, which is a significant tool to meet increasing wireless demand in 5G networks. However, the probability of failure of wireless backhaul is relatively high due to shadowing, device failure, high interference, etc.

In order to deploy a large number of small cells, operators must still face the challenge of backhauling the network traffic from small cells to the core network. A survey [20] showed that around 56% of operators consider backhaul as one of the greatest challenges in future

cellular communications. This is mainly because most of the small cells do not always have access to wired backhaul connectivity and because today the cost of the wireless backhaul equipment exceeds the cost of the small cell itself.

The 5G-xHaul project, http://www.5g-xhaul-project.eu, proposes the use of a redundant mmW backhaul link for self-healing in case on of them failed. This solution is excellent for low latency applications, however, it will consume double the resources needed for the regular backhauling. In [21], backhaul challenges for small cell BSs are discussed, and potential wired and wireless solutions together with their benefits and drawbacks are presented. The authors in [22], propose a solution for the scheduling, resource allocation and flow control problem for networks with self-backhauled half-duplex small cells. Their system-level simulation results are provided to quantify the performance gains of the proposed algorithms.

In [23], the authors overview the technologies that will pave the way for a novel cellular architecture that integrates access and backhaul networks based on mmW frequencies. The authors in [24] focus on the joint cost optimal fiber drop deployment, resource allocation and routing in an IAB network. They prove by results that IAB can significantly reduce the fiber drop deployment cost.

2.3 Energy Starved User and Energy Harvesting

There is significant on going research investigating a number of alternative ways to extract energy from the environment and convert it into electrical energy for energizing low power mobile devices directly, or store it for later use. One such energy source is Radio Frequency (RF) signals. RF energy is transmitted from billions of radio transmitters around the world, including mobile telephones, different Base Stations (BSs), and television/ radio broadcast stations. The ability to harvest energy from RF signals, enables wireless charging of low-power devices and has positive impact on product design, usability, and reliability. We focus on users that are going to detach from the network because of their depleted

battery. To the best of our knowledge, this work is the first to integrate Self-Healing and EH in the same scheme. Many existing studies focused on EH [63; 26; 27], while few of them have investigated battery starved users. In [28], the authors developed a comprehensive modeling framework for a K-tier uplink cellular networks with RF energy harvesting from the concurrent cellular transmissions. They used markov chain to model the level of stored energy in each user's battery. They showed that the gain of using RF EH can be highly improved by a proper choice of the network design parameters such as receiver sensitivity at the BSs and spatial densities of the BSs.

The authors in [29] investigated the performance of a cognitive radio network under harvesting of energy from combined RF signal and ambient sources. They presented a novel analytical expressions of harvested energy and throughput. In [30] , the authors modeled and analyzed cognitive and energy harvesting-based device-to-device (D2D) communication in cellular networks. The cognitive D2D transmitters harvest energy from ambient interference and use one of the channels allocated to cellular users (in uplink or downlink), which is referred to as the D2D channel, to communicate with the corresponding receivers. The same authors presented a framework for K-tier uplink cellular networks with RF energy harvesting from the concurrent cellular transmissions in [28].

2.4 Drone-based Communications in 4G/5G Networks

Few works in the literature investigated the deployment of the DBSs and its challenges. In [31], a placement technique that uses the drones as relays for cell overloading and outage compensation is proposed. Although an analytical model is provided for evaluating system performance in the downlink direction, the paper did not discuss the DBSs' coverage performance and did not suggest any deployment method. The authors in [32] discussed the optimal deployment position for drones that maximizes the average data rate while keeping the symbol error rate under a certain level. However, their work is limited to only one relaying drone. In [33], the authors proposed a computational method to find the optimal

and fast drone deployment in order to enhance the coverage performance in the case of public safety communications.

On the other hand, some works discussed the connectivity and safe path planing management for drone-based communication scenarios. For instance, improving the connectivity of ad-hoc networks using drones has been discussed in [34],[35]. The authors in [34] developed a simple heuristic suboptimal algorithm to optimize the drones movement by tracking changes in the network. Safe path planning algorithms with multiple drones are proposed in [36],[37] with the objective to ensure that the drones can return to the charging station before their energies are depleted.

Channel modeling also remains an important research direction that has extensively been discussed [38],[39],[40]. Indeed, one of the advantages of using flying DBSs is their ability to establish line of sight (LoS) link with ground users which helps in enhancing the signal quality. In [38], the authors analyzed the optimal altitude of one DBS for a certain coverage area that minimizes the DBS's transmit power. Moreover, they investigated the coverage of two DBSs positioned at a fixed altitude and interfering with each other over a certain coverage area. The probability of air-to-ground LoS link is determined in [39] for a dense urban area. It depends on the altitude, elevation angle, and the distance between the drone and the user. On the other hand, the air-ground path loss (PL) model for urban environment has been discussed in [40]. In [93], the authors provided closed-form expressions for predicted probability of LoS and PL model for air-to-ground environment using low altitude platform.

CHAPTER 3. BACKHAUL/FRONTHAUL OUTAGE COMPENSATION

In this chapter, we present two Backhaul/Fronthaul outage compensation schemes. The first one addresses fronthaul failures in 4G Cloud Radio Access Networks (CRAN) where a new radio is proposed to be added to each type of 4G BSs in order to mitigate the effect of fronthaul failures which may result from link failures or hardware failures. In the second scheme, the failures of the 5G networks' backhaul is considered especially the Millimeter Wave (mmW) link failures. The concepts of self-backhauling and Integrated Access and Backhaul (IAB) are introduced along with the 5G New Radio (NR) and how these technologies are used to mitigate the effects of the mmW backhaul link failures.

3.1 Fronthaul Cell Outage Compensation for 4G/5G Networks

3.1.1 Introduction

The main objective of 5G networks is to achieve the gigabits per second throughput level with high reliability and "limitless" connectivity from everything to everything, anytime, and anywhere. Many new and/or well-known technologies are proposed to be integrated in the 5G architecture such as CRAN, massive MIMO, millimeter Waves (mmW), Software Defined Networking (SDN), Self-Organizing Networks (SONs), dense heterogeneous networks (HetNets).

CRAN is a cloud computing based newly adapted cellular network architecture that is highly expected to be integrated in future cellular standards. Each conventional Base Station (BS) consists of a Baseband Unit (BBU), which is responsible for the baseband

processing, and radio heads which are responsible of the radio frequency functionalities. By separating the radio heads, which are now called Remote Radio Heads (RRHs), from the BBU, the baseband processing is migrated to the cloud and connected to the RRHs via high speed fronthaul links giving rise to the so called CRAN. CRAN provides several advantages compared to the conventional RANs such as faster network deployment and system performance improvement. Even more, by the interworking of SDN with CRAN in 5G networks, CRAN can gather more information to perform better global tasks and decisions [42].

It is expected that 5G data traffic will increase up to 1000 folds over that of 4G, implying that the 5G backhaul/fronthaul capacity has to carry significant amount of traffic. These high rates pose new requirements for backhaul/fronthaul links [1]. Achieving data rates on the order of 10 or 100 Gbps for access communications or fronthaul links is possible only if the available bandwidth is within 1 GHz, which is available only in the mmW bands [43]. Although 5G requires a multiple gigabits per second, tens or hundreds of megabits per second need to be guaranteed with very high availability and reliability in case of failures. In this section we are mainly focusing on the fronthaul outage of 4G/5G CRAN.

Self healing has been addressed by quite a few research works until 4G and in 5G networks it is still in its early stage. The authors in [44] addressed a variety of survivability issues, challenges, and mechanisms in multihop wireless networks. In [6] the authors surveyed the literature over the period of the last decade on the SONs as applied to wireless networks including self-healing.

3.1.2 The proposed HetNet CRAN Architecture

The new proposed HetNet CRAN architecture consists of the BBU pool and RRHs of different types of cells where the small cells (SCs), i.e., picocells and femtocells, are co-located within the macrocell footprint as shown in Fig. 3.1. Each macrocell is supposed to use fractional frequency reuse to avoid interference with other macrocells. The SDN

concept was included for the network flexibility and the Software Defined Wireless Network Controller (SDWNC) is used mainly to control the whole process of COC.

The different types of cell sites are fronthauled using different types of links. Macrocell is always connected to the BBU pool using fiber link(s). Picocells are connected to the BBU pool or to the macrocell either by using fiber or wireless point to point links. Femtocells can be fronthauled using any of the mentioned links in addition to coaxial cable, hybrid fiber-coaxial or copper pairs. If the former links are used, the Internet Service Provider (ISP) must have a low latency high speed connection to the cloud. This CRAN architecture is also compatible with the conventional BSs which are not CRAN based.

It should be noted that the heterogeneity in this architecture is in two directions. One direction is that the CRAN serves heterogeneous types of cell sites (macrocells, picocells and femtocells). The second direction is the different wired and wireless types of fronthaul connections.

3.1.3 The Proposed COC Approach

The conventional and well known approach for COC is to optimize the capacity and coverage of the outage zone by adjusting the antenna gain and transmission power of the neighboring BSs. The disadvantage of this approach is that it will degrade the performance of the users served by the neighboring BSs. Moreover, these BSs will consume a considerable time (compared to 1 ms) to change their power and antenna tilt. The proposed COC approach will not change the antenna tilt or the power of the neighboring cell sites. We propose to add a new radio, which is named Self-Healing Radio (SHR), to each cell site in the network. When a failure occur to the fronthaul of any cell site, the failed cell site will acquire its fronthaul connection from the neighboring cell sites using the SHRs. The neighboring cell will help the failed cell if it has available resources.

The network always operates in the normal mode which may last for days. The network is monitored for detection of any failure by the SDWNC. In case of failure, the COC

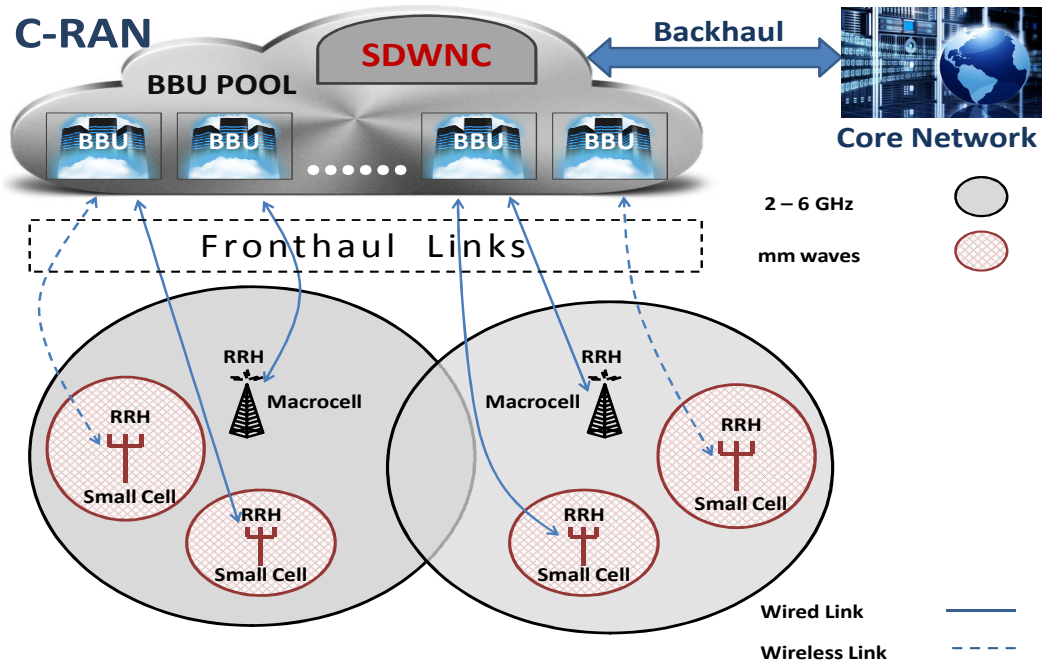

Figure 3.1: The System Model

strategy will be activated by the controller within a few milliseconds. System repair, which will be done by the operator maintenance personnel, can typically be done within hours and in this case, the COC approach will provide recovery that satisfies the minimum rate requirements in the failure region. Switching back to normal operation is performed in multiple of milliseconds and it is triggered by the SDWNC which will deactivate all SHRs for all cell sites.

There are many challenges and issues that had been addressed to provide a reliable network architecture which is able to mitigate any fronthaul failure such as the bands used for the macrocell tier and the SCs tier, the SHRs band, how to control the whole COC process and using pre-planned femtocells to help in the healing process. These issues are addressed below.

3.1.3.1 CRAN Architecture

CRAN architecture consists of three main components:

1) BBU pool which is composed of a set of servers, storage and switches. The BBU assignment for each RRH could be centralized or distributed. In our architecture we are considering the centralized implementation due to its advantages (flexible resource sharing, energy efficiency and interference avoidance).

2) RRHs are located at the remote cell sites. They transmit the radio frequency signals in the downlink and forward the baseband signals in the uplink for further processing in the BBU pool. They include radio frequency amplifier, up/down conversion mixer, analog-to-digital and digital-to-analog conversion.

3) Fronthaul Links can be wired or wireless. Although wireless fronthaul is cheaper and faster to deploy than wired, the best choice is the high speed optical fiber but microwave or mmW are also considered (reader is referred to [46] for an overview of possible wired and wireless backhaul/fronthaul technologies). Fronthaul antennas can be installed on top of roofs to ensure the existence of Line-of-Site (LOS) propagation. Also, reference [47] has more information regarding integrated fronthaul/backhaul architecture in 5G.

By implementing CRAN, 5G network will gain many advantages such as: 1) The equipment needed at the cell site is only RRHs, power supply and backup batteries which will result in shorter installation and repair time. 2) The cell site will consume less energy (no need for air conditioning) 3) The ease of communication between BBUs in the cloud will provide better performance for mobility management, interference cancelation and coordinated multi-point communication, which is expected to provide higher capacity and improve cell-edge coverage.

Backhaul failures of regular BSs is one type of many failures that can occur in BSs of 4G networks. But, after simplifying the BSs in CRAN into the RRHs and migrating all processing units (BBUs) to the cloud, fronthaul failures is the failure that has the most impact on the operation of the CRAN 5G network.

3.1.3.2 Millimeter Waves (mmW) Band

The mmW bands are typically sub-band free and high frequency reuse is possible due to very narrow directed beams. The so-called light spectrum licensing scheme provides lower total cost of ownership and lower cost per transmitted bit than the microwave bands.

Using mmW bands in 5G networks has already been proposed in the literature. The mmW band is used in short range LOS communications. It is not used in long distance communications due to the high attenuation and oxygen absorption of these waves [43]. The wireless fronthaul and access links are assumed to be out-of-band, that is, there is no interference between them. This will provide the 5G users with the target data rates, and SCs will rely on high-gain beamforming to mitigate pathloss [48].

The macrocell situation is complicated due to its wide area coverage. Using mmW with macrocells is still under intensive research because of the high attenuation associated with wide coverage area. As it is well known from 4G networks, 80% of network traffic is used indoor and only 20% is used outdoor [49], the 20% outdoor traffic will be carried out by the macrocell and the outdoor SCs. This trend is expected to continue in 5G, and this means that the traffic carried out by the macrocell in 5G networks is much lower than that carried by SCs.

In our proposed solution, mmW is used only in fronthaul connections and in SCs access links between SCs and users equipment (UEs). However, the macrocell will use the traditional cellular band (2 - 6 GHz) for communications with its UEs. The motivations behind using this band are better rates, lower penetration loss and eliminating the interference issue between SCs tier and macrocell tier. The only limitation of this band is its bandwidth but using massive MIMO, carrier aggregation and other technologies, can facilitate the achievement of macrocell gigabits per second throughput.

3.1.3.3 SHRs Band and Cognitive Radio Concept

The SHRs can use 1) mmW band, 2) The traditional cellular band, or 3) A new dedicated band. For the mmW band, it is difficult to be used because of the NLOS path between SHRs. Dedicating a portion of the traditional cellular band, which is also used by the macrocell, to the SHRs communication will affect the band utilization because SHRs are only activated if fronthaul failures occur. Finally, using a dedicated band (licensed for self-healing communications only) will dramatically increase the capital expenditure and also this band will not be fully utilized.

Cognitive Radio (CR) concept is one of the promising technologies for solving telecom problems such as spectrum scarcity or in case of disasters [50]. Our proposed solution is to use the CR for SHRs communications which optimizes the use of the available spectrum. The band used is the same as the second solution where a portion of the traditional cellular band will be dedicated to the SHRs. The main difference is that when SHRs are inactive, this portion will be available for the macrocell to use it as a secondary user. Therefore, if the macrocell is starved for bandwidth, it will sense the SHRs dedicated channels and if it is free then the secondary user (macrocell) will use the vacant channels until the primary users (SHRs) are activated. Once the primary user (SHR) is active (this means that a failure has occurred), the macrocell will vacate these channels.

Furthermore, in our model, the macrocell can avoid wasting time in spectrum sensing by acquiring the SHRs channel occupancy information from the SDWNC. If there is no failure, the macrocell will use the reserved portion of the band without sensing. If a failure happen, the SDWNC will immediately request from the macrocell to vacate the SHRs channels to be used by the primary users (SHRs). This will save the sensing power and time and will also increase the reliability of using CR in 5G networks.

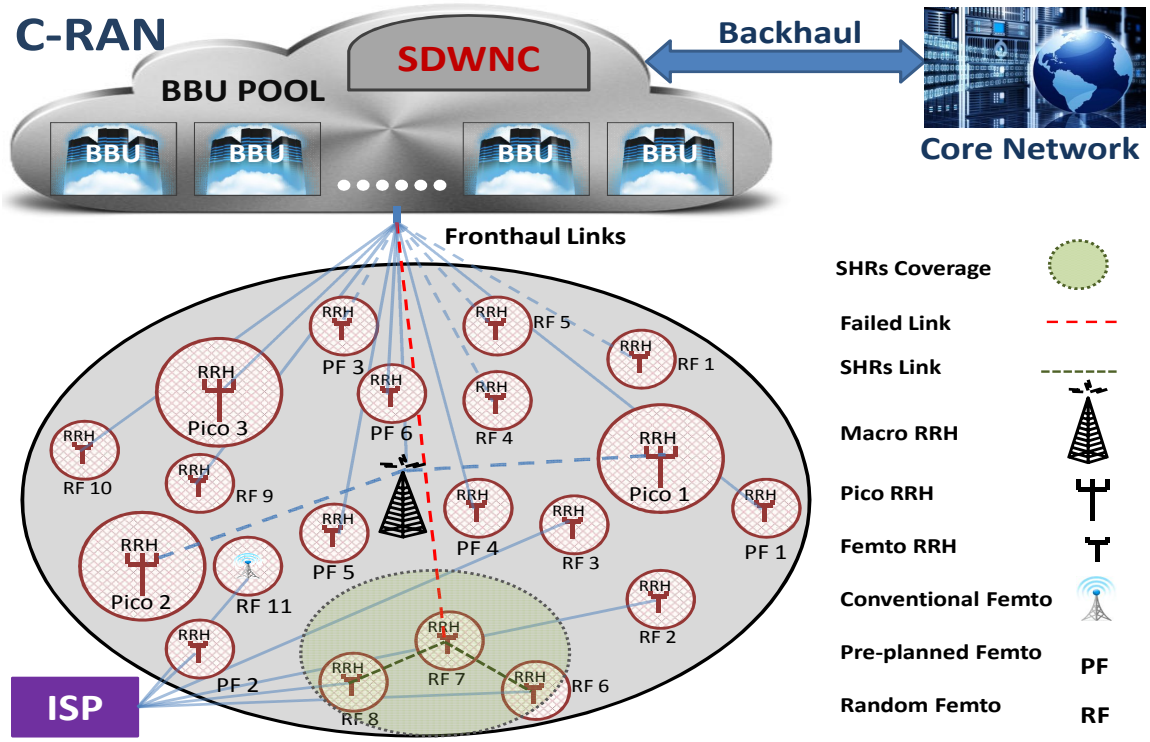

Figure 3.2: SC failure mitigation process

3.1.3.4 Types of Femtocells

As it is known from 4G, the femtocells may be deployed by network users; In this case they are randomly placed and are called Random Femtocells (RFCs) or femtocells may be deployed by the operator in pre-planned locations to enhance the capacity or to cover dead zones; In this case they are called Pre-planned Femtocells (PFs).

The main difference between the 4G PFs and the proposed 5G ones is that the latter are used mainly to self-heal the failed cell sites. In addition, they can be used also for capacity enhancement and dead zones coverage. The only constraint is that they must be located within the SHRs footprint of the target cell site and it is preferable that the PF be connected to a fiber fronthaul to guarantee the gigabits per second 5G throughput which will be used mainly to heal the failed cell sites and also for serving its own users.

3.1.3.5 Software Defined Wireless Network Controller (SDWNC)

The SDWNC is co-located within the cloud to gather the needed information in a fast and reliable way. The SDWNC is a mandatory component in our architecture as it acts as the supervisor, decision maker and administrator for all self-healing procedures applied to all network cell sites. Reference [51] has more details about SDN in wireless networks.

The co-location of the SDWNC in the cloud will help it to take optimal decisions in order to decide how to recover from fronthaul failures. This reduces the amount of information needed to be exchanged which will allow optimal recovery in a very short time.

The SDWNC activates SHRs for all cell sites in vicinity of the failed cell site. It also deactivates the SHRs after the failure is repaired. In addition, it deactivates the SHRs of the cells that are not participating in the self-healing process to save their power from being wasted.

3.1.4 Self-Healing Procedures

Fig. 3.1 shows the whole network but in Fig. 3.2 we zoom in on one of the macrocells coverage where each macrocell is associated with three PFs (one in each sector). Also, each picocell is associated with one PF. There are no PFs associated with RFCs. This is because macrocells and picocells are serving a large number of users compared to the RFCs. The latter will search for nearby SHRs, in case of failure, in order to heal their failed fronthaul link. This proposed CRAN architecture is compatible with the conventional BSs which are not CRAN based. RFC 11 in Fig. 3.2 shows an example of a BS backhauled from the ISP.

When a certain cell site fronthaul fails, it will automatically activate its own SHRs, but will be totally disconnected from the SDWNC and in this case the cloud, macrocell or ISP (depending on which one was fronthauling this cell site) will report to the SDWNC the failed cell details. The SDWNC will then activate the SHRs of all cell sites in the region surrounding the failed cell site. The process of detecting the failure and SHRs activation must be done within a very short time.

The failed cell will try to connect to the healing cell sites via SHRs according to a certain priority order depending on the cell site type, available resources and the Received Signal Strength (RSS). The failure of a fronthaul link may be permanent or transient. Our COC approach works with both, and the only difference is that in the case of a permanent failure, the SDWNC, after a certain threshold time, will inform the operator that there is a failure which requires maintenance personnel to embark on a field visit to the failed cell site. It should be noted that our proposed COC scheme can be classified as a hybrid approach according to the definition given in [44].

3.1.4.1 Single Failure Scenario

Single failure means that only one cell site fronthaul failed in the network. In this case, the SC will trigger the self-healing mode where it will activate its own SHRs and then try to connect to other cell sites' SHRs which are activated by the SDWNC. Following a priority

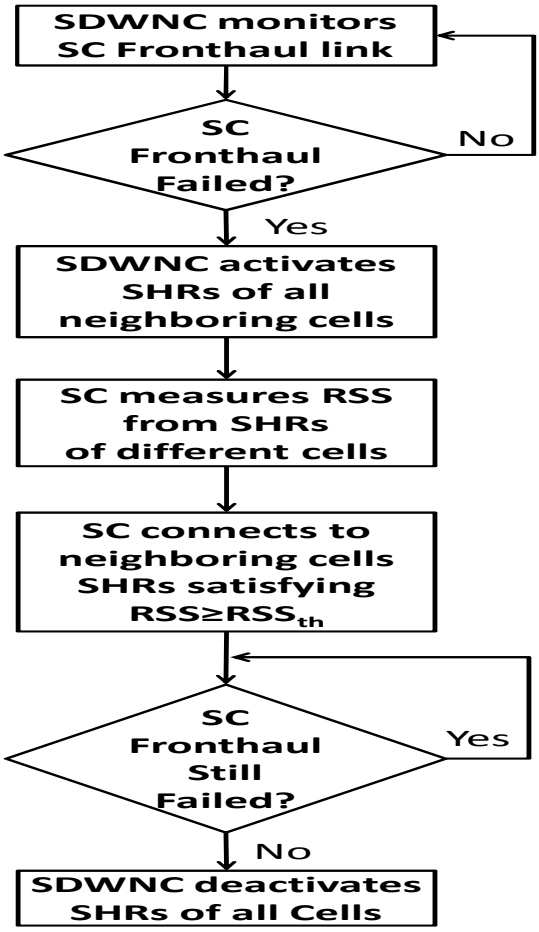

Figure 3.3: SC failure mitigation flow chart

order, the SC will first try to connect to a macrocell, then PFs, then picocell and finally RFCs. RFCs are assigned the lowest priority because they are personal properties and the operator will have to compensate the owners of these RFCs.

The flow chart in Fig. 3.3 shows the SC fronthaul failure mitigation process where the SDWNC always monitor the network to detect any fronthaul failure. If the fronthaul of any cell site failed, the failed SC will immediately activate its SHRs and at the same time the SDWNC will activate SHRs of all neighboring cell sites. At this point the failed SC will use its SHRs to measure the RSS levels from all neighboring cell sites and will update a list of healing cell sites with measured RSS levels higher than a certain RSS threshold.

The failed SC will use priorities to decide which cell sites' SHRs it will connect to. The SDWNC will continue to monitor the failed fronthaul link and when the failed link returns to work properly, the SDWNC will deactivate SHRs of all cell sites in the failure region and the network returns to operate in normal operation.

An example of failure scenario is shown in Fig. 3.2, where the fronthaul link of RFC 7 failed. The failed RFC will apply the priority order described above, but because it is out of SHRs' coverage of the macrocell, PFs and nearby picocells, it will connect to the SHRs of RFC 6 and RFC 8 to mitigate its fronthaul failure. Once the failure is repaired, the SHRs will be deactivated by the SDWNC and RFC 7 will return to serve its users using its own fronthaul link.

The failure of the macrocell fronthaul is not considered as a single failure because this will immediately cause the failure of all SCs fronthauled from the macrocell causing multiple failures in the network.

3.1.4.2 Multiple Failures Scenario

A multiple failures scenario refers to the situation where two or more fronthaul failures occur at the same time in the same region. There are two cases studied here.

• SCs Fronthaul Failure

This case can be seen as the failure of two or more SCs in the same region. The procedures in the flow chart above can be used to mitigate these failures when implementing the proposed algorithm for each failed cell site. For example, if two SCs failed, the SDWNC will activate the SHRs of cell sites in their region and each failed cell site will activate its SHRs and try to connect to the healing cell sites and as the number of failures increases the probability of healing each failed cell will depend on the number of nearby healing cell sites which can provide the temporary fronthauling connections. Thus, as expected in 5G networks, the dense deployment of SCs will enhance the performance of our self-healing approach especially in the multiple failures case.

• Macrocell Fronthaul Failure

The macrocell plays a vital role in HetNets where in addition to its main function, coverage for outdoor users, it provides wireless fronthaul links to other SCs that can't directly reach the cloud. In our architecture, two picocells acquire there fronthauling from the macrocell. Fig. 3.4 shows an example of the macrocell fronthaul failure and the mitigation process. The macrocell fronthaul failure (the solid red line) immediately results in the failure of two fronthaul links (Pico 1 and Pico 2). As can be seen from Fig. 3.4, the self-healing process will mitigate the effect of failure for the fronthauled picocells and the macrocell. The picocells will be recovered first using PFs and RFCs in their vicinity. For example, Pico 1 will be recovered by PF 1, RFC 1 and RFC 3. Similarly, Pico 2 will be recovered by PF 2, RFC 9 and RFC 11.

The next step, macrocell fronthaul recovery, will be done from two sources. The first source is using the mmW links between the macrocell and recovered picocells. The second source is the recovery from femtocells in its SHRs footprint. As shown in Fig. 3.4, PF 4, PF 5, PF 6, and RFC 4 provide the temporary fronthaul connections. Aggregating all received traffic, the macrocell will be able to guarantee the minimum requirements to its users until the failure is repaired, regardless of how long the failure will remain. A heuristic algorithm for the detailed macrocell self-healing procedures can be found in [45].

3.1.5 Simulation Model

Simulations were carried out for one macrocell with a footprint of radius 500m in an urban area. Within the macrocell footprint there are 6 picocells, 9 PFs and 50 RFCs randomly distributed over the entire area. The fronthaul rate to the macrocell is 100 Gbps, to the picocells is 10 Gbps, to the PFs is 5 Gbps and finally to the RFCs is heterogeneous and distributed among the RFCs as follow; 50% of RFCs with rate of 200 Mbps, 40% of RFCs with rate of 500 Mbps and 10% of RFCs with rate of 1 Gbps. The performance of our self-healing approach is evaluated in terms of Degree of Recovery (DoR) from failure.

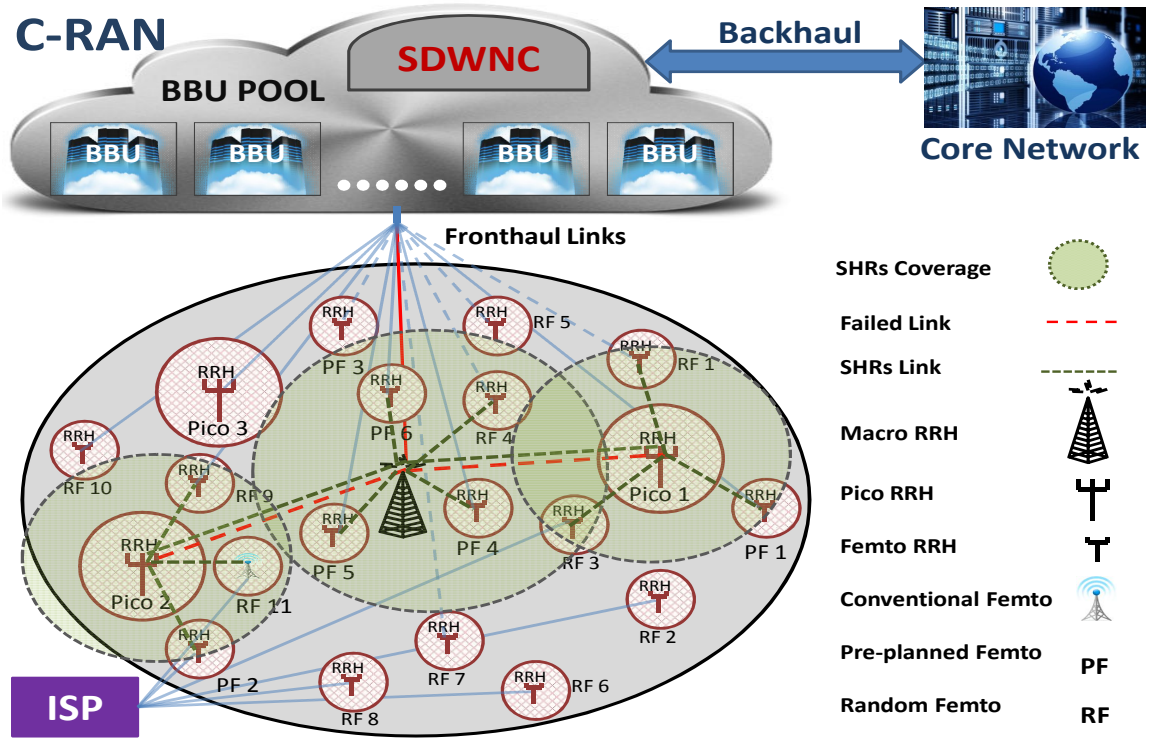

Figure 3.4: Macrocell failure mitigation process

The DoR of a certain BS is defined as:

$$DoR = \frac{Sum\ of\ recovered\ rates\ from\ other\ cell\ sites}{Original\ input\ rate\ of\ the\ failed\ cell\ site}$$

where the original input rate of the failed cell site is the same as the input rate of that cell site except for the macrocell because it fronthauls other picocells, so the actual input rate for the macrocell depends on the number of macrocell fronthaul connections.

3.1.5.1 Simulation Results

In this section, we study the performance of our proposed COC algorithm by investigating the effect of increasing the number of SHRs on the DoR of the failed cell sites. Two scenarios are considered; single failure and multiple failures. First, we assess the DoR of the macrocell failure which is the worst case and is considered as multiple failures. The DoR is evaluated with respect to the number of SHRs in both macrocell and picocells. Second we assess the DoR of RFC in case of single failure with respect to the number of SHRs in RFCs and picocells.

Fig. 3.5 addresses the failure scenario of macrocell fronthaul. It shows the DoR of macrocell when the number of SHRs of macrocell and picocells is increased from 1 to 4. When the number of SHRs in picocells is fixed, the DoR increases with the increase of SHRs in macrocell. On the other hand, when fixing the number of SHRs in the macrocell and increasing them in picocells, the DoR will also increase. However, increasing the number of picocells' SHRs has a great influence on the DoR of the macrocell. For example, fixing macrocell SHRs to 1 and increasing picocell SHRs from 1 to 4 can improve the macrocell DoR by approximately 50%, but fixing picocell SHRs to 1 and increasing macrocell SHRs from 1 to 4 will improve the DoR by less than 10%. The DoR significantly depends on the number of SHRs in picocells because in addition to recovering from surrounding femtocells, it recovers also from the recovered picocells using the already deployed LOS links between picocells and macrocell. It is obvious that the incremental increase in the DoR decreases with increasing the SHRs.

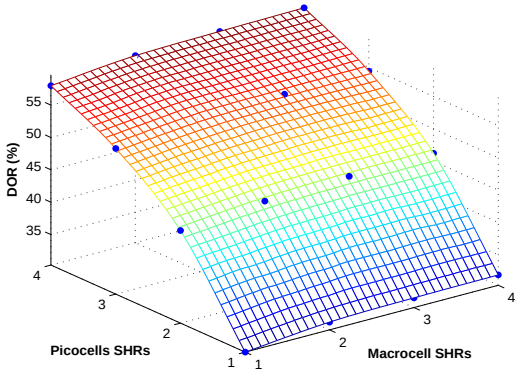

Figure 3.5: Macrocell DoR vs. number of SHRs in the macrocell and picocells.

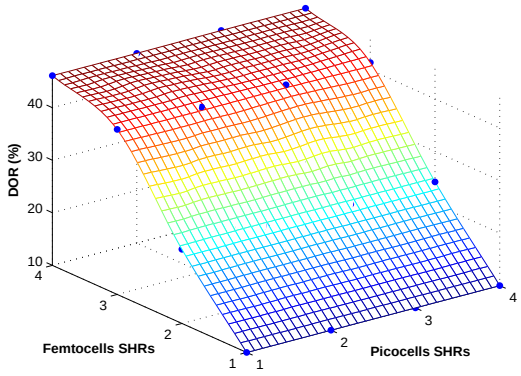

Figure 3.6: Femtocell DoR vs. number of SHRs in the femtocells and picocells

Fig. 3.6 addresses the failure scenario of a femtocell fronthaul. It shows the DoR of a femtocell when the number of SHRs of femtocells and picocells is increased from 1 to 4. As can be seen clearly from the figure, as the femtocells SHRs increases the DoR of femtocells increases. However, the number of SHRs in picocells has a slight or even no effect on the DoR of the failed femtocell. This shows that the DoR of femtocells is not directly dependent on the number of SHRs in picocells but it is dependent on the number of cell sites located within the failed femtocell's SHRs coverage area, regardless of the cell site type. It is clear that using 2 SHRs in femtocells we can recover up to 20% of the original

rate of the failed femtocell fronthaul link. Using 3 SHRs in femtocell will recover around 40%. Further increase of the SHRs will not increase the DoR by a significant percentage.

Based on the simulation setup in [45], Fig. 3.7 evaluates the DoR of picocell when increasing the picocell SHRs from 1 to 7 under single and multiple failure scenarios. In case of single failure, the DoR increases rapidly from 10% to 20% by increasing the SHRs from 1 to 4. Further increase in the SHRs results in negligible increase in the DoR which proves that the recommended number of SHRs to be used by picocells is 4.

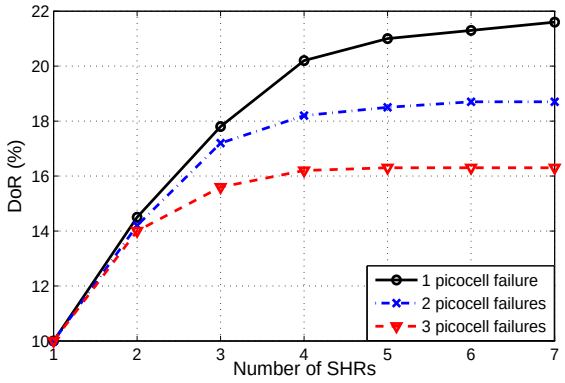

Figure 3.7: DoR of picocells vs. number of SHRs.

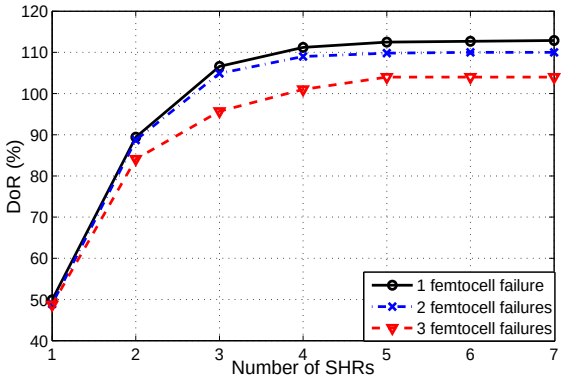

Figure 3.8: DoR of femtocells vs. number of SHRs.

Also we can see in Fig. 3.7 in the case of multiple failure that all failed picocells can recover their rates by 10% using 1 SHR. This is because, as mentioned before, each picocell has a dedicated PF in its SHRs range. Therefore, under multiple failures each failed picocell

can find at least 1 PF to connect to. As the number of SHRs increases the DoR of the 2 failure case and 3 failure case decreases. This is because by adding more SHRs in each picocell, the network resources will be consumed and not all SHRs in each failed picocell will succeed to get enough resources. Also it can be seen that further increase than 4 SHRs per picocell introduces negligible improvement and the DoR is almost constant. In the next scenario, the picocells SHRs will be fixed to 4 SHRs.

We observe from Fig. 3.8 that when femtocells have only 1 SHR, the DoR of femtocells is up to 50%. This is because the femtocells most of time are recovered from other BSs which have much higher rates. This also explains the reason for exceeding the 100% DoR for femtocells having 3 SHRs or more. Using 2 SHRs can recover up to 90% of the failed femtocell rate which is acceptable rate in the presence of failure. Recovering more than 100% is not acceptable from the operator point of view. As the number of SHRs increases, the DoR of 2 failures and 3 failures decreases which is similar to picocell multiple failure case. Even in case of 3 failures, the DoR is approximately 85% using 2 SHRs. This indicates that our approach is robust under multiple failures.

The price of RRHs ranges from $2000 for macrocell to $100 for femtocell (this is an approximate market price taken from different vendors) and the price of a typical cellular transceiver is much less than these values. So adding more SHRs to macrocells or picocells will not dramatically increase the capital expenditure. For femtocells only 1 or 2 SHRs can be added to keep its price low. The operator will pay for the extra cost of the SHRs if the user agrees to be involved in the self-healing process. Otherwise, the user will purchase the regular femtocell (without SHRs). From the DoR results and the approximate cost stated above, it is recommended to equip each macrocell sector with 3 SHRs, and use 4 SHRs per picocell. The latter plays a crucial rule in recovering the macrocell fronthaul failure. Using 2 SHRs per femtocell is sufficient to guarantee the minimum requirements in the presence of failures, as confirmed by the results.

3.2 Self-backhauling Failure Mitigation Using 5G New Radio

3.2.1 Introduction

The 5G Radio Access Network (RAN) will be architecturally very different from past generations. Network equipment manufacturers and service providers are faced with new technologies, architectures, access methods, applications, and traffic compared to past generations. They will need to troubleshoot never-before-seen issues in the previous cellular generations or the rigorous R&D validation environment. 5G introduces higher frequencies (millimeter wave), wider bandwidths, advanced multi-antenna access schemes, small cells, and network slicing including network function virtualization, and orchestration [52].

The 5G era will mean a connected society, in which people, machines, and things are always connected. According to small cell forum [53], deployments of 5G small cells will cross the one million mark in 2020 and will rise steeply after that to reach 5.2 million in 2025. Moreover, around 67% of the operators have already deployed indoor small cells (i.e., femtocells). AT&T has also announced the deployment of more than 40,000 outdoor small cells (i.e., metrocells) [20].

Therefore, network densification using millimeter wave or sub-6 GHz small cells is considered to be a key solution in the future networks. The deployment of small-cell networks in a given area is a promising technique that provides a huge capacity gain and brings small cells closer to users' devices. Nevertheless, the great deployment of small-cells presents several challenges in network management, including interference alignment, extensive backhauling, and cell selection within Heterogeneous Networks (HetNets).

3.2.2 Motivation

Cellular network operators spend nearly a quarter of their revenue on network maintenance and management. A significant amount of that budget is spent on resolving outages that degrade cellular services.

Network densification, driven by the need to meet capacity and data rate requirements of 5G mobile cellular networks, means that future mobile cellular networks will have to handle far more network nodes and links (wired or wireless) than before. Hence, the classic methods of manual outage compensation will not suffice. To address this challenge autonomous mechanisms need to be developed. Higher cell densities coupled with technologies such as millimeter wave spectrum utilization, and more configurable parameters will result in frequent network outages driven by link failures.

In order to deploy a large number of small cells, operators must still face the challenge of backhauling the network traffic from small cells to the core network. A survey [20] showed that around 56% of operators consider backhaul as one of the greatest challenges in future cellular communications. This is mainly because most of the small cells do not always have access to wired backhaul connectivity.

Wireless backhaul allows densification of mobile networks without incurring additional fiber deployment cost. This, in turn, leads to high spatial reuse, which is a significant tool to meet increasing wireless demand in 5G networks. Integrated access and backhaul (IAB), where access and backhaul network share the same standard wireless technology (e.g. 5G new radio (NR) standard), allows interoperability among different IAB manufacturers and flexible operation between access and backhaul. These tools are very promising solutions to tackle the problem of backhaul failure. 5G requires Gbps backhaul capacity, which requires new spectrum (e.g. mmWave) for both access and backhaul.

Wireless backhaul links, especially those using millimeter waves, are vulnerable to blockage, e.g., due to moving objects such as vehicles, due to seasonal changes (foliage), or due to infrastructure changes (new buildings). Such vulnerability also applies to mmW IAB-small cells [104]. 5G networks are characterized by high speed connections so backhaul failure for a few seconds with gigabits per second speeds can cause the loss of hundreds of gigabits. This motivates us to focus on the small cells backhaul failure in 5G networks where IAB are used by the small cells which adapt the 5G NR.

Providing a reliable connectivity between the small cells and the core network is a challenge, and it may require pre-planning efforts. This is why we present a planning model in this section that allows the failure of the backhaul of an arbitrary 5G small cell without interrupting service to its users. This is achieved by applying a novel Backhaul Outage Compensation (BOC) mechanism that mitigates the effect of the failure using 5G NR while utilizing the concept of IAB. An optimization problem is formulated aiming to maintain the connectivity of the users affected by the backhaul failure. We assume that only one small cell will fail at a given time. This is a reasonable assumption since usually in the time it takes the small cell to be repaired, there is a very small probability that another small cell will fail. In the following subsections, we will introduce the 5G NR, the IAB and ways to mitigate their failures using self-healing.

3.2.2.1 5G New Radio (NR)

NR is a completely new air interface being developed for 5G. It is being developed from the ground up in order to support the wide variety of services, devices, and deployments 5G will encompass, and across diverse spectrum, but it will build on established technologies to ensure backward and forward compatibility. It is also designed to significantly improve the performance, flexibility, scalability, and efficiency of current mobile networks, and to get the most out of the available spectrum, whether it is licensed, shared or unlicensed, across a wide variety of spectrum bands.

The 5G NR specifications defined two modes. Non Stand-alone (NSA) and Stand-alone (SA). According to the recent 3GPP Release 15 standard [66], the first wave of networks and devices will be classed as NSA, which is to say the 5G networks will be supported by existing 4G infrastructure. Here, 5G-enabled smartphones will connect to 5G frequencies for data-throughput improvements but will still use the existing LTE radio for non-data duties such as talking to the cell towers and servers. The NSA 5G NR variant was to be finalized by March 2018 but in fact was approved in December 2017. The SA mode is to

be completed by September 2018 and implies full user and control plane capability using the 3GPPs new 5G core network architecture. The agreement also defined a framework to ensure commonality between the two variants. It also puts compatibility at the heart of 5G NR design.

To deliver the new levels of performance and efficiency that will enable the wide range of 5G services. There are three general designations of 5G services; 1) Enhanced Mobile Broadband (eMBB), 2) Ultra-reliable and Low-latency Communications (uRLLC) and 3) Massive Machine Type Communications (mMTC). eMBB is defined as the data-intensive applications that need lots of bandwidth, like video streaming. The technologies that will bring eMBB to a reality is massive MIMO, mmWave, spectrum sharing and advanced channel coding. uRLLC is describing the latency-sensitive services needing extremely high reliability and availability, such as autonomous driving and real-time command and control for cellular drone communications. Finally, mMTC is the support of a large number of low cost, low energy devices with small data volumes, such as mart cities. This new radio could support one million devices in a single square kilometer.

While the use of mmWave spectrum will be critical to meeting the extreme data throughput expected in 5G mobile broadband, frequency bands below 6 GHz will also be used for all three use cases: eMBB, ULLRC, and mMTC. Sub-6 GHz spectrum is well-understood, and many countries are freeing up spectrum for sub-6 GHz initial releases. Sub-6 GHz has some challenges, but using wider carrier bandwidths at mmWave frequencies are where we will see a new set of issues not previously experienced in commercial mobile communications. 5G NR has specified frequency use up to 52.6 GHz, and there are several countries conducting trials in the 26, 28, and 39 GHz bands.

For 5G NR with millimeter wave cell deployment, researchers will need to consider additional metrics. This is because millimeter waves have a very high pathloss leading to natural loss of coverage even at a distance of a few hundred meters. However, to optimize signal strength at the mobile device, NR uses a combination of analog and digital beamforming.

The idea of beamforming is not new as LTE networks extensively use digital beamforming. With 5G the challenges of signal propagation and smaller antenna sizes motivate the use of extensive analog beamforming techniques. Above 24 GHz, analog beamforming of narrower beamwidths gives 5G BSs the ability to steer downlink signals more efficiently. Using this approach, the recipient of the downlink transmission benefits from higher signal strength particularly by using higher order modulation schemes.

3.2.2.2 Integrated Access and Backhaul (IAB)

IAB can provide seamless integration between access and backhaul links where the summation of the allotted bandwidth among access and backhaul links is fixed. This can meet the dynamic traffic demand by splitting the threshold for access and backhaul bandwidth differently at different BSs of the network. A key benefit of IAB is enabling flexible and very dense deployment of NR cells without densifying the transport network proportionately. A diverse range of deployment scenarios can be envisioned including support for outdoor small cell deployments, indoors, or even mobile relays (e.g. on buses or trains).

The move toward self-backhauling or IAB was motivated by the capacity bottleneck which has shifted from air interface to the backhaul. In addition, fiber backhaul is costly and cannot be deployed everywhere. Point-to-point (PTP) microwave has limited connectivity and is not suitable for bursty small cell traffic. Also, Point-to-multi-point (PTMP) microwave has a limited data rate.

An IAB node can follow the same initial access procedure as a UE, including cell search and random access, in order to initially set up a connection to a parent IAB-node or a IAB-donor, which is providing backhaul to the IAB-node [104]. There are different options for sharing the wireless channel resources (Time, Frequency, and Space): a) Orthogonal (no shared channels between access and backhaul), b) Partial reuse (some channels are shared) and c) Full reuse (all channels are shared). The benefits of integrated access and backhaul (IAB) are crucial during network rollout and the initial network growth phase. To leverage

these benefits, IAB needs to be available when NR rollout occurs. Consequently, postponing IAB-related work to a later stage may have an adverse impact on the timely deployment of 5G NR access.

Due to the expected larger bandwidth available for NR compared to LTE (e.g. mmWave spectrum) along with the native deployment of massive MIMO or multi-beam systems in 5G NR creates an opportunity to develop and deploy IAB concept. This may allow easier deployment of a dense network of self-backhauled 5G NR cells in a more integrated manner by building upon many of the control and data channels/procedures defined for providing access to UEs.

In-band- and out-of-band backhauling with respect to the access link represent important use cases for IAB. In-band backhauling includes scenarios, where access- and backhaul link at least partially overlap in frequency creating half-duplexing or interference constraints, which imply that the IAB node cannot transmit and receive simultaneously on both links. In the present context, out-of-band scenarios are understood as not posing such constraints. It is critical to study in-band backhauling solutions that accommodate tighter interworking between access and backhaul in compliance with half-duplexing and interference constraints [104].

3.2.2.3 Related Works

3GPP 5G NR standard, set to be published with 3GPP Release 15 and further updates will be published in the upcoming 3GPP releases. White papers from Qualcomm and Mediatek [58; 59] describe the technology behind the NR and its main use cases.

The authors in [60] offer a comprehensive overview of the state-of-the-art development of NR, including deployment scenarios, numerologies, frame structure, new waveform, multiple access, initial/random access procedure, and enhanced carrier aggregation (CA) for resource requests and data transmissions. Akdeniz and collaborators in [57] investigate the path loss in mmW bands. They see that their propagation models at both 28 and 73 GHz predict

path losses that are approximately 20 to 25 dB higher than the 3GPP model at 2.5 GHz. Self-healing has been addressed by quite a few research works until 4G. In 5G networks, it is still an unexplored area. The survey article in [61] provides a taxonomy of existing literature on self-healing. Challenges and prospective research directions for developing 5G self-healing solutions are also discussed. They identify that the most demanding challenges are the difficulty of meeting 5G low latency and the high quality of experience requirements. Researchers and network operators consider the failure of the backhaul results in the failure of the BS and there is a considerable work considering healing the network BSs [63; 64; 65].

The authors in [62] present a novel approach for mitigating fronthaul failures in CRAN networks using a new radio added to each BS in the network. They also utilized the cognitive radio concept to provide the needed resources to the new proposed radio. The only drawback here is that adding new radio to each BS in the network impractical except if it is included in the early stage of the new 5G standard.

3.2.3 The Proposed System Model

The system consists of 1 eNB which is considered as macrocell which could accommodate lower-priority/low rate communications over the 4G network. In addition, this macro eNB provides control plane (c-plane) connectivity to a set of $\mathcal{M}$ IAB-gNBs and also performs the radio resource assignment and management in an optimized control/data splitting dense urban network where the eNB provides the signaling service for the whole area and the gNBs provide the users with resources for high-rate transmission using 5G NR with a light control overhead.

It is worth noting that the gNB in 5G network is comparable to the eNB in LTE/4G network given that in our proposed model gNBs are considered as small cells where they are covering a circular area with radius no more than 30 meters. Operators in the U.S. including Verizon and AT&T are promising commercial services based on the NSA 5G New Radio (NR) specification by the end of 2018. These services will use the LTE radio access

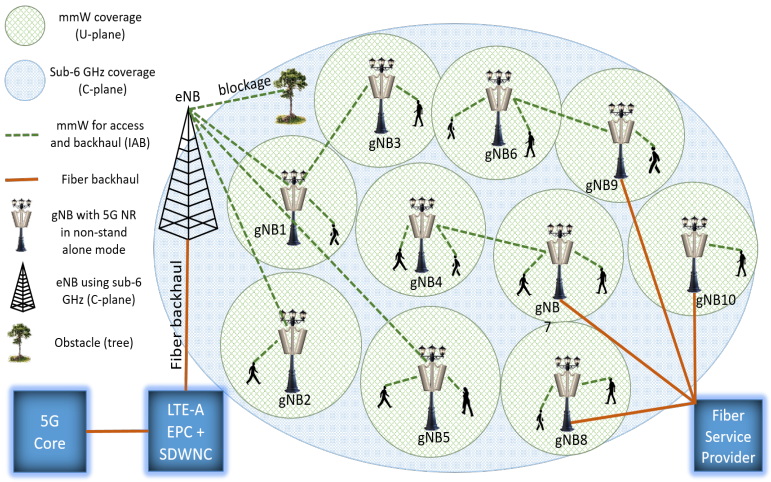

Figure 3.9: System model during normal operation.

and core network to control the users while the data plane is delivered by the 5G gNBs. The idea is that operators can leverage massive investments in LTE networks to rapidly commercialize 5G. The standalone variant of the 5G specification will operate in tandem with an LTE network. As such, a standalone 5G network will require new base stations, new backhaul mechanisms and a new core network.

Each gNB is equipped with a 5G NR which operates in the NSA mode where the LTE Evolved Packet Core (EPC) is used to supply the control plan to gNBs' users. This is controlled by the LTE eNB as the responsible of the control plane for its coverage area.

Fig. 3.9 shows the system model of an ultra dense 5G network. The gNBs are shown to be in the street level, however, they can be indoors or mounted on top of buildings. The eNB is responsible for the C-plane which is connected to the LTE EPC. Also, eNB provides backhaul links to nearby/Line of Site (LoS) gNBs using mmW. The gNBs can also be backhauled using fiber links wherever available. The gNBs are backhauled wired or wirelessly, however, we are considering the failure of the wireless links since the wired links (fiber) have five nines reliability which is much higher than that of the mmW links.

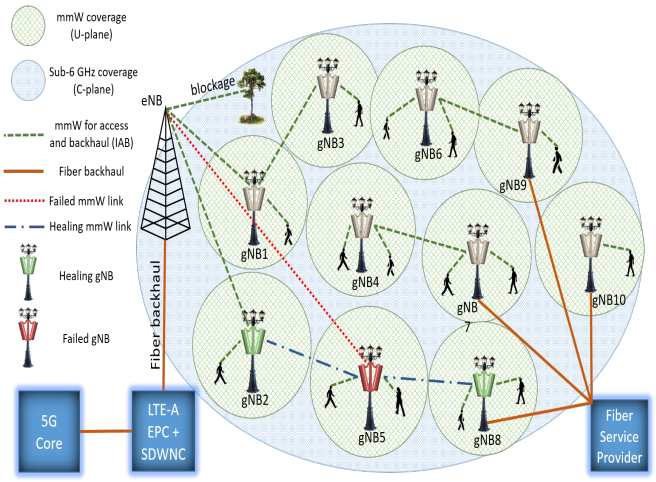

Figure 3.10: System model during one failure.

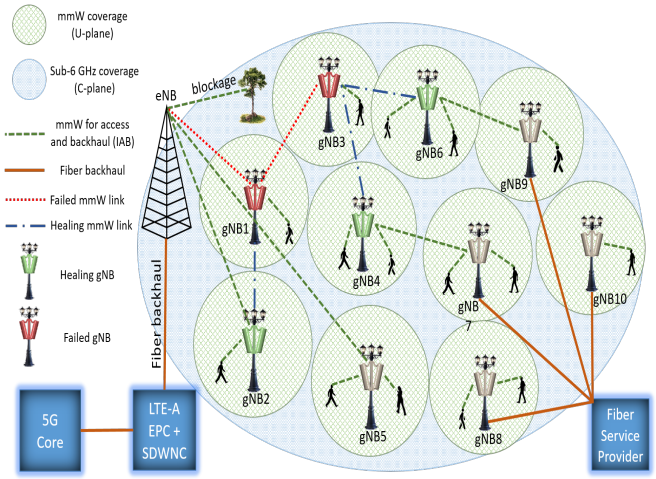

Figure 3.11: System model during multiple failures.

3.2.3.1 Backhaul Outage Compensation (BOC) Approach

The conventional and well known approach for BOC is to optimize the capacity and coverage of the outage zone by adjusting the antenna gain and transmission power of the neighboring BSs. The disadvantage of this approach is that it will degrade the performance of the users served by the neighboring BSs. Moreover, these BSs will consume considerable time (compared to 1 ms) to change their power and antenna tilt. Our proposed BOC approach will not change the antenna tilt or the power of the neighboring gNBs. We

propose to utilize the 5G NR and its IAB feature to provide the failed gNB with the needed backhaul connection from neighboring gNBs. When a failure occurs to the backhaul of any gNB, the failed gNB will acquire its backhaul connection from the neighboring gNBs utilizing the IAB feature supported by the NR. The neighboring gNBs will help the failed cell if it has available resources. These resources can be access or backhaul resources based on the IAB concept.

In case of failure, the BOC strategy will be activated by the controller/eNB. System repair, which will be done by the operator's maintenance personnel if needed, can typically be done within hours. In this case, the BOC approach will provide recovery that satisfies the minimum rate requirements in the failure region. After recovering the failed mmW link, switching back to normal operation is triggered by the co-located controller with the eNB. This controller is called Software Defined Wireless Network Controller (SDWNC). The SDWNC will reset all the backhaul connections to its original configuration, i.e., normal operation configuration.

Fig. 3.10 shows a scenario where the mmW backhaul between the eNB and gNB5 failed. This failure will result in a full outage to the users served by gNB5. Using the BOC approach, the eNB controller, i.e., SDWNC, will trigger gNB5's neighbors to provide portion of their access and/or backhaul resources to backhaul gNB5. This is subject to resources availability where a particular gNB may not be able to serve the failed gNB due to limitation of its resources which is used by its own users. In this case, gNB2 and gNB8 will provide the needed alternate backhaul connections to gNB5 in order to be able to serve its own users.

Figure 3.11 shows a more complicated scenario where the mmW backhaul between the eNB and gNB1 failed. Since gNB1 was relaying the backhaul of gNB3, then gNB3 backhaul will fail as well. This triggers a multiple failure situation, i.e., two failures in this particular scenario, which will be handled in the same way of healing a single failure except if we still cannot satisfy the users under the failed gNBs, in this case, the minimum requirement of

the users in the failed region will be lowered as it will be shown in the following section. From the figure, we can observe that gNB2 is healing gNB1 by providing the required backhauling, however, gNB4 and gNB6 are healing gNB3.

3.2.4 BOC Problem Formulation

In this section, we present the channel propagation model, the resource allocation and the data rate models.

3.2.4.1 Channel Propagation Model

We consider the alpha-beta channel model for modeling the access and backhaul mmW channels. The access channels are considered to be Non-Line-of-Site (NLoS) between the gNB and the users while the backhaul channels are considered to be LoS between different gNBs or between the gNB and the eNB. We adopt the alpha-beta model which is named also as floating intercept model. This channel model is determined by two parameters: slope α and intercept β which is estimated by least-squares linear regression. The floating intercept model can be used to characterize mmW channels in both LOS and NLOS environments. The alpha-beta 28 GHz pathloss model for LoS is given as follows [68]:

$$PL_{\mathrm{AB}}^{\mathrm{LoS}}(g_1, g_2, m) = \alpha^{\mathrm{LoS}} + \beta^{\mathrm{LoS}} log_{10}(d_{g_1,g_2}) + \chi_{\sigma}^{\mathrm{LoS}}(m) \tag{3.1}$$

The alpha-beta pathloss model for NLoS, i.e., $PL_{\mathrm{AB}}^{\mathrm{NLoS}}$, is given by [68]:

$$PL_{\mathrm{AB}}^{\mathrm{NLoS}}(g, u, m) = \alpha^{\mathrm{NLoS}} + \beta^{\mathrm{NLoS}} \log_{10}(d_{g,u}) + \chi_{\sigma}^{\mathrm{NLoS}}(m) \tag{3.2}$$

where d is the distance between the gNB and the user, in case of access links, or the gNB and the gNB, in case of backhaul links. The distance is measured in meters. $\chi_{\sigma}^{\mathrm{LoS}}$ and $\chi_{\sigma}^{\mathrm{NLoS}}$ are zero mean Gaussian random variables modeling the shadow fading factor with a standard deviation σ in dB for LoS and NLoS, respectively.

Taking into account shadowing fluctuations in addition to the pathloss, the channel gain, $\Gamma^m_{g_1,g_2}$ in dB between any two gNBs can be expressed as $\Gamma^m_{g_1,g_2} = -PL^{\text{LoS}}_{\text{AB}}(g_1, g_2, m)$ and the channel gain between a particular gNB g and its user u is given by $\Gamma^m_{g,u} = -PL^{\text{LoS}}_{\text{AB}}(g_1, g_2, m)$.

3.2.4.2 User Association, Resource Allocation and Data Rate

The SINR received at UE u from gNB g on sub-channel m is given by:

$$\gamma^m_{g,u} = \frac{p^m_{g,u}\Gamma^m_{g,u}}{\sum\limits_{\substack{j\in\mathcal{G}\\ j\neq g}}\sum\limits_{\substack{i\in\mathcal{U}\\ i\neq u}} p^m_{j,i}\Gamma^m_{j,u} + \sigma^2} \tag{3.3}$$

where $p^m_{g,u}$ is the downlink power from gNB g to UE u using sub-channel m, $\Gamma^m_{g,u}$ is the channel gain between gNB g and UE u using sub-channel m.

The SINR received at UE u from the failed gNB ξ on sub-channel m is given by:

$$\gamma^m_{\xi,u} = \frac{p^m_{\xi,u}\Gamma^m_{\xi,u}}{\sum\limits_{\substack{j\in\mathcal{G}\\ j\neq g}}\sum\limits_{\substack{i\in\mathcal{U}\\ i\neq u}} p^m_{j,i}\Gamma^m_{j,u} + \sigma^2} \tag{3.4}$$

The SINR received by the failed BS, ξ from neighboring BS, g, via 5G NR is given by:

$$\gamma^r_{g,\xi} = \frac{p^r_{g,\xi}\Gamma^r_{g,\xi}}{\sigma^2} \tag{3.5}$$

where $r + m$ is the total IAB resources and r is the resources dedicated to the backhaul . It is worth noting that frequency reuse/interference is not allowed when the failed BS and the neighboring gNB are communicating using 5G NR. This is why a dedicated band is assigned.

Accordingly, the achievable per sub-channel downlink rate from BS g to UE u is given by:

$$R^m_{g,u} = \log_2(1 + \gamma^m_{g,u}) \tag{3.6}$$

Similarly, the achievable per sub-channel downlink rate from the failed BS ξ to UE u is given by:

$$R^m_{\xi,u} = \log_2(1 + \gamma^m_{\xi,u}) \tag{3.7}$$

Finally, the achievable per sub-channel rate from the neighboring gNB to the failed gNB is given by:

$$R^r_{g,\xi} = \log_2(1 + \gamma^r_{g,\xi}) \tag{3.8}$$

Then, the downlink rate achieved by UE u served by gNB g is given by:

$$\hat{R}_{g,u} = x_{g,u} \sum_{m \in \mathcal{M}} R^m_{g,u} \tag{3.9}$$

where $x_{g,u}$ is a decision variable indicating the association of user u with gNB g.

The downlink rate achieved by UE u served by the failed gNB ξ is given by:

$$\hat{R}_{\xi,u} = x_{\xi,u} \sum_{m \in \mathcal{M}} R^m_{\xi,u} \tag{3.10}$$

The rate achieved by failed gNB ξ from neighboring gNB g is given by:

$$\hat{R}_{g,\xi} = \delta_{g,\xi} \sum_{m \in \mathcal{M}} R^m_{g,\xi} \tag{3.11}$$

3.2.5 Problem Formulation

3.2.5.1 Normal Operation Optimization Problem

This problem is aiming to find the resource allocation and gNB association for all users in normal operation (no failure).

$$(\mathbf{P1A}): \max_{p^m_{g,u},\Phi^m_{g,u},x_{g,u},\rho^N_R} \quad \rho^N_R \tag{3.12a}$$

subject to:

$$\rho^N_R \leq \sum_{g\in\mathcal{G}}\sum_{m\in\mathcal{M}} \log_2(1+\frac{p^m_{g,u}\Gamma^m_{g,u}}{\sum\limits_{\substack{j\in\mathcal{G}\\ j\neq g}}\sum\limits_{\substack{i\in\mathcal{U}\\ i\neq u}} p^m_{j,i}\Gamma^m_{j,u}+\sigma^2}) \ \forall u\in\mathcal{U} \tag{3.12b}$$

$$\rho^N_R \geq R^{\text{th}}_{\text{nor}} \tag{3.12c}$$

$$\sum_{g\in\mathcal{G}} x_{g,u} \leq 1 \qquad \forall \ \ u\in\mathcal{U} \tag{3.12d}$$

$$p^m_{g,u} \leq x_{g,u}\Phi^m_{g,u}\ p^{\max} \qquad \forall \ \ g\in\mathcal{G}, u\in\mathcal{U}, m\in\mathcal{M} \tag{3.12e}$$

$$\sum_{u\in\mathcal{U}}\sum_{m\in\mathcal{M}} p^m_{g,u} \leq P^{\max} \qquad \forall \ \ g\in\mathcal{G} \tag{3.12f}$$

$$p^m_{g,u} \geq 0 \qquad \forall \ \ g\in\mathcal{G}, u\in\mathcal{U}, m\in\mathcal{M} \tag{3.12g}$$

The objective function (3.12a) along with constraint (3.12c) formulate the well-known max-min objective function. Constraint (3.12d) guarantees that each user is associated with only one gNB. Moreover, constraint (3.12e) which integrates the association and resource allocation to the power, is used to simplify constraint (3.12c). In other words, if this constraint is not used, we have to replace each $p^m_{g,u}$ in constraint (3.12b) with $x_{g,u}*\Phi^m_{g,u}*p^m_{g,u}$, reader is referred to [69] in order to get more details by following how **P1** is transformed to **P2**. Constraint (3.12f) limit the maximum power that a gNB can transmit in the downlink. Finally, constraint (3.12g) set the lower limit on the downlink power transmitted from the gNB to a certain user over sub-channel m. This problem is the well-known 4G/5G resource allocation problem. It is solved in the literature (readers are referred to [70; 71; 72] for

detailed solution of this problem). **P1** is presented since the results of this problem will be used in **P2**.

3.2.6 Failure Operation Optimization Problem

In this problem, we are aiming to maximize the minimum rate of the network users. This is a weighted version of the well-known max-min problem which guarantee fairness among users. The optimization problem during failure is shown below.

$$(\mathbf{P1B}): \underset{(\Phi^m_{g,u}),(t^r_{g,\xi}),(\rho^F_R)}{\text{maximize}} \rho^F_R \tag{3.13a}$$

subject to:

$$\rho^F_R \leq \sum_{g\in\mathcal{G}\cup\xi}\sum_{m\in\mathcal{M}} \log_2(1+\frac{p^m_{g,u}\Gamma^m_{g,u}}{\sum\limits_{\substack{j\in\mathcal{G}\\ j\neq g}}\sum\limits_{\substack{i\in\mathcal{U}\\ i\neq u}} p^m_{j,i}\Gamma^m_{j,u}+\sigma^2}) \ \forall u\in\mathcal{U} \tag{3.13b}$$

$$\rho^N_R \geq R^{\text{th}} \tag{3.13c}$$

$$\alpha^r_{g,\xi} \geq \frac{\gamma^r_{g,\xi}-\beta^{\text{th}}_g}{Q} \qquad \forall \ \ g\in\mathcal{G} \tag{3.13d}$$

$$\alpha^r_{g,\xi} \leq \frac{\gamma^r_{g,\xi}}{\beta^{\text{th}}_g} \qquad \forall \ \ g\in\mathcal{G} \tag{3.13e}$$

$$t^r_{g,\xi} \leq \log_2(1+\frac{p^r_{g,\xi}\Gamma^r{}_{g,\xi}}{\sigma^2}) \qquad \forall g\in\mathcal{G} \tag{3.13f}$$

$$\frac{t^r_{g,\xi}}{Q} \leq \delta^r_{g,\xi} \qquad \forall g\in\mathcal{G} \tag{3.13g}$$

$$\delta^r_{g,\xi} \leq \alpha^r_{g,\xi} \qquad \forall \ \ g\in\mathcal{G} \tag{3.13h}$$

$$\sum_{g\in\mathcal{G}}\sum_{r\in\mathcal{R}} t^r_{g,\xi} \geq \varrho \sum_{u\in\mathcal{U}}\sum_{m\in\mathcal{M}} \log_2(1+\frac{p^m_{\xi,u}\Gamma^m_{\xi,u}}{\sum\limits_{\substack{j\in\mathcal{G}\\ j\neq\xi}}\sum\limits_{\substack{i\in\mathcal{U}\\ i\neq u}} p^m_{j,i}\Gamma^m_{j,u}+\sigma^2}) \tag{3.13i}$$

$$p^m_{g,u} \leq x_{g,u}\Phi^m_{g,u}p^{\max} \qquad \forall \ \ g\in\mathcal{G}\cup\xi, u\in\mathcal{U}, m\in\mathcal{M} \tag{3.13j}$$

$$p^r_{g,\xi} \leq \delta_{g,\xi}p^{\max} \qquad \forall \ \ g\in\mathcal{G}, r\in\mathcal{R} \tag{3.13k}$$

$$\sum_{u\in\mathcal{U}}\sum_{m\in\mathcal{M}} p^m_{g,u} + \sum_{m\in\mathcal{R}} p^r_{g,\xi} \leq P^{\max} \qquad \forall \ \ g\in\mathcal{G} \tag{3.13l}$$

Similar to (**P1A**), the objective function (3.13a) along with constraint (3.13b) formulate the well-known max-min objective function where we are aiming to maximize the minimum achievable rate of the network users including those users served by the failed gNB ξ. Constraint (3.13c) guarantees that the minimum achievable rate among the users is greater than a certain threshold R^{th}. Constraints (3.13d) and (3.13e) together decide which neighboring gNBs are able to heal the failed one. If the SINR between the failed gNB and the neighboring gNB is greater than a certain threshold, β_g^{th}, this neighboring gNB will be in the healing set. The decision variable $\alpha_{g,\xi}^r$, which indicates the healing set, is equal to 1 when the SINR between gNB g and the failed gNB ξ is greater than the threshold.

Constraints (3.13f)-(3.13i) are managing the backhaul healing links where $t_{g,\xi}^r$ is the traffic between the failed gNB, ξ, and the neighboring gNB, g given sub-channel r. Also, $\delta_{g,\xi}$ is a decision variable indicating that gNB g is going to heal failed gNB ξ. Constraint (3.13f) sets the upper bound on the traffic between gNB g and failed gNB ξ using sub-channel r where no interference allowed here since all neighboring gNBs. Constraints (3.13g) and (3.13h) set together the value of $\delta_{g,\xi}$ where the traffic will equal zero if $\delta_{g,\xi}^r$ equals to zero. Also, $\delta_{g,\xi}^r$ will equal to zero if $\alpha_{g,xi}^r$ equals to zero. Finally, constraint (3.13i) assure that the incoming backhaul traffic to the failed gNB is greater than or equal to the requested traffic from its users. Note that ϱ is a scaling factor between 0 and 1 used to limit/control the achievable rate of the users served by the failed gNB. This helps to cure infeasibility of the problem if constraint (3.13i) is not satisfied.

Constraint (3.13j) integrates the association and resource allocation to the power similar to constraint (3.12e) in Problem (**P1A**). For example, if the association binary variable equals to zero then the power will equal to zero. Constraint (3.13k) is the same as the last constraint but between a neighboring gNB g and the failed gNB ξ so if $delta_{g,xi}$ equals zero then the power will equal to zero. Finally, constraint (3.13l) sets the upper limit for the gNB maximum power for access and backhaul transmissions. **(P1B)** is a non-convex optimization problem due to the non-convex constraints (3.13b and 3.13i) and

actually is NP-hard due to the binary decision variables. Hence, the problem is intractable. Now, we will show the detailed procedures for converting constraint (3.13b) to a convex constraint. Since constraint (3.13i) will follow the same procedures, we will not show it here. Considering constraint (3.13b), note that the RHS can be written as a difference of two concave functions with respect to $p_{g,u}^m$. This can be rewritten as:

$$\begin{aligned}
\rho &\leq \sum_{\substack{j\in\mathcal{G}\cup\xi \\ j\neq g}} \sum_{m\in\mathcal{M}} \log_2(1+\frac{p_{g,u}^m \Gamma_{g,u}^m}{\sum\limits_{\substack{j\in\mathcal{G}\cup\xi \\ j\neq g}} \sum\limits_{\substack{i\in\mathcal{U} \\ i\neq u}} p_{j,i}^m \Gamma_{j,u}^m + \sigma^2}) \\
\rho &\leq \sum_{m\in\mathcal{M}} \log_2(\frac{\sum_{g\in\mathcal{G}} \sum_{u\in\mathcal{U}} p_{g,u}^m \Gamma_{g,u}^m + \sigma^2}{\sum\limits_{\substack{j\in\mathcal{G}\cup\xi \\ j\neq g}} \sum\limits_{\substack{i\in\mathcal{U} \\ i\neq u}} p_{j,i}^m \Gamma_{j,u}^m + \sigma^2}) \\
\rho &\leq \underbrace{\sum_{m\in\mathcal{M}} \log_2(\sum_{g\in\mathcal{G}} \sum_{u\in\mathcal{U}} p_{g,u}^m \Gamma_{g,u}^m)}_{\tilde{R}1} \\
&\quad \underbrace{- \sum_{m\in\mathcal{M}} \log_2(\sum_{\substack{j\in\mathcal{G}\cup\xi \\ j\neq g}} \sum_{\substack{i\in\mathcal{U} \\ i\neq u}} p_{j,i}^m \Gamma_{j,u}^m + \sigma^2)}_{\tilde{R}2}
\end{aligned} \tag{3.14}$$

To handle the non-convex constraint of (3.13b), we apply the successive convex optimization technique to approximate $\tilde{R}2$ with a convex function in each iteration. By defining $\tilde{R}(\{p_{g,u}^m\}) = \tilde{R}1(\{p_{g,u}^m\}) - \tilde{R}2(\{p_{g,u}^m\})$, we present the following Lemma:

Lemma 1: Given a feasible transmission power $\hat{p}_{g,u}^m$, there is a lower bound for $\tilde{R}\{p_{g,u}^m\}$ given by the following inequality:

$$\begin{aligned}
\tilde{R}\{p_{g,u}^m\} \geq & \tilde{R}(\{p_{g,u}^m\}, \{\hat{p}_{g,u}^m\}) \\
&= \tilde{R}1(\{p_{g,u}^m\}) - \sum_{m\in\mathcal{M}} \tilde{R}2(\{\hat{p}_{g,u}^m\}) \\
&\quad \underbrace{- \sum_{m\in\mathcal{M}} \langle \nabla \tilde{R}2(\{\hat{p}_{g,u}^m\}), \{p_{g,u}^m\} - \{\hat{p}_{g,u}^m\} \rangle}_{\tilde{R}2a}
\end{aligned} \tag{3.15}$$

where the term $\tilde{R}2a$ can be rewritten as:

$$\tilde{R}2a = \sum_{\substack{l\in\mathcal{G}\\ l\neq g}} \frac{\Gamma^m_{l,u}\log_2(e)}{\sum_{j\in\mathcal{G}}\sum\limits_{\substack{i\in\mathcal{U}\\ i\neq u}} p^m_{j,i}\Gamma^m_{j,u}+\sigma^2}\left(p^m_{g,u}-\hat{p}^m_{g,u}\right) \tag{3.16}$$

Proof: Since $\tilde{R}2$ is concave, based on the first order condition of a concave function, we have $\tilde{R}2(\{p^m_{g,u}\}) \leq \tilde{R}2(\{\hat{p}^m_{g,u}\}) + \langle \nabla\tilde{R}2(\{\hat{p}^m_{g,u}\}), \{p^m_{g,u}\} - \{\hat{p}^m_{g,u}\}\rangle$ at any given point $\{p^{\hat{m}}_{g,u}\}$. Thus, $\tilde{R}(\{p^m_{g,u}\}) \geq \tilde{R}(\{p^m_{g,u}\}, \{\hat{p}^m_{g,u}\})$. Moreover, if $\{p^m_{g,u}\} = \{\hat{p}^m_{g,u}\}$, there is $\tilde{R}(\{p^m_{g,u}\}) = \tilde{R}(\{p^m_{g,u}\}, \{\hat{p}^m_{g,u}\})$. So $\tilde{R}(\{p^m_{g,u}\}, \{\hat{p}^m_{g,u}\})$ provides a tight lower bound for function $\tilde{R}(\{p^m_{g,u}\})$ at $\{\hat{p}^m_{g,u}\}$. Obviously, the new approximated function $\tilde{R}(\{p^m_{g,u}\}, \{\hat{p}^m_{g,u}\})$ is a concave function.

After approximating constraint (3.13b), the problem is converted from maximizing the minimum rate to maximizing the minimum lower bound on the rate. This will lead to a sub-optimal solution to the original problem. The approximated constraint is given as:

$$\begin{aligned}\rho^F_R \leq & \sum_{m\in\mathcal{M}} \log_2\Big(\sum_{g\in\mathcal{G}}\sum_{u\in\mathcal{U}} p^m_{g,u}\Gamma^m_{g,u}+\sigma^2\Big)\\ & - \sum_{m\in\mathcal{M}} \log_2\Big(\sum_{\substack{j\in\mathcal{G}\cup\xi\\ j\neq g}}\sum_{\substack{i\in\mathcal{U}\\ i\neq u}} \hat{p}^m_{j,i}\Gamma^m_{j,u}+\sigma^2\Big)\\ & - \sum_{m\in\mathcal{M}}\sum_{\substack{l\in\mathcal{G}\\ l\neq g}} \frac{\Gamma^m_{l,u}\log_2(e)}{\sum\limits_{\substack{j\in\mathcal{G}\cup\xi\\ j\neq g}}\sum\limits_{\substack{i\in\mathcal{U}\\ i\neq u}} p^m_{j,i}\Gamma^m_{j,u}+\sigma^2}\left(p^m_{g,u}-\hat{p}^m_{g,u}\right)\end{aligned} \tag{3.17}$$

Using Lemma 1 and following the same approach for approximating constraint (3.13b), we can approximate constraints (3.13i) in the same way. The only remark is that the approximation will be done for the first log term. This is because constraint (3.13i) has the opposite inequality compared to constraint (3.13i). This will result in a convex optimization problem which can be solved efficiently.

3.2.6.1 System Model Assumptions

The proposed system model is considering the following assumptions:

- The eNB is always backhauled using fiber link (we assume its backhaul failure probability is 0).
- 5G NR dual connectivity feature is not adapted in our model.
- The user association will not change in the transition from the normal operation to the failure operation modes. In this case, we can use the user association provided from **P1A** in to **P1B**.
- We assumed that each user is only using one resource block when getting the optimal solution to simplify the problem and minimize the exhaustive search space.

3.2.7 Simulation Results

In this section, numerical results are provided to investigate the benefits of utilizing 5G NR and IAB technology in mitigating backhaul failures in 5G networks. The simulation model consists of 5 gNBs where one of them fails at a time. Extensive simulations for different failure scenarios have been conducted by varying the number of users in the network. Also, we use two Power Models (PMs) for evaluating our proposed scheme. The first power model (PM 1) considers the 5G NR total transmission power is shared between the access and backhaul transmissions. However, the second power model (PM 2) considers each one has its own maximum power.

The formulated optimization problem was solved using General Algebraic Modeling System (GAMS). GAMS is a high-level modeling system for mathematical programming and optimization. It is designed for modeling and solving linear, nonlinear, and mixed-integer optimization problems. It consists of a language compiler and integrated high-performance solvers. GAMS is tailored for complex, large scale modeling applications, and

allows to build large maintainable models that can be adapted quickly to new situations. The simulation parameters are shown in Table 4.2.

Table 3.1: Simulation Parameters

Parameter	Value	Parameter	Value
α^{LoS}	45.3 dB	α^{NLoS}	57.6
β^{LoS}	2.9 dB	β^{NLoS}	4.7
$\chi_{\sigma}^{\mathrm{LoS}}$	0.04 dB	$\chi_{\sigma}^{\mathrm{NLoS}}$	10
Carrier Frequency	28 GHz	σ^2	-87 dBm
$P^{\max}$	30 dBm	$p^{\max}$	20 dBm
R^{th}	1 Mbps	β^{th}	0.01
Q	1000	ϱ	0-1

We evaluate our BOC approach in terms of Degree of Recovery (DoR) from failure. The DoR is defined as the ratio between the recovered achievable rate and the normal operation achievable rate for the users associated with the failed gNB.

Fig. 3.12 shows the optimal solution of the optimization problem compared to the sub-optimal solution of the proposed approach. Note that the optimal solution was obtained using exhaustive this is why the scale of the problem was reduced to minimize the runtime of the exhaustive search. We present different scenarios where the number of gNBs and UEs is varied ranging from 3 to 4 and 5 to 8, respectively. It is obvious that the optimal solution is outperforming the proposed solution, however, the gap increases as the number of gNBs decrease or the number of UEs increases. For large-scale networks, the number of UEs served by a given gNB must be kept within a certain ratio in order to guarantee a realistic sub-optimal solution from the proposed approximation approach.

Fig. 3.13 and Fig. 3.14 show two different single failure scenarios. These scenarios are having 5 gNBs, however, the number of UEs is 8 in the first scenario and 16 in the second scenario. Also, two different power models are used in each scenario known as PM 1 and PM 2. Fig. 3.13 shows a scenario where we have 5 gNBs, one of them failed which is gNB 3. This failed gNB will acquire its healing backhaul connection from gNB 5. Although the

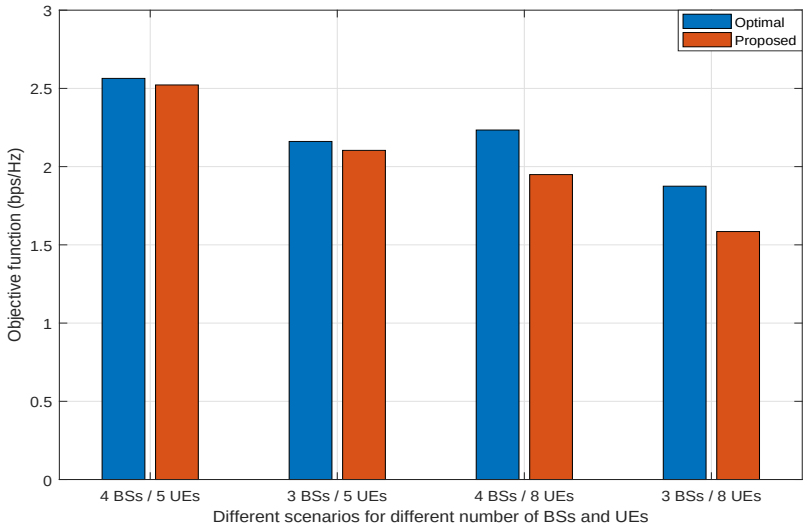

Figure 3.12: Optimal solution versus proposed model.

number of UEs is relatively small, the DoR is 501 % only and this is mainly because PM 1 is used.

In Fig. 3.14, although we are using PM 2, the degree of recovery is still low and this is because the IAB resources are limited and the number of UEs increased compared to the first scenario. In this case, the number of resources available for the backhaul healing process is limited. Note that both gNB 2 and gNB 5 are healing gNB 3. This can not be achieved if PM 2 is applied to this scenario since gNB 2 is serving 3 UEs where the remaining transmission power will not be sufficient to heal gNB 3.

Fig. 3.15 shows the DoR from failure when increasing the number of UEs in the network from 8 to 20. The lower set of curves represents the first power model (PM 1) where the total 5gG NR power is shared between access and backhaul transmissions. On the other hand, the upper set of curves represents the second power model where the power for access and backhaul transmissions is not shared. The reason for choosing this metric is that the proposed 5G NR considered PM 1 which appears to negatively affect the self-healing process. Note that as the number of UEs increases the DoR decreases. However, as the

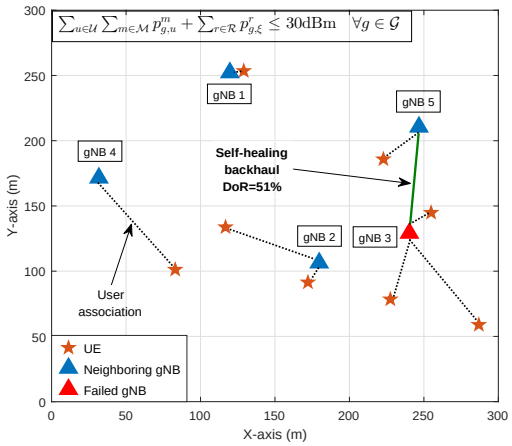

Figure 3.13: BOC scenario with gNB 3 failed and 8 UEs.

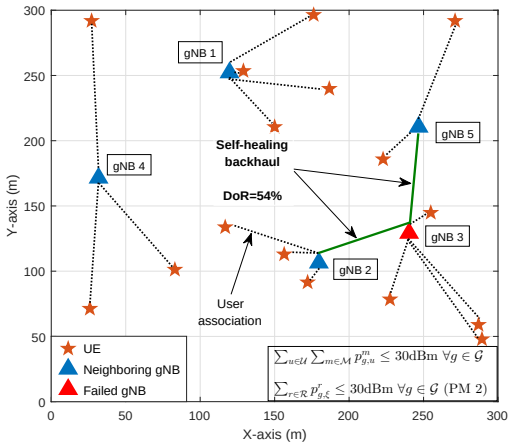

Figure 3.14: BOC scenario with gNB 3 failed and 16 UEs.

number of UEs approaches 16 and higher, the DoR is strongly degraded. This is mainly because the IAB resources are limited so when adding more UEs there are less resources for healing the failed backhaul. The superior performance achieved using PM 2 motivates the integration of this model in the upcoming 5G NR standard.

Table 3.2 shows results from the multiple failures scenario. We consider two gNBs concurrent failures and three gNBs concurrent failures. In the first scenario, the only infeasible case is when gNBs 1 and 4 fail. In this case, gNB 4 will not find any neighboring gNB to acquire its backhauling from. The other 5 cases each failed gNB successfully connected to at least on gNB and acquired its backhauling. The failure of gNBs 3 and 5 results in the least average DoR because gNB 1 which is healing gNB 5 is relatively far which results in high pathloss between them. The highest average DoR achieved when gNBs 3 and 4 failed. This is because gNB 3 is healed from 2 other gNBs.

On the other hand, the three gNBs concurrent failures scenario, where more than 50% of the network gNBs failed, is suffering from infeasibility. The reason for this feasibility is that the available resources and/or power are not sufficient to heal all failed gNBs. In addition, if only one gNB is not healed, the problem will turn out to be infeasible. In the

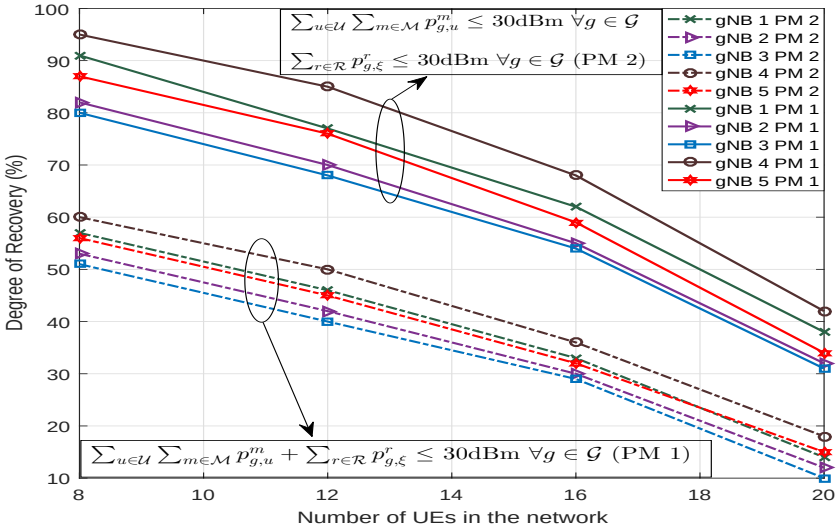

Figure 3.15: The gNB degree of recovery.

other 2 cases, the average DoR is very low and this is due to the concept of IAB where the access and backhaul resources are shared to be used to heal all the failed gNBs.

3.3 Chapter Summary

In the first part, we present the new technologies proposed for use by 5G networks. These technologies are CRAN, massive MIMO, mmW, SDWN, 5G NR, IAB, etc. Applying

Table 3.2: Multiple Failures Scenario.

Two concurrent failures			**Three concurrent failures**		
Failed gNBs	Healing gNB(s)	Avg. DoR	Failed gNBs	Healing gNB(s)	Avg. DoR
(1/2)	(4/3,5)	23.6 %	(1/2/3)	(4/5/5)	5.8 %
(1/3)	(4/2,5)	29.5 %	(1/2/4)	N/A	Infeasible
(1/4)	N/A	Infeasible %	(1/2/5)	N/A	Infeasible
(2/3)	(1/5)	24.5 %	(1/4/5)	N/A	Infeasible
(3/4)	(2,5/1)	31.1 %	(2/3/5)	N/A	Infeasible
(3/5)	(2/1)	16.6 %	(3/4/5)	((2/1/2))	7.1 %

all these and other technologies to 5G will increase the fronthauling load. We propose a scheme to guarantee a minimum throughput to 5G users in the presence of temporarily or permanently fronthaul failures. A novel pre-planned reactive cell outage compensation approach is presented to mitigate the fronthaul failure effects and its main concepts can be summarized as follows:

• Two tier CRAN architecture with SCs use mmW band for connecting their users, and macrocell uses traditional cellular bands for macrocell users access.

• SDWN implementation provides flexible network operation where the SDWNC, which is co-located in the cloud, monitors and implements the self-healing procedures and acts as a database for the macrocell to avoid spectrum sensing during the CR phase.

• Multiple failures scenario is complicated and always results in an obvious degradation in the DoR metric.

Performance was evaluated using system simulation and it shows that at least 20% of the fronthauling rate can be guaranteed during the fronthaul failure of any cell site type.

In the second part, we present the problem of backhauling failure for the 5G network which will consider the dense deployment of gNBs, i.e., 5G small cells, to increase network coverage and capacity. However, in order to install a large number of small cells, operators will face the challenge of backhauling their traffic to the core network in a cost-effective manner. Although, IAB using 5G NR is a promising solution to solve the dilemma of gNBs' backhauling, densifying the network will increase the probability of failure of these links. To cope with this problem, we formulated an optimization problem aiming to maximize the UEs' minimum rate during failures. We considered single and multiple failures when solving the optimization problem. The results show that the IAB is a promising solution, however, the power model for 5G NR must consider separating the transmission power for the access and backhaul traffic. Our proposed model can mitigate single and multiple failures up-to two concurrent failures at a time. More than two failures.

CHAPTER 4. SELF-HEALING BATTERY STARVED USERS USING ENERGY HARVESTING

4.1 Introduction and Motivation

RF Energy Harvesting (EH) techniques have recently been considered as alternative methods to power the next generation wireless networks, especially those using low-power such as Internet of Things (IoT) objects. RF EH has been used to power remote devices. For example, RF energy has been used to power individual nodes in a wireless sensor networks [73].

RF energy sources can be categorized into two categories [74]:

• Ambient RF: This RF energy is freely available. The frequency range of ambient RF transmission is 0.2-2.4 GHz, and this includes most of the radiations from domestic appliances, e.g., Television, Bluetooth, WiFi, mobile devices, in addition to different transmitting BSs.

• Dedicated RF: This on-demand supply generally has a relatively higher power density due to directional transmission, and it is used to recharge the nodes or mobile devices that require predictable and high amount of energy. As RF EH from dedicated RF sources is fully controllable, it is better suited for supporting applications with Quality-of-Service (QoS) constraints. Also, the harvester of this dedicated RF energy must pay for this dedicated service.

Delivering on-demand RF energy to the mobile devices is the same as giving Energy as a Service (EaaS) to them. In the next generation networks, the operator will be able to deliver energy via RF signals to the network users or even objects (i.e., Internet of Things

(IoT) objects). EaaS is a promising service that will have high demand in 5G networks due to the large number of connected devices and at anytime there will be a number of devices that their battery is starved and they need a supplementary amount of energy to survive.

Two EH protocols are used: time switching and power splitting. In time switching, the time slot is partitioned into an EH period and a communication period. In power splitting, however, a portion of the received signal is used for EH and the remaining signal will be used to extract the information from the received signal.

There are three EH and transmission schemes defined in the literature: 1) harvest-use-store, 2) harvest-store-use and 3) harvest-use. In the latter, the node uses the harvested energy without storing it for future use. In the harvest-use-store, the harvested energy is immediately used, then the remaining energy, if any, is stored. Finally, in harvest-store-use, the harvested energy is partially/fully stored before it is used. These three different schemes are used depending on the nature of the mobile device and the transmission requirements.

Mobile devices are now part of everyone daily life. These devices are not used only in calls or even daily communications, they are now used in sensitive applications/purposes such as wireless transactions (Samsung pay or Apple pay), home security, remotely controlling other devices and emergency calls. In certain critical situations, the mobile user cannot use his mobile device or particulary cannot initiate an emergency call due to a depleted battery, especially if the mobile user cannot charge his device using the regular wired/wireless charger. In this chapter, we consider the scenario of high density UEs in a small area where the users have no access to any power outlets. This scenario appears in games such as football, soccer or Olympic games where fans enter the stadium 2 or 3 hours before the game and stay there for another 2 or 3 hours.

Our proposed solution is to introduce a win-win situation where the user will be able to use his mobile device for an extended period of time and the operator will charge the mobile user for extending his battery life. The operator will offer this emergency service using a cooperative Self-healing of Users equipment by Rf Energy transfer (SURE) scheme.

This scheme will depend mainly on the nearby Base Stations (BSs) and Users Equipment (UEs) where all of them will dedicate RF energy to the battery starved user in order to be able to deliver enough energy for extending the battery life.

The procedures to implement the SURE scheme is that when a certain user has a very low battery level and needs to urgently use his UE for extended time, he will send a request to the network to extend the life time of his battery. The operator will start gathering the needed information from this target UE and the surrounding UEs (the cooperative UEs only) using Minimization of Drive Test (MDT) reports [76], these reports contain number of measurements measured by the UE itself. Then, the operator will decide which BSs and which cooperative UEs will be involved in the SURE scheme.

The MDT reporting schemes have been defined in LTE Release 10 specification [77]. The release proposes to construct a data base of MDT reports from the network using Immediate or Logged MDT reporting conguration. The release proposes to construct a data base of MDT reports from the network using Immediate and/or Logged MDT reports from UEs. Following are the key features of MDT: a) The ability of the UE to include location information as part of UE radio measurement reporting b) The ability of the UE to log radio measurements during the UEs idle state. The measurements including Reference Signal Received Power (RSRP) and quality of serving BS as well as of the three strongest neighboring BSs and the Channel Quality Indicator (CQI). These information are sent by the UE in a single vector $\mathcal{V}$ as follows:

$$\begin{aligned}\mathcal{V} =&[RSRP_s, RSRP_{n1}, RSRP_{n2}, RSRP_{n3}, RSRQ_s, \\ &RSRQ_{n1}, RSRQ_{n2}, RSRQ_{n3}, CQI, XYZ]\end{aligned} \tag{4.1}$$

where the subscripts s and n denote the serving and neighboring cells, respectively. RSRQ is the reference signal received quality and XYZ refers to the location of the UE.

The MDT report of the target UE will help the network to detect which BSs can be involved in the SURE scheme. However, the MDT reports received from the cooperative

users in the area will be used to determine which UEs will heal the target UE. The target UE will also relay his UL data to one of the healing UEs in order to minimize transmission power. This relay UE is chosen such that the transmission power of the target UE is minimized compared to sending his data directly to the serving BS given that the relay UE is much closer than the serving BS.

The remainder of this paper is organized as follows: Section II is the literature review of the previous work. In Section III, we explain the technical details of our proposed approach with a detailed description of the system model. In Section IV, the detailed formulation of the optimization problem is preseneted. Section V introduces three solvers which solve the exact formulated problem, a relaxed version of it and finally a linearized version of it. This is followed by Section VI which presented the simulation results of our SURE scheme. Finally, Section VII concludes our work.

4.2 The Proposed System Model

We consider a heterogeneous network with different BSs tiers (macrocells and small cells) in addition to two UE categories which are cooperative (agreed to cooperate in the healing process) and non cooperative UEs (regular UEs without any cooperation) in which macrocells are overlaid with uniformly distributed small cells and randomly located UEs. As can be seen in Fig. 4.1, the battery starved UE (in the center) has initiated a healing request to the network after sending his latest MDT report. The serving BS will communicate with the neighboring BSs to inform them to start the healing process. Also, the serving BS requests the MDT reports from the cooperative UEs located in the target UE's vicinity and depending on the position, compared to the target UE, and mobility, the serving BS will determine which UEs can heal the target UE. Finally, the target UE will harvest and aggregate the energy coming from all sources (different BS tiers and UEs tier). The healing process will continue until a certain metric is achieved such as threshold battery level or after the delivery of a predetermined amount of energy [78].

Fig. 4.2 shows one time slot of the target UE where the time switching technique is used so that the time slot is partitioned into tree portions to accommodate the EH period. The harvesting process is done in the first portion where the target UE first harvests from neighboring BSs and from a subset of the cooperative UEs. Then the target user begins its regular transmission with its serving BS (downlink and uplink). The downlink, as usual, is received from the serving BS. However, the uplink phase is done using relaying so that the target UE will relay its data to the nearest cooperative UE which will forward this data to the serving BS. This UL relying is implemented to minimize the uplink power consumption of the target UE [78].

4.2.1 Selection Criteria

The UEs involved in this cooperation approach must pre-register in the SURE scheme. Also, during the healing process, they must have sufficient energy in their batteries (if a cooperative UE does not have sufficient energy, it will be removed from the cooperative UE's list). Upon their cooperation and as an incentive, they are compensated by the network operator for their role in the healing process. In [75], the authors proved that cooperation schemes bring significant gains for both the operator and the cooperative users compared to a non cooperative scenario.

In SURE scheme, we introduce two selection criteria: 1) Selecting the BSs and UEs that will help the target UE to recharge its depleted battery. 2) Selecting the relay UE that will relay the target UE's UL data to minimize its battery consumption.

4.2.1.1 Selecting Cooperative UEs

The selection process can be done within the target UE's serving BS or a central control BS (i.e., macrocell). This selection process will return the BSs and UEs that are capable of transferring energy to the target UE. The cooperative BSs are chosen based on the target UE's MDT report where the three strongest neighboring BSs are chosen.

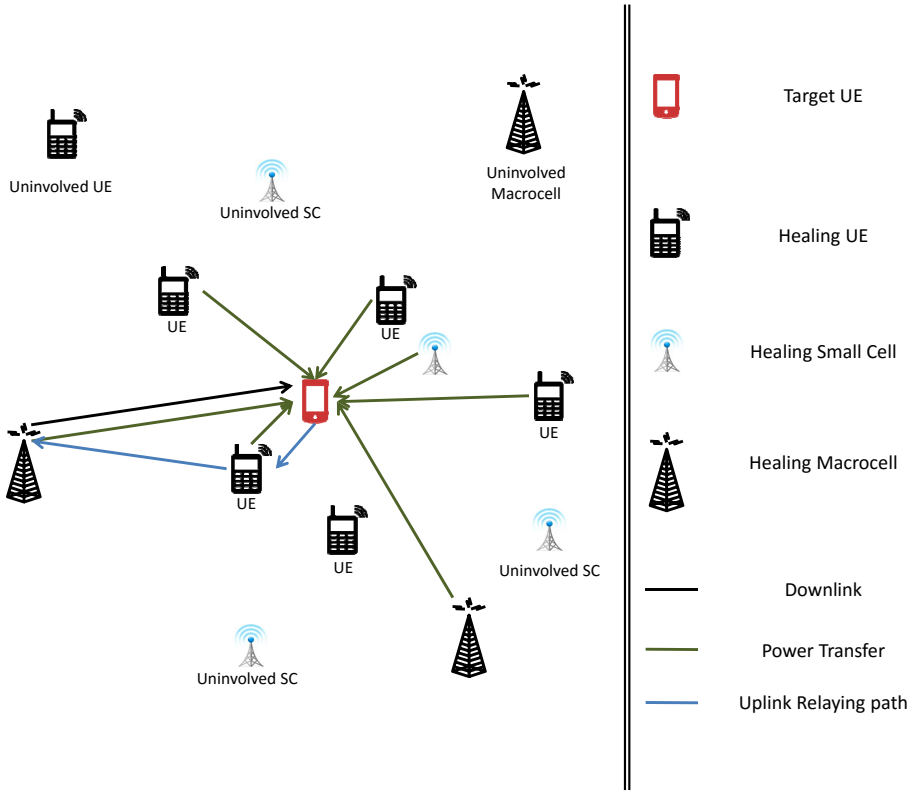

Figure 4.1: Healing the target UE using SURE scheme.

On the other hand, the selection criteria for the cooperative UEs is totally different than that of the BSs. This is because the MDT report does not include any mutual information between the target UE and the helping UEs. However, the location of each UE is known from its MDT reports.

In order for the target UE to harvest RF energy from cooperative UEs, the input power to the target UE must exceed a predesigned threshold to activate the EH electronic circuit [79]. Thus, to harvest RF energy, the target UE received power from its nearby UEs cannot be small, which means that these UEs must be within a certain region around the target UE. This region is called the EH Region (EHR). The EHR consists of circles with radii r_{h_u} centered at each cooperative UE, where r_{h_u} is given by [80]:

$$r_{h_u} = (\xi \frac{P_u}{V_{th}})^{1/\nu} \tag{4.2}$$

where $\xi \in (0,1]$ is the EH efficiency factor of UE, V_{th} is the EH threshold to activate the EH circuit, and ν is the path loss exponent in EH transmission. It should be noted that the transfer distance in EHRs is generally short, which results in line-of-sight power transfer. As such, ν is not necessarily the same as the path loss exponent in data link transmission [80]. Then if the target UE falls in the EHR of any nearby UE, then this UE is chosen as a helping UE in the healing process.

This selection process is done offline because all the needed information (locations and transmission power of UEs) are known. In a real implementation of the SURE scheme scenario, the location of each UE is known from the MDT report sent to the serving BS from each UE including the target UE. Then the central BS will calculate the distances between the target UE and all UEs that are willing to cooperate.

Eq. (4.2) is used to check if the target UE lies within the EHR of each UE. When this condition is satisfied, this UE is added to the cooperative UE's set. This set of cooperative UEs is supposed to heal the target UE through the EH process.

Figure 4.2: Time slot partitioning to include EH slot.

4.2.1.2 Selecting UL Relay UE

Harvesting energy from surrounding BSs and UEs is sufficient but will not guarantee continue service and extended life time for the target UE battery. This is why we are trying here to minimize the UL transmission power of the target UE by relaying its UL data to one of the cooperative UEs. These cooperative UEs are already in the target UE vicinity. Assuming that all helping UE has enough battery level, then the selected UE relay must provide the best data rate to the target UE. Also, it will minimize the target UE's UL transmit power because the target UE will send its UL data to the best relay UE instead of sending its UL data directly to the serving BS. This selection criterion is done online and it will be discussed in detail in Section III.

4.2.2 Target UE Channel Model

The target UE has a starved battery, and for this reason the target UE relays its data in the UL via one of the cooperative UEs to communicate with the serving BS. This will minimize the target UE's energy consumption which will help extend the battery life and will effectively help in the healing process. The relay UE is chosen online to maximize the transmission rate and minimize the UL power of the target UE.

There are two types of relays; Amplify-and-forward (AF) relays which retransmit the signal without decoding while decode-and-forward (DF) relays decode the received signal, encode the signal again, and transmit. Each of these two types has its advantages and disadvantages (for more details reader is referred to [81]).Our system model and formulation is based on the DF protocol. However, AF protocol is also applicable to our model.

The maximum rate of the DF protocol $R_o^t(DF)$ can be expressed as:

$$R_o^t(DF) = \min(R_{m,o}^t, R_{m,d}^t) \tag{4.3}$$

where $R_{m,o}^t$ is the data rate of the wireless link between the target UE and the relay UE, $R_{m,d}$ is the data rate of the wireless link between the relay UE and the serving BS. The equations for these rates are given by Eqs. (4.4) and (4.5), respectively:

$$R_{m,o}^t = \frac{1}{2}\log_2(1 + \frac{P_o^t|h_{m,o}^t|^2}{N_o}) \tag{4.4}$$

$$R_{m,d}^t = \frac{1}{2}\log_2(1 + \frac{P_m^t|h_{m,d}^t|^2}{N_o}) \tag{4.5}$$

where P_o^t is the UL power of the target UE in time slot t, P_m^t is the UL power of the relay UE in time slot t, $h_{m,o}^t$ is the channel gain between the target UE and the relay UE and $h_{m,d}^t$ is the channel gain between the relay UE and the serving BS and N_o is the noise power.

Also, AF protocol can be used instead of DF protocol in this case the target UE data rate $R_o^t(AF)$ will be given as follows [82]:

$$R_o^t(AF) = \frac{1}{2}\log_2(1 + \frac{P_o^t P_m|h_{m,o}^t|^2|h_{m,d}^t|^2}{N_o(P_o^t|h_{m,o}^t|^2 + P_m^t|h_{m,d}^t|^2 + N_o)}) \tag{4.6}$$

4.2.3 Energy Harvesting Model

Most of prior work assumed that the UEs can harvest the ambient energy received from all BSs. However, since wireless energy decays rapidly, as such, the received power from BSs located far away from the UE may be too low to be harvested by the UE. This can be overcome by using MDT reports to pre-determine the BSs and UEs that can effectively heal the target user. The stored energy in the target UE's battery at the end of time slot t is given as follows:

$$B^t = \max(0, B^{t-1} + E_h^t - E_c^t) \tag{4.7}$$

where B^{t-1} is the battery charge in the previous time slot, E_h^t is the harvested energy in time slot t, E_c^t is the consumed energy in the UL stage and is equal to $p_o^t T^{UL}$. The max operator used to make sure that the battery level at time t will never go to zero.

The target UE's total harvested energy during a certain time slot t E_h^t is defined as the total harvested energy from the BSs tier and from the UE tier. The E_h^t is given as follows:

$$E_h^t = T_H(\xi_1 \sum_{m=1}^{M} P_m^t |h_{m,o}|^2 + \xi_2 \sum_{k=1}^{K} P_{b_k}^t |h_{b_k,o}|^2) \tag{4.8}$$

where ξ_1 *and* ξ_2 are the EH efficiency factors of UEs and BSs, respectively. P_m^t is the transmit power of the m^{th} cooperative UE. $P_{b_k}^t$ is the transmit power of the k^{th} BS depending on the type of the BS (macrocell or SC).

4.3 Formulating The Optimization Problem

The objective of this section is to formulate an optimization problem that will maximize the target UE's UL rate while minimizing the UL power and satisfying the energy constraints, power constraints and decision variables constraints.

4.3.1 The Objective Function

The objective function as shown in Eq. (4.9) has two main terms; the fractional term which, in the numerator, maximizes the overall data rate of the target UE and, in the denominator, minimizes the total UL energy of the same UE. The second term is introduced to minimize the harvested energy. However, this minimization is constrained by achieving the target amount of energy (E^{target}) which the network operator is guaranteeing to the target UE. The objective function is given in Eq. (4.9).

$$\max_{\epsilon_m^t, P_o^t, u^t} \frac{\sum_{t=1}^{T}\sum_{m=1}^{M} \epsilon_m^t T^{UL} \min(R_{m,o}^t, R_{m,d}^t)}{\sum_{t=1}^{T} P_o^t \; T^{UL}} - \alpha \sum_{t=1}^{T} E_h^t u^t \tag{4.9}$$

where ϵ_i^t is a decision binary variable that is used to determine the relay UE that the target UE will depend on to relay his data to the serving BS in order to minimize his UL transmission power in each time slot t, T^{UL} is the uplink duration in each time slot, α is a scaling factor used to control the contribution of the second term to the objective function, given that $0 \leq \alpha \leq 1$, T is the total number of time slots and this number is constant within each SURE scheme, E_h^t is the harvested energy in time slot t, u_t is a decision binary variable used to terminate the EH process when the target UE harvests a certain amount of energy E^{target}.

4.3.2 Rate Constraint

A minimum rate must be guaranteed to the target UE. This rate is guaranteed because the objective function implicitly minimizes the target UE UL power. The rate constraint is given by Eq. (4.10)

$$\sum_{m=1}^{M} \epsilon_m^t \min(R_{m,o}^t, R_{m,d}^t) \geq R_{min} \tag{4.10}$$

where ϵ_m^t will equal to 0 for all m except for the relay UE where it will be equal to 1 (given that we have only one relay UE). Then, the rate between either the target UE and the relay UE or the relay UE and the serving BS must be greater than or equal to R_{min}.

4.3.3 Energy Constraints

In the optimization problem, we added two energy constraints; battery capacity constraint and energy causality constraint, as shown in the following subsections.

4.3.3.1 Battery Capacity Constraint

Although the target UE has a starved battery and this battery level is less than 10% of the maximum, we must guarantee that the harvested energy at each time slot plus the battery level at the previous time slot does not exceed the maximum. Referring to the time slot partitioning in Fig. 4.2, this constraint is considered to be evaluated after the harvesting duration and before any energy consumption either in the uplink or the downlink (considered at the boundary between T^H and T^D). This constraint is formulated as shown in Eq. (4.11).

$$B^{t-1} + E_h^t \leq B^{max}, \quad \forall\ t = 1, ..., T \tag{4.11}$$

where B^{t-1} is the target UE's battery level at the previous time slot and B^{max} is the maximum capacity of the target UE's battery.

4.3.3.2 Energy Causality Constraint

It is required that energy can not be consumed before it is harvested in each time slot which means that the consumed energy in uplink or downlink transmission or even consumed energy by the electronic devices must be less than or equal to the harvested energy in this time slot plus the battery charge at the previous time slot. Since the capacity of the battery is assumed to be finite,the harvested energy that can not be consumed in each slot will be stored in the battery for further use is constrained by Eq. (4.11). From the long term operation perspective, we obtain the energy causality constraint as shown in Eq. (4.12).

$$E_U^t + E_D^t + E_X \leq E_h^t + B^{t-1}, \quad \forall\ t = 1, ..., T \tag{4.12}$$

where E_U^t is the target UE's UL energy at time slot t, E_D^t is the target UE's DL energy at time slot t, E_X is the target UE's circuit consumed energy including energy dissipated in the electronic circuits and leakage energy.

4.3.4 Power Constraints

The power constraints in our formulation is simply an upper and lower limits on the target UE's UL power P_o^t in each time slot t. During the healing process, the upper limit of the target UE's UL power is set to P_{max}^{SH} where this limit is less than the upper limit in normal operation. This is because we are trying to minimize the power consumption of the target UE during the EH stage. Also, during the healing process the target UE relays its UL transmission to a relay UE, hence resulting in the target UE consuming much less power than sending the UL transmission directly to the serving BS, given that the relay UE is in the target UE's vicinity.

The upper and lower limits of the target UE's UL power are given in Eq. (4.13) and (4.14), respectively.

$$P_o^t \leq P_{max}^{SH}, \quad \forall\ t = 1, ..., T \tag{4.13}$$

$$P_o^t \geq P_{min}, \quad \forall\ t = 1, ..., T \tag{4.14}$$

where P_{min} is the lower limit of the target UE's UL power and this is the same during the SURE scheme or during the normal operation.

4.3.5 Decision Variables Constraints

In this formulation, we have two binary decision variables (ϵ_m^t and u^t). The former is used to choose the relay UE among the cooperative UEs. The latter is used to control the EH process. Following is a detailed explanation of the role of each decision variable.

4.3.5.1 Relay UE Decision Constraint

The relay UE selection is done online at each time slot t depending on which relay maximizes the target UE's rate. In each time slot, one UE is selected among the cooperative

UE's to relay the target UE's data to the serving BS. This selection is done by limiting the selected UEs to only one at each time slot t using Eq. (4.15).

$$\sum_{m=1}^{M} \epsilon_m^t \leq 1 \tag{4.15}$$

Then from the objective function (Eq. (4.9)), it is obvious that ϵ_m^t is used to select UE m which maximizes the target UE's UL rate.

4.3.5.2 Energy Harvesting Decision Constraint

The target UE's battery is starved and the network operator main task is to extend the life time of this UE's battery by supplying a certain amount of energy E^{target}. The EH process is done during T time slots. There are two possibilities during these T time slots. The first possibility is that the energy supplied to the target UE is less than E^{target}. This can be due to the shortage in cooperative UEs or BSs. In this case, the operator will re-initiate the healing process for another T time slots until providing the target energy to the starved UE.

The second possibility is that the operator supplied the target UE with E^{target} within T time slots. In this case and from the operator point of view, any additional supplied energy more than E^{target} is considered a waste of resources because the operator has to compensate the cooperative UEs for their exerted efforts in the healing process, in addition to the resources and energy consumed from the operator's network side. This is the motivation behind terminating the EH process after reaching a certain threshold (E^{target}).

This termination process is done with the aid of the binary decision variable u^t. This decision variable equals 1 as long as the harvested energy E_h^t did not exceed E^{target}. When it exceeds E^{target}, u^t is set to 0 and the whole harvesting process will terminate. Observe that when u^t goes to 0 it never goes to 1 again. This can be represented mathematically by Eqs. (4.16) and (4.17).

$$u^{t+1} \leq u^t, \quad \forall\, t = 1, ..., T \tag{4.16}$$

$$u^{t+1} \geq \frac{E^{target} - \sum_{i=1}^{J} E_h^i u^i}{K}, \quad \forall\ t = 1, ..., T, \quad \forall J = 1, ..., t, \tag{4.17}$$

where $\sum_{i=1}^{J} E_h^i u^i$ is the accumulated harvested energy at a certain time slot t given that J is from 1 until the current time slot t. K is a very large positive number used to limit the right hand side of Eq. (4.17) to be between -1 and 0 if $\sum_{i=1}^{J} E_h^i u^i$ is greater than E^{target} and between 0 and 1 if E^{target} is greater than $\sum_{i=1}^{J} E_h^i u^i$.

Eq. (4.16) is used to guarantee the following; if u^{t+1} goes to 0 it will never return back to 1 given that u^t has an initial value equals to 1. For example, if u^t equals to 1 then from Eq. (4.16), u^t in the following time slot $(u^t + 1)$ can take the values 0 or 1. However, if u^t equals to 0 then u^{t+1} cannot take any value except 0.

Eq. (4.17) is used to set u^{t+1} to 0 or 1 depending on the value of accumulated harvested energy $\sum_{i=1}^{J} E_h^i u^i$ and target threshold E^{target} at each time slot. If the accumulated harvested energy is less than E^{target} then the numerator of the left hand side will be positive and given that K is a very large positive number, then this value will be between 0 and 1. Because the right hand side u^t must be greater than or equal to the right hand side, then u^{t+1} is forced to be set to 1.

On the other hand, if the accumulated harvested energy is greater than E^{target} then the numerator of the right hand side will be negative and given that K is a very large number, then this value will be between -1 and 0. Because the left hand side u^t must be greater than or equal the right hand side, then u^{t+1} can be set to either 0 or 1. Recalling the last term in Eq. (4.9), this is equivalent to minimizing u^t. Although 0 or 1 are valid according to Eq. (4.17), u^{t+1} will be forced by the minimization pressure to be 0 and not 1. At this point, u^{t+1} goes to 0 and it will never go back to 1 again during the remaining time slot before the whole process is terminated by the aid of Eq. (4.16).

Although u^t is a decision variable, it has limited combinations due to its special nature. Given $T = 10$ and u^t as a binary variable, then normally u^t will have 2^{10} different combinations. However, in our unique formulation (if it goes to 0 it will never go to 1 again), u^t

has only 10 different combinations given that initially u^1 equals to 1 since the target UE is using the SURE scheme to harvest at least in the first time slot. For example, if E^{target} was reached in the 5^{th} time slot, then the final vector of u^t will be [1 1 1 1 1 0 0 0 0 0].

4.3.6 The Optimization Problem Formulation

BAsed on the above detailed derivation of the objective function and different constraints , the optimization problem for SURE scheme is given by:

$$\max_{\epsilon_m^t, P_o^t, u^t} \frac{\sum_{t=1}^{T}\sum_{m=1}^{M} \epsilon_m^t T^{UL} \min(R_{m,o}^t, R_{m,d}^t)}{\sum_{t=1}^{T} P_o^t \; T^{UL}} - \alpha \sum_{t=1}^{T} E_h^t u^t$$

subject to

$$\sum_{m=1}^{M} \epsilon_m^t \min(R_{m,o}^t, R_{m,d}^t) \geq R_{min}, \quad \forall\, t = 1, ..., T,$$

$$B^{t-1} + E_h^t \leq B^{max}, \quad \forall\, t = 1, ..., T,$$

$$E_U^t + E_D^t + E_X \leq E_h^t + B^{t-1}, \quad \forall\, t = 1, ..., T,$$

$$P_o^t \leq P_{max}^{SH}, \quad \forall\, t = 1, ..., T$$

$$P_o^t \geq P_{min}, \quad \forall\, t = 1, ..., T$$

$$\sum_{m=1}^{M} \epsilon_m^t \leq 1, \quad \forall\, t = 1, ..., T$$

$$u^t \geq u^{t+1}, \quad \forall\, t = 1, ..., T$$

$$u^t \geq \frac{E^{target} - \sum_{i=1}^{J} E_h^i u^i}{K}, \quad \forall\, t = 1, ..., T, \quad \forall J = 1, ..., t$$

$$u^t \;\epsilon\; \{0, 1\}, \quad \forall\, t = 1, ..., T$$

$$\epsilon_m^t \;\epsilon\; \{0, 1\}, \quad \forall\, t = 1, ..., T, \quad \forall m = 1, ..., M$$

The formulated optimization problem is Mixed-Integer Nonlinear Programming (MINLP), non-convex and NP-hard due to the binary decision variables (ϵ_m^t and u^t) and the continues variable P_o^t in addition to the nonlinearity in the objective function and constraints.

4.4 The Proposed Solutions

Non-convex nonlinear functions as imposed by discrete variables easily lead to problems that are NP-hard in theory and computationally demanding in practice. Solving the aforementioned optimization problem is hard and this is why we will try to solve the problem heuristically. Three approaches (solvers) are used to solve this problem: 1) Basic Open-source Nonlinear Mixed Integer Programming (BONMIN) 2) Solving Constraint Integer Programs (SCIP) 3) Interior Point OPTimizer (IPOPT). All these solvers are integrated in General Algebraic Modeling System (GAMS). For more details about GAMS and its solvers: *https://www.gams.com/*.

GAMS is a high-level modeling system for mathematical programming and optimization. It is designed for modeling and solving linear, nonlinear, and mixed-integer optimization problems. It consists of a language compiler and integrated high-performance solvers. GAMS is tailored for complex, large scale modeling applications, and allows to build large maintainable models that can be adapted quickly to new situations.

Both BONMIN and SCIP linearize the MINLP before solving which results in Mixed Integer Linear Problem (MILP). However, to solve the problem with IPOPT, we relax the decision variables of the MINLP resulting in Non Linear Problem (NLP).

4.4.1 Linearization of The Problem

The non-linearity of the original optimization problem appears in the objective function Eq. (4.9) and the rate constraint Eq. (4.10). Linearizing the objective function requires first eliminating the "min" operator. To do that we will introduce a new variable R_x to the objective function and add two more constraints as shown in Eq. (4.18) , Eq. (4.19) and Eq. (4.20) , respectively.

$$\max_{\epsilon_m^t, P_o^t, u^t} \frac{\sum_{t=1}^{T}\sum_{m=1}^{M}\epsilon_m^t T^{UL} R_x^t}{\sum_{t=1}^{T} P_o^t \; T^{UL}} - \alpha \sum_{t=1}^{T} E_h^t u^t \tag{4.18}$$

$$R_x^t \leq R_{m,o}^t \tag{4.19}$$

$$R_x^t \leq R_{m,d}^t \tag{4.20}$$

The same approach will be used with the rate constraint Eq. (4.10) to eliminate the "min" operator which will result in 2 new constraints. Then the linearization step is done within each solver where the logarithmic function is linearized using piecewise approximation. Following is the explanation for each linearization solver.

4.4.1.1 BONMIN Solver

BONMIN is an open-source solver for MINLPs [84]. BONMIN can handle MINLP models and it implements 3 different algorithms for solving MINLPs: a) B-BB (default): a simple branch-and-bound algorithm based on solving a continuous linear program at each node of the search tree and branching on integer variables which is based on spatial branch and bound sBB b) B-OA: an outer-approximation based decomposition algorithm based on iterating solving and improving of a MIP relaxation c) B-QG: an outer-approximation based branch-and-cut algorithm based on solving a continuous linear program at each node of the search tree. In our simulation, we used the first algorithm.

As BONMIN is an exact solver only for convex problems, but taking into consideration that the values of the heuristic solutions obtained using this approach are usually very close to the optimal ones.

A linearization step allows obtaining a linear programming relaxation of the main problem, which can be easily embedded in the sBB Algorithm. It is worth to mention that if the branching can be done over a binary variable or a continuous variable, the algorithm chooses the binary variable. The main difference between sBB with a usual BB algorithm for solving MILPs is that branching might occur on a continuous variable. It also uses a

linear outer-approximation of the nonlinear problem for bounding purposes. The detailed description of the sBB algorithm can be found in [85].

4.4.1.2 SCIP Solver

SCIP includes capabilities to handle nonlinear functions that are specified via algebraic expressions. Similar to BONMIN, MINLPs are solved via an sBB algorithm using linear relaxations. The tightness of this relaxation depends heavily on the variable bounds, thus tight bounds for the nonlinear variables are crucial for SCIP. However, SCIP uses sBB based on a linear outer-approximation, which is computed by a reformulation of the MINLP [86].

4.4.2 Relaxation of The Problem

Although the linearization is done automatically inside the solver (BONMIN or SCIP), the decision variables relaxation must be done manually before solving the problem using any NLP solver. Relaxation arises by replacing the binary constraints by weaker constraints, that each variable belongs to the interval [0,1]. This relaxation will be applied to the two binary variables in our problem (ϵ_m^t and u^t) where after relaxation they will be bounded as follows:

$$0 \leq \epsilon_m^t \leq 1$$

$$0 \leq u^t \leq 1$$

After solving the relaxed NLP version of the original MINLP, the relaxed variables are rounded up to 1 or down to 0 depending on a certain threshold (0.5 in most cases) to return back to its binary nature, taking into consideration the constraints satisfaction, and then the objective function is evaluated.

4.4.2.1 IPOPT Solver

IPOPT is a software library for large scale nonlinear optimization of continuous systems. IPOPT implements a primal-dual interior point method, and uses line searches based on

Filter methods. It tries to minimize the gap between the primal and dual solution of the NLP problem (reader is referred to [87] for more details regarding the IPOPT solver). Since IPOPT is not a MINLP solver, the relaxation and rounding are done manually before and after running IPOPT where the manual relaxation converts our original MINLP into NLP and then the rounding step is done after IPOPT returned the solution and before doing the evaluation of the objective function.

4.5 Simulation Results

Table 4.1: Simulation Parameters (Section 4.5)

Parameter	Value
Macrocell maximum power	43 dBm
SCs maximum power	30 dBm
UE max power	23 dBm
P_{max}^{SH}	20 dBm
R_{min}	20 b/s/Hz
B^{max}	40 KJ
$B^{initial}$	2 KJ
Target UE's battery charge	2.915 Ah
Target UE's battery voltage	3.82
E^{target}	8.5 KJ
E_X	50 J
Total number of macrocells	1
Total number of SCs	3
Total number of UEs	12
T	10
T^{UL}	$\frac{1}{3}$ time slot
T^{H}	$\frac{1}{3}$ time slot
N_o	-174 dBm/Hz
ξ	0.5
K	100000
α	0.01

In this section, numerical results are presented to prove the validity of the proposed SURE model to heal the energy starved users. The formulated optimization problem was solved using GAMS. GAMS is connected to a group of third-party optimization solvers. Among these solvers, three are used to solve our optimization problem which are: BONMIN, SCIP and IPOPT. The simulation parameters are shown in Table II.

4.5.1 Offline Cooperative UEs Selection

In our simulation model, the UEs and different types of BSs are distributed using PPP. Then the distance between the target UE and all other UEs is calculated via the central BS. Using Eq. (4.2), a UE is selected as a cooperative UE if the target UE lies in its EHR.

According to the locations of the UEs distributed randomly except the target UE which is located at the orgin, an average of 8 cooperative UEs are selected from set of 12 UE. This average number of cooperative UEs is considered high due to the high density distribution of the UEs in limited space according to the proposed scenario. However, this scenario is realistic in the anticipated high dense 5G networks or in 4G networks in special high dense events such as Olympic games or football matches.

4.5.2 Online Relay UE Selection

Table 5.1 shows an example for ϵ_m^t, where m=8 and T=10, from our simulation to show that relay UE is changing from one time slot to the other. Also, a relay can be chosen in two different or successive time slots such as relay UE 1 and UE 3. A relay UE may not be chosen at anytime slot such as relay UE 4 and UE 7.

4.5.3 Harvested Energy

4.5.3.1 Target UE's Harvested Energy

The harvested energy during the SURE scheme depends mainly on the number of cooperative UEs and BSs. Fig. 4.3 shows the target UE's harvested energy versus time for

Table 4.2: Relay UE online assignment for m=8 and T=10

ϵ_m^t	t=1	t=2	t=3	t=4	t=5	t=6	t=7	t=8	t=9	t=10
ϵ_1^t	0	1	0	0	0	0	0	1	0	0
ϵ_2^t	1	0	1	0	0	0	0	0	0	0
ϵ_3^t	0	0	0	0	1	1	0	0	0	0
ϵ_4^t	0	0	0	0	0	0	0	0	0	0
ϵ_5^t	0	0	0	0	0	0	1	0	1	0
ϵ_6^t	0	0	0	0	0	0	0	0	0	1
ϵ_7^t	0	0	0	0	0	0	0	0	0	0
ϵ_8^t	0	0	0	1	0	0	0	0	0	0

different numbers of cooperative UEs and BSs. It is assumed that the target UE's battery initially holds only 5%(2 KJ) of its full battery level B^{max}. This explains why the starting point of the vertical axis is above 2 KJ. Also, all cooperative UEs and BSs are set to transmit using their maximum power. This configuration is used here to show the maximum energy that can be delivered to the target UE.

It is clear from the figure that as the number of cooperative UEs and/or BSs increases, the harvested energy increases. Because the BSs' (macrocells or small cells) transmission power is much greater than the UEs' transmission power, increasing the number of cooperative BSs (maximum k=4), the harvested energy, at the target UE, increases with higher rate than increasing the number of cooperative UEs. This appears clearly by comparing the set of green curves (k=4) with the other two sets (beside the cooperative UEs, one set has 1 BS and the other has no BSs). Moreover, For m=8 UEs and k=4 BSs, the green curve achieve the target energy threshold (E^{target}) at t=8 mins, then it remains constant because in this case the harvested energy will be greater than E^{target} and u^t will go to 0 and the harvesting process will be forced to terminate.

For (m=4 UEs and k=1 BS) and (m=8 UEs and k=0 BSs), these two curves (the intersecting blue and brown curves) give an indication that harvesting from 1 BS is equivalent to harvesting from 4 UEs, taking into consideration that the cooperative UEs are much closer

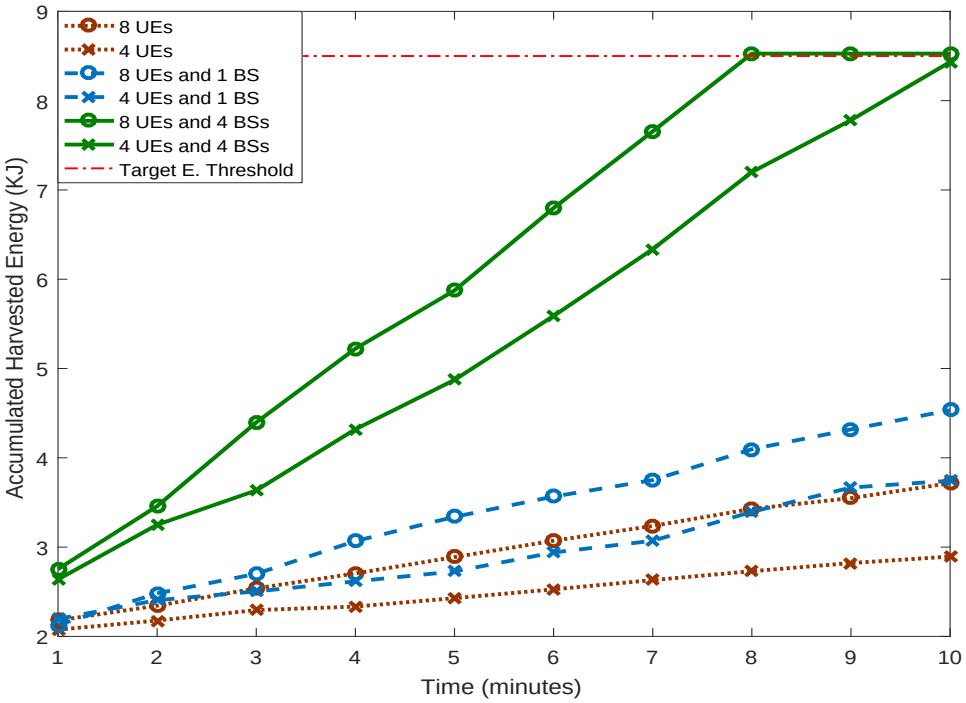

Figure 4.3: Harvested Energy Versus Time

to the target UE than any BS. For m=8 UEs and k=0 BSs, the cooperative UEs can supply the target UE with almost double its initial battery level without the help of any BS.

4.5.3.2 Cooperative UEs Energy Consumption

Cooperative UEs are giving away a portion of their battery energy for being involved in the SURE scheme and in return they are rewarded/compensated from the network operator which results in a win-win situation. The operator must decide how many cooperative UEs are required to start any SURE scheme and how much energy they will give away. Fig. 4.4. (a) shows the consumed energy from each cooperative UE's battery when the number of cooperative UEs range from 2 to 8. As it is shown in the figure, as the number of UEs increases the consumed energy from each cooperative UE decreases. For m=8 UEs, almost all UEs have the same energy consumption. The differences in energy consumption appear because each time slot a cooperative UE is chosen to relay the target UE's data.

Fig. 4.4. (b) shows the amount of harvested energy at the target UE from the cooperative UEs only. It is obvious that as the number of cooperative UEs increases the amount of harvested energy at the target UE increases. By looking at Fig. 4.4. (a) and (b), we can see that having only 2 cooperative UEs is not a good choice to start the SURE scheme. At least 4 cooperative UEs are required (beside the cooperative BSs) to start the SURE scheme.

4.5.4 Energy Efficient and Sum Rate

After solving the optimization problem, the energy efficiency and sum rate equations are defined as in Eq. (4.21) and Eq. (4.22), respectively.

$$\sum_{t=1}^{T}\sum_{m=1}^{M}\epsilon_m^t \min(R_{m,o}^t, R_{m,d}^t) \tag{4.21}$$

$$\frac{\sum_{t=1}^{T}\sum_{m=1}^{M}\epsilon_m^t T^{UL}\min(R_{m,o}^t, R_{m,d}^t)}{\sum_{t=1}^{T} P_o^t\ T^{UL}} \tag{4.22}$$

where $R_{m,o}^t$ and $R_{m,d}^t$ are defined in Eq. (4.4) and Eq. (4.5), respectively, and the energy efficient equation is simply the sum rate over the total target UE's UL energy.

In Fig. 4.5, the sum rate and energy efficiency are presented using three different solvers; IPOPT (solving relaxed NLP), SCIP and BONMIN (both solving linearized MIP). Fig. 4.5. (a) shows the energy efficient versus the number of cooperative UEs. BONMIN solver has the highest values among the other two solvers (the zoomed sub figure shows that BONMIN is higher than SCIP). However, comparing BONMIN and SCIP with IPOPT shows that IPOPT has very poor energy efficiency values. Moreover, BONMIN is the best to satisfy the shown tradoff. This gives an indication that solving the MINLP using linearization (MILP) is much better than solving it using relaxation of the decision variables (NLP).

Fig. 4.5. (b) shows the target UE's UL sum rate when changing the number of cooperative UEs from 2 to 8. By increasing the number of cooperative UEs, the sum rate increases because the target UE will have more UE choices from which the target UE can choose the

best UE's channel conditions to relay his UL data. Although the sum rate of IPOPT is the best among the other two solver, it has the poorest energy efficient values which indicates that the target UE's UL power is very high in this case. From Fig 4.5. (a) and (b) it can be inferred that BONMIN is the best solver for this problem where it has the best energy efficient values and its sum rate is higher than that of the SCIP solver.

4.6 Chapter Summary

The growing number of wireless transmitters naturally results in increased Radio Frequency (RF) power density and availability. On demand energy transfer will be universally present over an ever-increasing range of frequencies and power levels, especially in highly populated urban areas. In this chapter, a novel scheme named Self-healing of Users equipment by Rf Energy transfer (SURE) proposed to heal battery starved users using on demand RF energy transfer. We formulated a Mixed Integer Non Linear Programming (MINLP) optimization problem for the SURE scheme to maximize the sum rate and meanwhile minimize the UL power of the target UE. The formulated problem belongs to MINLP that is hard to solve directly. To achieve better scalability, we used three different heuristic algorithms to solve the problem named Interior Point OPTimizer (IPOPT), Solving Constraint Integer Programs (SCIP) and Basic Open-source Nonlinear Mixed Integer Programming (BONMIN). The simulation results show that BONMIN is the best solver for this problem. Also, it is recommended that the SURE scheme starts with at least four cooperative UEs beside the cooperative BSs in order to charge the target UE's battery with 5% (at least) of its full capacity.

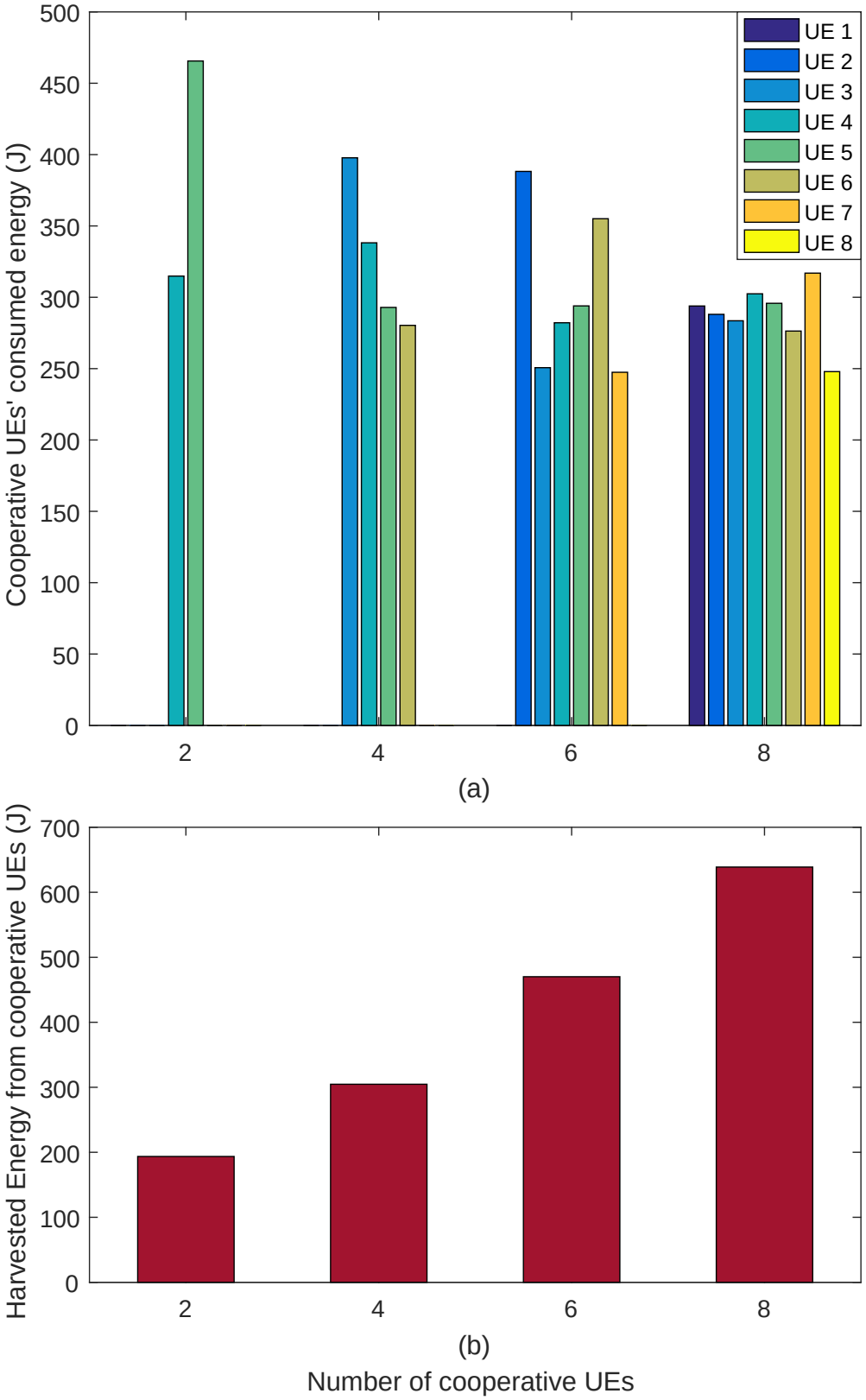

Figure 4.4: (a) Cooperative UEs' consumed energy versus number of cooperative UEs (b) Target UE's harvested energy versus number of cooperative UEs

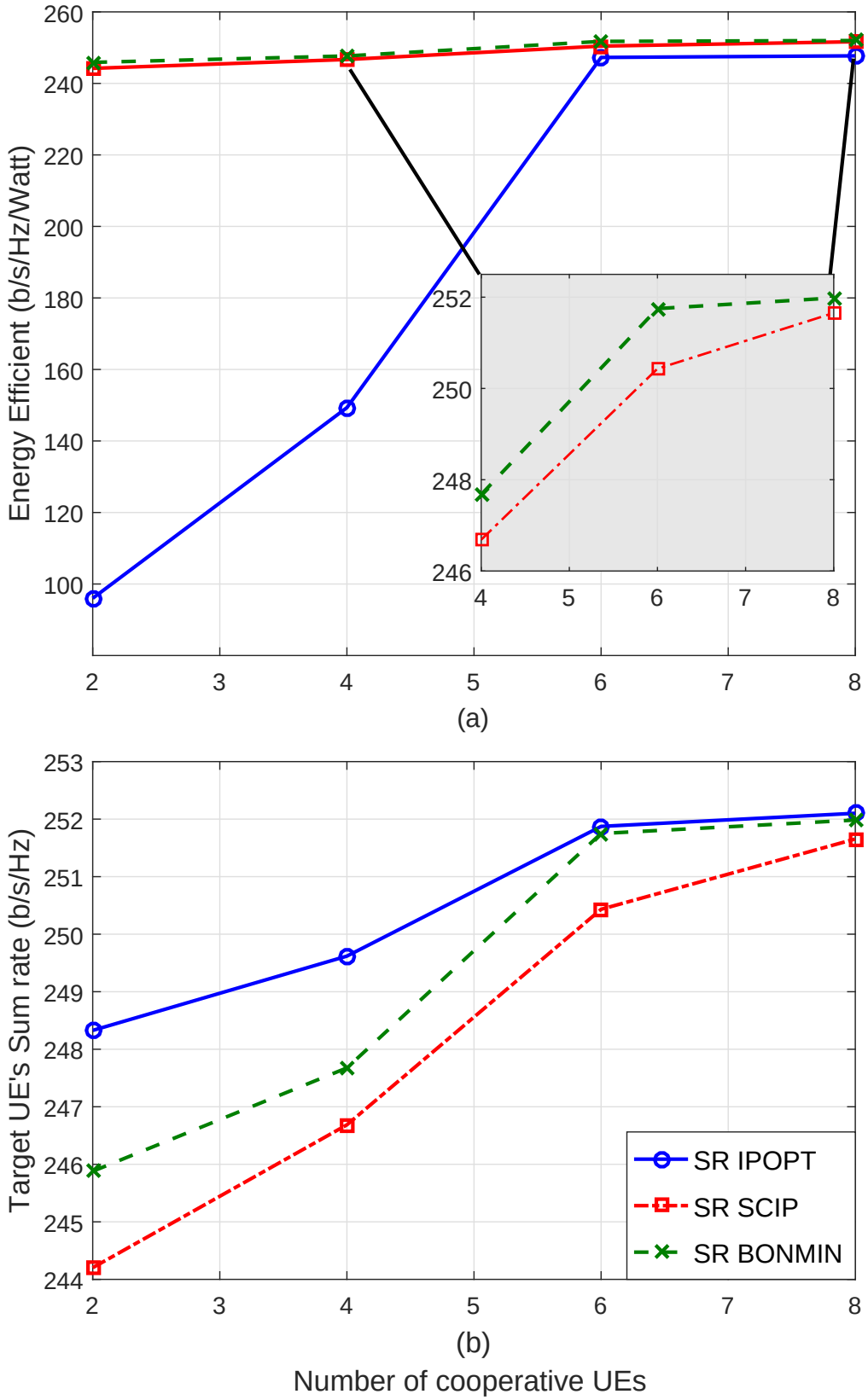

Figure 4.5: (a) Target UE's energy efficient versus number of cooperative UEs (b) Target UE's sum rate versus number of cooperative UEs

CHAPTER 5. CELL OUTAGE COMPENSATION IN 5G USING UAVS

In this chapter a number of cell outage compensation frameworks for 4G/5G network supported by dynamic Drone Base-stations (DBSs) is proposed.

In the first framework, we present a novel cell outage compensation (COC) framework to mitigate the effect of the failure of any outdoor Base Station (BS) in 5G networks. Within our framework, the outage compensation is done with the assistance of sky BSs (UAVs) and Ground BSs (GBSs). An optimization problem is formulated to jointly minimize the energy of the Drone BSs (DBSs) and GBSs involved in the healing process which accordingly will minimize the number of DBSs and determine their optimal 2D positions. In addition, the DBSs will mainly heal the users that the GBS cannot heal due to capacity issues. Simulation results show that the proposed hybrid approach outperforms the conventional COC approach. Moreover, all users receive the minimum quality of service in addition to minimizing the UAVs' consumed energy.

In the second framework, we propose to use drones or helikites to mitigate GBS failures based on the type and duration of the failure. Our proposed short-term and long-term cell outage compensation framework aims to mitigate the effect of the failure of any GBS in 5G networks. Within our framework, outage compensation is done with the assistance of sky BSs (UAVs). An optimization problem is formulated to jointly minimize communication power of the UAVs and maximize the minimum rates of the Users' Equipment (UEs) affected by the failure. Also, the optimal placement of the UAVs is determined. Simulation results show that the proposed framework guarantees the minimum quality of service for each UE.

5.1 Hybrid Cell Outage Compensation: Sky-Ground Approach

5.1.1 Introduction

Unmanned aerial vehicles (UAVs) enabled communications have attracted considerable attention recently due to the inherent agility [88]. On demand UAVs can rapidly provide network access to be used in various applications. As reported by AIAA (www.aiaa.org), the global market for commercial UAV applications will skyrocket to as much as 127 billion dollars by 2020. UAVs are gaining increasing popularity in Information Technology (IT) applications due to their high flexibility for on-demand deployments. According to Nokia (www.nokia.com), in May 2016, they launched a rapidly deployable 4G solution that can be carried by drones to provide connectivity at high-traffic events. Also, project Loon by Google (www.google.com/loon) provided internet access worldwide by leveraging the UAV technology.

In particular, employing UAVs as aerial Base-Stations (BSs) is envisioned as a promising solution to tackle the challenges facing the existing 4G, and forthcoming 5G networks. One of the main challenges facing these networks is the failure of BSs and how to self-heal or mitigate this failure in an autonomous way [6; 19].

Drones are a special type of UAVs that are popular for remote sensing and surveillance. Recently drones were used by Nokia to provide connectivity to smart cities (www.nokia.com). Although drones are very popular in UAV-based communications, there are other types of UAVs which are strong candidates to be used as flying Base-Stations (BSs) in 5G. The most relevant and well-known UAV types are [100]:

•**Drones**: are a special type of UAVs that are used in many applications nowadays and they are gaining increasing popularity in information technology applications due to their high flexibility for on-demand deployments. Due to their relatively low capacity, they are generally restricted to low altitudes.

• **Aircrafts**: powered by fuel or batteries, are capable of remaining aloft for several days. This category of UAVs possesses favorable features such as low-power and energy-efficient lightweight structures with sufficient payload capacity which allow efficient trajectory management and positioning tools [101].

• **Airships**: are much more flexible in terms of weight, size and power consumption. They have been designed to fly up to 20 km. They are capable of staying in the air for long periods of time, which may be even months. A well-know example of already deployed airships is project Loon powered by Google (www.google.com/loon).

• **Helikites**: exploits both wind and helium for its lift. The aerodynamic lift is essential to combat the wind meanwhile its power consumption is very low. Helikites are very popular low altitude platforms operable independent of weather conditions and can stay in air for a few weeks [102].

Table 1 summarizes the capabilities of the aforementioned UAVs [103].

Table 5.1: Comparing different types of UAVs

UAVs Capabilities	**Drones**	**Aircraft**	**Airship**	**Helikite**
High Payload	Based on size	Yes	Yes	Yes
Moving Coverage	Yes	Yes	Yes	No
Instant Deployment	Yes	Yes	No	Yes
Weather Resistance	No	Yes	No	Yes
Easily Handled	Yes	No	No	Based on size
Power Consumption	High	High	High	Low

When a failure occurs at any BS in the network, the conventional and well-known cell outage compensation technique changes the neighboring BSs' antennae tilt and transmission power levels to serve the users of the failed BS. The advantage of this self-healing technique is that it is fast and guarantees minimum Quality of Service to the users under the failed BS. However, its disadvantage is that the users of the neighboring BSs will be affected by the change in their BSs' antennae configurations. To make use of the advantage of the conventional self-healing technique and avoid its disadvantage, we propose a novel approach

where DBSs will serve users that are not connected to any neighboring Ground BS (GBS) or those users that overloading neighboring GBS and affecting its original users. The proposed approach aims to minimize the number of used DBSs by minimizing the energy of the healing process which consequently minimizes the number of used DBSs and ensures that each user is attached to at least one BS (DBS or GBS) and is receiving the minimum required achievable rate.

Although there has been significant amount of work on using DBSs in cellular networks, using DBSs in self-healing is still at its infancy. In [89], the positioning of aerial relays is discussed to compensate cell outage and cell overload. The authors in [90] show the improvement in the coverage by assisting the network with DBSs at a certain altitude, in case of failure of the network BS.

In [91], the optimal altitude of a DBS that achieves a required coverage with minimum transmission power is found. Also providing maximum coverage with two DBSs in the presence and absence of interference is investigated. The authors in [106] designed an offloading scheme using UAVs where UAVs flies cyclically along the cell edge to serve cell-edge users and help offload data from the GBS.

5.1.2 System Model

As shown in Fig. 5.1, we consider a wireless communication system with a heterogeneous network and D DBSs which are employed to heal a group of U UEs under the failed GBS given one failure at a time or multiple failures in different geographical locations.

The set $\mathcal{U} = \{1, 2, \ldots, U\}$ denotes the set of active UEs under the failed BS and they are at known locations where the horizontal coordinate of each UE u is fixed at $\mathbf{g}_u = [x_u, y_u]^T$, $u \in U$. The set $\mathcal{D} = \{1, 2, \ldots, D\}$ denotes the set of DBSs used to heal the failed BS where all DBSs are assumed to navigate at a fixed altitude h and the horizontal coordinate of DBS $d \in D$ at discrete time instant n where $n = 1, ..., N$ is denoted by $\mathbf{J}_d^n = [x_d^n, y_d^n]^T$ where N is a total discrete period.

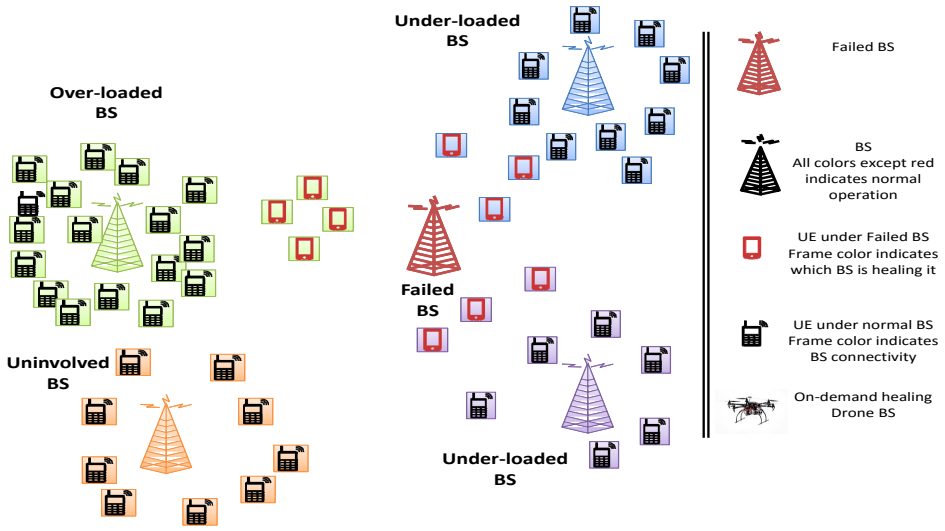

Figure 5.1: Conventional self-healing approach.

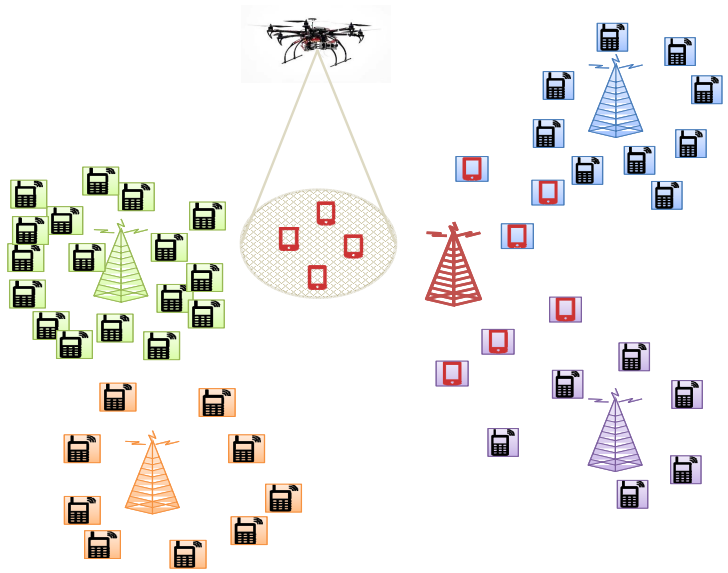

Figure 5.2: Hybrid self-healing approach.

We denote that DBS d is used in time block n by κ_d^n which acts as a decision variable in our formulation. The UEs under the failed BS are associated with either a DBS or a GBS. We denote $\zeta_{u,d,m}^n$ as the binary variable which indicates that UE u is associated with DBS d and using sub-channel m during time block n. Similarly, $\epsilon_{u,l,m}^n$ is defined for GBS l.

Assume that the DBS-UE communication channels are dominated by LoS links. Though simplified, the LoS model offers a good approximation for practical DBS-UE channels and enables us to investigate the main objective of the optimization problem presented later. Under the LoS model, the DBS-UE channel power gain follows the free space path loss model. Given that $\mathbf{J}_d^n$, $\mathbf{J}_l$ and g_u as the coordinates of DBS d, GBS j and UE u at discrete time instant n, respectively, then the distance from DBS d to UE u in time block n can be expressed as:

$$\delta_{u,d}^n = \sqrt{h_d^2 + ||\mathbf{J}_d^n - \mathbf{g}_u||^2} \tag{5.1}$$

Similarly, the distance from GBS l to UE u in time block n can be expressed as:

$$\delta_{u,l} = \sqrt{h_l^2 + ||\mathbf{J}_l - \mathbf{g}_u||^2} \tag{5.2}$$

where $\mathbf{J}_l$ is constant, h_l is the height of the GBS.

5.1.2.1 DBS and GBS Channel and Achievable Rate Models

Under this LoS model, the DBS-UE channel power gain is given as follows:

$$\Gamma_{u,d}^n = \rho_o(\delta_0/\delta_{u,d}^n)^2 = \frac{\rho_o}{h^2 + ||\mathbf{J}_d^n - \mathbf{g}_u||^2} \tag{5.3}$$

where ρ_o is a unitless constant, measured at the reference distance $\delta_0 = 1$ m, that depends on the antenna characteristics and frequency. Moreover, the channel gain for the communication links between GBS-UE is following the urban path loss model which is:

$$\Gamma_{u,l} = \rho_o(\delta_0/\delta_{u,l})^{\alpha} = \frac{\rho_o}{\left(\sqrt{h_l^2 + ||\mathbf{J}_l - \mathbf{g}_u||^2}\right)^{\alpha}} \tag{5.4}$$

Let $\mathcal{M} = \{1, 2, \ldots, M\}$ be the set of self-healing sub-channels that each DBS and GBS can use during the self-healing process. These sub-channels will be further divided and allocated to the UEs associated with each DBS and GBS. We assume that each DBS d and GBS l transmits with a constant per sub-channel transmit power $p_{d,m}$ and $p_{l,m}$, respectively. If sub-channel m is not assigned to DBS d then $p_{d,m}$ will be zero. For simplicity, we assume that there is no interference between the DBS tier and the GBS tier. Hence, the received Signal to Interference plus Noise Ratio (SINR) between DBS d and UE u per sub-channel m during time block n can be expressed as:

$$\gamma^n_{u,d,m} = \frac{p_{d,m}\ \Gamma^n_{u,d}}{\sum\limits_{\substack{j\in\mathcal{D}\\ j\neq d}} p_{j,m}\Gamma^n_{u,j} + \sigma^2} = \frac{\frac{p_{d,m}\ \rho_o}{h^2+||\mathbf{J}^n_d - \mathbf{g}_u||^2}}{\sum\limits_{\substack{j\in\mathcal{D}\\ j\neq d}} \frac{p_{j,m}\ \rho_o}{h^2+||\mathbf{J}^n_j - \mathbf{g}_u||^2} + \sigma^2} \tag{5.5}$$

Similarly, we can express the received SINR between GBS l and UE u per sub-channel m during time block n as:

$$\gamma_{u,l,m} = \frac{p_{l,m}\ \Gamma_{u,l}}{\sum\limits_{\substack{i\in\mathcal{L}\\ i\neq l}} p_{i,m}\Gamma_{u,i} + \sigma^2} = \frac{\frac{p_{l,m}\ \rho_o}{\left(\sqrt{h_l^2+||\mathbf{J}_l - \mathbf{g}_u||^2}\right)^{\alpha}}}{\sum\limits_{\substack{i\in\mathcal{L}\\ i\neq l}} \frac{p_{i,m}\ \rho_o}{\left(\sqrt{h_l^2+||\mathbf{J}_l - \mathbf{g}_u||^2}\right)^{\alpha}} + \sigma^2} \tag{5.6}$$

where σ^2 is the power of the Additive White Gaussian Noise at the receiver. The first term in the denominator of equations (6.2) and (5.6) represents the co-channel interference caused by the transmissions of all other DBS/GBSs on the same sub-channel m, respectively. Thus the achievable per sub-channel rate of UE u connected to DBS d during time block n is $R^n_{u,d,m} = \log_2(1 + \gamma^n_{u,d,m})$ bps/Hz. Moreover, the achievable per sub-channel rate of UE u connected to GBS l during time block n is $R_{u,l,m} = \log_2(1 + \gamma_{u,l,m})$ bps/Hz.

5.1.2.2 Base Stations Power Model

In order for any GBS to serve its connected users during a time block n, GBS l consumes a certain amount of power. This amount of power can be expressed as [95]:

$$P_l^{n(noSH)} = \alpha_l P_{U_N} + \beta_l, \tag{5.7}$$

where α_l is the scaling parameter, U_N is the total number of users served by the GBS, P_{U_N} is the total power used by this GBS to serve all its users during normal operation and β_l models a constant power which is consumed independently of the radiated power of GBS.

Upon the failure of any BS, the neighboring GBSs will heal the users under the failed BS by applying the conventional self-healing approach, i.e., changing antenna tilt and power. Then the additional power consumed by neighboring GBS l during the self-healing period $P_l^{n(SH)}$ is the power radiated to heal those users. This can be expressed as:

$$P_{l,m}^{n(SH)} = \tilde{\alpha}_l \sum_{u=1}^{U} \epsilon_{u,l,m}^{n} p_{l,m} \tag{5.8}$$

where $\tilde{\alpha}_l$ is a scaling parameter which takes into consideration the increase of the BS antenna power during the healing process where $\tilde{\alpha}_l \geq \alpha_l$. $\epsilon_{u,l,m}^{n}$ is a binary variable indicating the association of the user u with BS l using sub-channel m and $p_{l,m}$ is the fixed amount of power radiated from the GBS to each user connected to it. Note that the additional independent power β_l is not accounted in the case of failure since this power is already consumed whether there is a failure or no and in Eq. (5.8) we are only considering the excess consumed power due to the healing process.

5.1.2.3 Drone Power Model

There are three sources draining power from the DBS battery: 1) The hardware power 2) The hovering power 3) The DBS transmission power. We assume that all drones move with a fixed speed denoted by v_d. The hovering and hardware drone power levels, denoted by P_{hov} and P_{har}, can be expressed, respectively, as [96]:

$$P_{\text{hov}} = \sqrt{(m_{\text{tot}} g)^3 / 2\pi r_p^2 n_p \rho}, \tag{5.9}$$

$$P_{\text{har}} = \frac{P_{\text{full}} - P_s}{v_{\max}} v_d + P_s, \tag{5.10}$$

where m_{tot}, g, and ρ are the drone mass in (Kg), earth gravity in (m/s^2), and air density in (Kg/m^3), respectively. r_p and n_p are the radius and the number of the drone's propellers, respectively. $v_{\max}$ is the maximum speed of the drone and in our model it is equal to v_d. P_{full} and P_s are the hardware power levels when the drone is moving at full speed and when the drone is in idle mode, respectively. When the DBS is flying to a destination, it will consume P_{har}. Finally, the total flying power of DBS d can be calculated as $P_f = P_{\text{hov}} + P_{\text{har}}$.

The DBS transmission power can be modeled exactly in the same way of the regular BS with the new parameters α_d and β_d. This can be seen in the second term of Eq. (5.12).

5.1.2.4 System Model Assumptions

The proposed system model is considering the following assumptions:

- Each macro-BS in the target area is pre-equipped with 2 DBSs. This minimize the fly time of the DBSs when any small-BS fail.
- During failure, each UE is either associated with a GBS or a DBS.
- The user association is assumed to be fixed during each time block "n".
- The DBSs are assumed to fly from their initial location to the failure area in a fixed time named T_f. This means that all DBSs are initialized from the same location and the distance flown is proportional to the flying time given that the DBS speed is constant.

5.1.3 Problem Formulation and Proposed Solution

In this section, we formulate an optimization problem aiming to minimize the total energy of GBSs and DBSs during the hybrid self-healing mechanism which will determine when to use the healing DBSs given capacity and rate constraints. The optimization problem starts after the detection of the failure and hence applying the conventional self-healing technique to serve the affected UEs. Once all UEs are served by the neighboring GBSs, the optimization problem will work mainly on minimizing the overall system energy in addition to serving users of the failed GBS, hence minimizing the number of DBSs used in the healing process.

The total energy consumed by BS l to heal the UEs of the failed BS during time block n is given by the total duration of healing T multiplied by the healing power as follows:

$$E^n_{l,m} = TP^{n(SH)}_l = T\tilde{\alpha}_l \sum_{u=1}^{U} \epsilon^n_{u,l,m} p_{l,m} \tag{5.11}$$

The total energy consumed by any DBS d to heal the users of the failed BS is given by:

$$E^n_{d,m} = \kappa^n_d \big(T_f(P_{\text{har}}) + T(P_{\text{har}} + P_{\text{hov}})\big) + T[\alpha_d \sum_{u=1}^{U} \zeta^n_{u,d,m}\ p_{d,m} + \beta_d] \tag{5.12}$$

where κ^n_d is a binary variable indicating whether or not DBS d is used in time block n and T_f is the time the DBS takes to travel from its initial position to the position from which it will serve the users.

5.1.3.1 Problem Formulation

The optimization problem minimizing the energy of the healing BSs (ground and sky BSs) to heal the UEs under the failed OSC is given by:

$$(\mathbf{P1}): \underset{\mathbf{J_d^n},\epsilon^n_{u,l,m},\zeta^n_{u,d,m},\kappa^n_d}{\text{minimize}} \sum_{n=1}^{N}\sum_{l=1}^{L}\sum_{m=1}^{M} E^n_{l,m} + \sum_{n=1}^{N}\sum_{d=1}^{D}\sum_{m=1}^{M} E^n_{d,m} \tag{5.13}$$

subject to:

$$\sum_{l=1}^{L}\sum_{m=1}^{M} \epsilon^n_{u,l,m} + \sum_{d=1}^{D}\sum_{m=1}^{M} \zeta^n_{u,d,m} = 1 \quad \forall\ u,n \tag{5.14}$$

$$\sum_{d=1}^{D}\sum_{m=1}^{M} \zeta^n_{u,d,m} R^n_{u,d,m} + \sum_{l=1}^{L}\sum_{m=1}^{M} \epsilon^n_{u,l,m} R_{u,l,m} \geq R^{\text{th}}_u \quad \forall\ u,n \tag{5.15}$$

$$R^{th}_u\Big(\sum_{u=1}^{U}\sum_{m=1}^{M} \epsilon^n_{u,l,m} + \overline{U}^n_l\Big) \leq R^{\max}_{GBS} \quad \forall\ l,n \tag{5.16}$$

$$R^{th}_u\Big(\sum_{u=1}^{U}\sum_{m=1}^{M} \zeta^n_{u,d,m}\Big) \leq R^{\max}_{DBS} \quad \forall\ d,n \tag{5.17}$$

$$\kappa^n_d < 1 + \frac{\sum_{u=1}^{U}\sum_{m=1}^{M} \zeta^n_{u,d,m}}{Q} \quad \forall\ d,n \tag{5.18}$$

$$\kappa^n_d \geq \frac{\sum_{u=1}^{U}\sum_{m=1}^{M} \zeta^n_{u,d,m}}{Q} \quad \forall\ d,n \tag{5.19}$$

$$\mathbf{J}^{\min}_d \leq \mathbf{J}^n_d \leq \mathbf{J}^{\max}_d, \quad \forall\ d,n \tag{5.20}$$

$$\kappa^n_d, \zeta^n_{u,d,m}, \epsilon^n_{u,l,m} \in \{0,1\} \tag{5.21}$$

Constraint (6.9d) forces UE u to be associated with DBS d or GBS l. Constraint (5.15) indicates that the rate of UE u, which is associated with either DBS d or GBS l, is lower bounded by a threshold rate R^{th}_u. Constraints (5.16) and (6.9c) define an upper bound for the maximum rate for GBS and DBS, respectively, given that $\overline{U}^n_l$ is the number of UEs served by GBS l at time block n. Since κ^n_d indicates whether DBS d is used in time block n or not, constraints (5.18) and (5.19) are used to extract this information from $\zeta^n_{u,d,m}$ where when $\zeta^n_{u,d,m} = 0$ then consequently $\kappa^n_d = 0$ and when $\zeta^n_{u,d,m} = 1$ for any UE u and resource block M then $\kappa^n_d = 1$. Note that Q is a very large number. Constraint (5.36e) is used to limit the 2D coordinates of DBS d where $\mathbf{J}^{\min}_d = [x^{\min}_d, y^{\min}_d]^T$ and $\mathbf{J}^{\max}_d = [x^{\max}_d, y^{\max}_d]^T$.

P1 is not easy to solve due to the following: 1) the decision variables κ^n_d, $\zeta^n_{u,d,m}$, $\epsilon^n_{u,l,m}$ are binary and thus the objective function (6.9a) and constraints (6.9d)-(5.19) involve integer

constraints. 2) Even if we fixed the decision variables, constraint (5.15) is still non-convex with respect to DBS coordinates variable $\mathbf{J}_d^n$. Therefore, problem (6.9a) is mixed-integer non-linear non-convex problem, which is difficult to be solved optimally.

5.1.3.2 Proposed Solution

In general, **P1** has no standard method for solving it efficiently. In the following, we propose an efficient iterative algorithm for solving **P1**. Specifically, for a given coordinate $\mathbf{J}_d^n$, we optimize the decision variables, i.e. ζ, κ and ϵ, by solving a Linear Program (LP) after relaxing the decision variables. For any given ζ, κ and ϵ, the DBS coordinates $\mathbf{J}_d^n$ are optimized based on the Successive Convex Approximation (SCA) technique [97]. Finally, an iterative algorithm is given to solve **P1** efficiently.

• Solving for Decision Variables

By fixing the DBS coordinates, the resulting problem will be an Integer LP (ILP) which can be solved optimally but not efficiently due to the large number of binary variables. In this case, relaxing the binary variables and then reconstructing them will allow us to solve this problem efficiently (reconstruction phase is skipped due to space limitation). Hence, for any given $\mathbf{J}_d^n$, the variables of **P1** can be optimized by solving the following problem:

$$(\mathbf{P2}): \underset{\epsilon_{u,l,m}^n, \zeta_{u,d,m}^n, \kappa_d^n}{\text{minimize}} \quad \sum_{n=1}^{N}\sum_{l=1}^{L} E_l^n + \sum_{n=1}^{N}\sum_{d=1}^{D} E_d^n \tag{5.22}$$

subject to:

$$\text{Constraints}(6.9d) - (5.19)$$

$$0 \leq \kappa_d^n, \zeta_{u,d,m}^n, \epsilon_{u,l,m}^n \leq 1 \quad \forall\, u, d, l, n \tag{5.23}$$

Note that in **P2**, $R_{u,d,m}^n$ is not a variable anymore since we fixed the DBS coordinates. The relaxed **P2** is an LP which can be solved using any LP solver.

• Solving for DBS Coordinates

For any given decision variable, the DBS coordinates $\mathbf{J}_d^n$ can be optimized by solving the following problem:

$$(\mathbf{P3}): \underset{\mathbf{J_d^n}}{\text{minimize}} \quad \sum_{n=1}^{N}\sum_{l=1}^{L} E_l^n + \sum_{n=1}^{N}\sum_{d=1}^{D} E_d^n \tag{5.24}$$

subject to:

$$\text{Constraints}(5.15), (5.36e)$$

In **P3**, Constraints (6.9d), (5.16)-(5.19) and (5.21) are not involved in **P3** since the decision variables are now fixed and their values are iteratively updated from **P2**. The objective function and all constraints of **P3** are convex except for constraint (5.15). This constraint is neither concave nor convex with respect to the DBSs' coordinates which appears in $R_{u,d,m}^n$. It is worth noticing that the second term of the same constraint is not a function of the DBSs' coordinates, hence it is linear. Returning back to the first term of constraint (5.15), call it $\tilde{R}$, which can be expanded as follows:

$$\begin{aligned}
\tilde{R} &= \sum_{d\in\mathcal{D}}\sum_{m\in\mathcal{D}} \zeta_{u,d,m}^n \log_2\Big(1 + \frac{\frac{p_{d,m}\ \rho_o}{h^2+||\mathbf{J}_d^n-\mathbf{g}_u||^2}}{\sum\limits_{\substack{j\in\mathcal{D}\\ j\neq d}} \frac{p_{j,m}\ \rho_o}{h^2+||\mathbf{J}_j^n-\mathbf{g}_u||^2} + \sigma^2}\Big) \\
&\quad \sum_{d\in\mathcal{D}}\sum_{m\in\mathcal{D}} \zeta_{u,d,m}^n \log_2\Big(\frac{\sum_{j\in\mathcal{D}} \frac{p_{j,m}\rho_o}{h^2+||\mathbf{J}_j^n-\mathbf{g}_u||^2} + \sigma^2}{\sum\limits_{\substack{j\in\mathcal{D}\\ j\neq d}} \frac{p_{j,m}\ \rho_o}{h^2+||\mathbf{J}_j^n-\mathbf{g}_u||^2} + \sigma^2}\Big) \\
&= \sum_{d\in\mathcal{D}}\sum_{m\in\mathcal{D}} \zeta_{u,d,m}^n \Big(\underbrace{\log_2\Big(\sum_{j\in\mathcal{D}} \frac{p_{j,m}\rho_o}{h^2+||\mathbf{J}_j^n-\mathbf{g}_u||^2} + \sigma^2\Big)}_{\tilde{R}^1} \\
&\quad \underbrace{-\log_2\Big(\sum_{\substack{j\in\mathcal{D}\\ j\neq d}} \frac{p_{j,m}\ \rho_o}{h^2+||\mathbf{J}_j^n-\mathbf{g}_u||^2} + \sigma^2\Big)}_{\tilde{R}^2} \Big)
\end{aligned} \tag{5.25}$$

Our main goal is to convert Eq. (5.25) to a concave form in order for **P3** to be convex. Both terms of $\tilde{R}$ are neither concave nor convex. $\tilde{R}^2$ is not concave with respect to $\mathbf{J}_j^n$,

however, it is concave with respect to $||\mathbf{J}_j^n - \mathbf{g}_u||^2$. This motivates us to introduce the slack variable $\mathbf{\Psi} = \left\{\Psi_{u,j}^n = ||\mathbf{J}_j^n - \mathbf{g}_u||^2, \forall j \in \mathcal{D}, j \neq d, u, n\right\}$ to make $\tilde{R}^2$ concave in $\mathbf{\Psi}$. After introducing this slack variable to $\tilde{R}^2$, we have to add a new constraint to **P3** which is expressed as [98]:

$$\Psi_{u,j}^n \leq ||\mathbf{J}_j^n - \mathbf{g}_u||^2 \qquad \forall j \in \mathcal{D}, j \neq d, u, n \tag{5.26}$$

Back to the first term of $\tilde{R}$, i.e., $\tilde{R}^1$, this term is neither concave nor convex. Even with the slack variable, $\tilde{R}^1$ will not be concave (it will be convex). To tackle the non-concavity of $\tilde{R}^1$, the SCA technique is applied where in each iteration, the original function is approximated by a more tractable function at a given local point. Define $\mathbf{J}_d^n(r)$ as the given location of DBS d in the r-th iteration. Recall that $\tilde{R}^1$ is convex in $||\mathbf{J}_j^n - \mathbf{g}_u||^2$ and since any convex function can be globally lower-bounded by its first order Taylor expansion [99], hence, given $\mathbf{J}_d^n(r)$ in iteration r, we obtain the following lower bound:

$$\begin{aligned}\tilde{R}^1 \geq \log_2\Big(\sum_{j\in\mathcal{D}} \frac{p_{j,m}\rho_o}{h^2 + ||\mathbf{J}_j^n(r) - \mathbf{g}_u||^2}\Big) \\ - \sum_{j\in\mathcal{D}} Z_{u,d}^n(||\mathbf{J}_j^n - \mathbf{g}_u||^2 - ||\mathbf{J}_j^n(r) - \mathbf{g}_u||^2) = \tilde{\tilde{R}}^1\end{aligned} \tag{5.27}$$

$$\text{where} \quad Z_{u,d}^n = \frac{\frac{p_{j,m}\rho_o}{h^2 + (||\mathbf{J}_j^n(r) - \mathbf{g}_u||^2)^2}\log_2(e)}{\sum_{k\in\mathcal{D}} \frac{p_{k,m}\rho_o}{h^2 + ||\mathbf{J}_k^n(r) - \mathbf{g}_u||^2} + \sigma^2} \tag{5.28}$$

After using SCA with $\tilde{R}^1$ and using a slack variable with $\tilde{R}^2$, now Eq.(5.25) is concave. Hence, with any given local point $\mathbf{J}_j^n(r)$, problem **P3** can be approximated to $\overline{\mathbf{P3}}$ as follows:

$$(\overline{\mathbf{P3}}) : \underset{\mathbf{J_d^n},\mathbf{\Psi_{u,j}^n}}{\text{minimize}} \qquad \sum_{n=1}^{N}\sum_{l=1}^{L} E_l^n + \sum_{n=1}^{N}\sum_{d=1}^{D} E_d^n \tag{5.29}$$

subject to:

$$\sum_{d=1}^{D}\sum_{m=1}^{M} \zeta_{u,d,m}^n \Big(\tilde{\tilde{R}}^1 - \log_2(\sum_{\substack{j\in\mathcal{D}\\ j\neq d}} \frac{p_{j,m}\ \rho_o}{h^2 + ||\mathbf{J}_j^n - \mathbf{g}_u||^2} + \sigma^2)\Big)$$

$$+ \sum_{l=1}^{L}\sum_{m}^{M} \epsilon_{u,l,m}^n R_{u,l,m} \geq R_u^{\text{th}} \quad \forall\ u, n \tag{5.30}$$

$$\Psi_{u,j}^n \leq ||\mathbf{J}_j^n - \mathbf{g}_u||^2 \qquad \forall j \in \mathcal{D}, j \neq d, u, n \tag{5.31}$$

$$\mathbf{J}_d^{\min} \leq \mathbf{J}_d^n \leq \mathbf{J}_d^{\max}, \quad \forall\ d, n \tag{5.32}$$

Note that the value of R_u^{th} is selected sufficiently low in order to make constraint (30) feasible while taking into consideration inequality (27).

Finally, we propose an iterative algorithm to solve **P1**. The variables in **P1** are partitioned into two blocks, i.e., association and coordinates. Then they are alternately optimized (solving **P2** then $\overline{\mathbf{P3}}$ iteratively). Furthermore, the obtained solution in each iteration is used as the input to the next iteration. The details of this algorithm are summarized in Algorithm 1.

5.1.4 Simulation Results

In this section, numerical results are provided to investigate the benefits of utilizing DBSs in mitigating GBS failures in 5G networks. The simulation model consists of 5 GBSs where one of them fails. We initialized 4 standby DBSs to be used in case the conventional self-healing approach cannot accommodate the users originally served by the failed BS.

The simulation area is 400×400 m^2 where the failed GBS is centered at the origin and the UEs of the failed BS are distributed randomly over this area. The UEs of the failed GBS are static, however, the number of users within each neighboring GBS changes randomly

Algorithm 1: Iterative approximate solution for **P1**

Input: $\mathbf{J}_d^n(0)$

Output: $\mathbf{J}_d^n(r+1), \kappa_d^n(r+1), \zeta_{u,d,m}^n(r+1), \epsilon_{u,l,m}^n(r+1)$

while $r \neq$ *maximum iteration* **do**
- Solve Problem **P2** for given $\mathbf{J}_d^n(r)$.
- Reconstruct the binary variables, check their feasibility and then denote them as $\kappa_d^n(r+1)$, $\zeta_{u,d,m}^n(r+1)$ and $\epsilon_{u,l,m}^n(r+1)$
- Solve Problem $\overline{\mathbf{P3}}$ for given $\kappa_d^n(r+1), \zeta_{u,d,m}^n(r+1), \epsilon_{u,l,m}^n(r+1)$.
- Denote the optimal solution of $\overline{\mathbf{P3}}$ as $\mathbf{J}_d^n(r+1)$
- Update r=r+1
- **if** *The fractional increase of the objective value* $\leq \varepsilon^{th}$ **then**
  - Break
- **end**

end

Table 5.2: Simulation parameters (Section 5.1)

Parameter	Value	Parameter	Value	Parameter	Value
f (GHz)	2.1	$R_{GBS}^{\max}$ (bps/Hz)	100	$\mathbf{J}_d^{\min}$ (m)	**-200**
$p_{d,m}$ (mW)	100	$R_{DBS}^{\max}$ (bps/Hz)	10	$\mathbf{J}_d^{\max}$ (m)	**200**
$P_{l,m}$ (mW)	100	R_u^{th} (bps/Hz)	2	h_l (W)	30
σ^2 (dBm/Hz)	-174	β_d (W)	1	h_d (min)	100
T (min)	60	α_d	2.6	ρ_o	0.01
T_f (min)	0.5	α_l	4.7	Q	1000

per time block. The parameters used to calculate P_{hov} and P_{har} are initialized as in [96]. The remaining parameters are presented in Table I.

Table 2 shows the users association (DBS or GBS) and rates for 10 UEs during 2 time blocks. The remaining time blocks are not shown due to space limitations. For time block 1, only DBS 1 is used from a set of 4 DBSs and all other UEs are served by GBSs. Since DBS 1 is serving UE 3, UE5 and UE 9, their corresponding rates are relatively high. UE 1 is associated with the same GBS during time blocks 1 and 2. However, its rate decreases during time block 2. This is due to the change of the capacity of GBS 1 since GBS 1 has to serve its own UEs first and participate in the healing process by the available capacity. During time block 2, DBS 4 is serving UE 3, UE 5 and UE 9. According to these UEs'

Table 5.3: Association and rates for 10 UEs

UEs	**Time block 1 (n=1)**		**Time block 2 (n=2)**	
	Association	**R (bps/Hz)**	**Association**	**R (bps/Hz)**
UE1	GBS1	2.82	GBS1	2.28
UE2	GBS2	2.43	GBS2	2.66
UE3	DBS1	3.28	DBS4	3.59
UE4	GBS3	2.41	GBS3	2.33
UE5	DBS1	3.00	DBS4	3.37
UE6	GBS2	2.28	GBS2	2.25
UE7	GBS4	2.17	DBS4	3.12
UE8	GBS3	3.07	GBS3	2.71
UE9	DBS1	2.80	GBS1	2.30
UE10	GBS2	2.00	GBS2	2.00

locations, DBS 4 optimizes its location to serve each of them.

Figure 5.4 shows the accumulated consumed energy for both DBSs and GBSs for different numbers of UEs. It is worth noting that the GBS energy is the excess energy consumed to serve the users originally served by the failed BS. On the other hand, the energy consumed by the DBS is the hovering, hardware and communication power which is significantly high compared with the excess energy consumed by the GBS. As the number of UEs increases from 4 to 10, the number of used DBS is increasing since the GBSs are serving their own UEs and serving the targeted UEs using only the available capacity. At a certain point, all DBSs are used to satisfy the target UEs minimum rate requirement.

Fig. 5.3 shows different scenarios of the proposed scheme where there are 8 UEs connected to the failed BS and there are 4 neighboring GBSs and 4 DBSs ready to participate. In Fig. 5.3(a), the GBSs are serving all the UEs without any help from the DBSs. This occurs at the detection of the failure or if the GBSs are non loaded with their own users and they can satisfy all UEs rate requirements. In Fig. 5.3(b), UE 3 and UE 5 are not achieving their minimum rate R_u^{th} by associating to GBS 4 and GBS 1, respectively. In this case these two UEs are associated with DBS 1. Although attaching them to DBS 1 will not reduce the energy, this will satisfy UE 3 and UE 7 threshold rates.

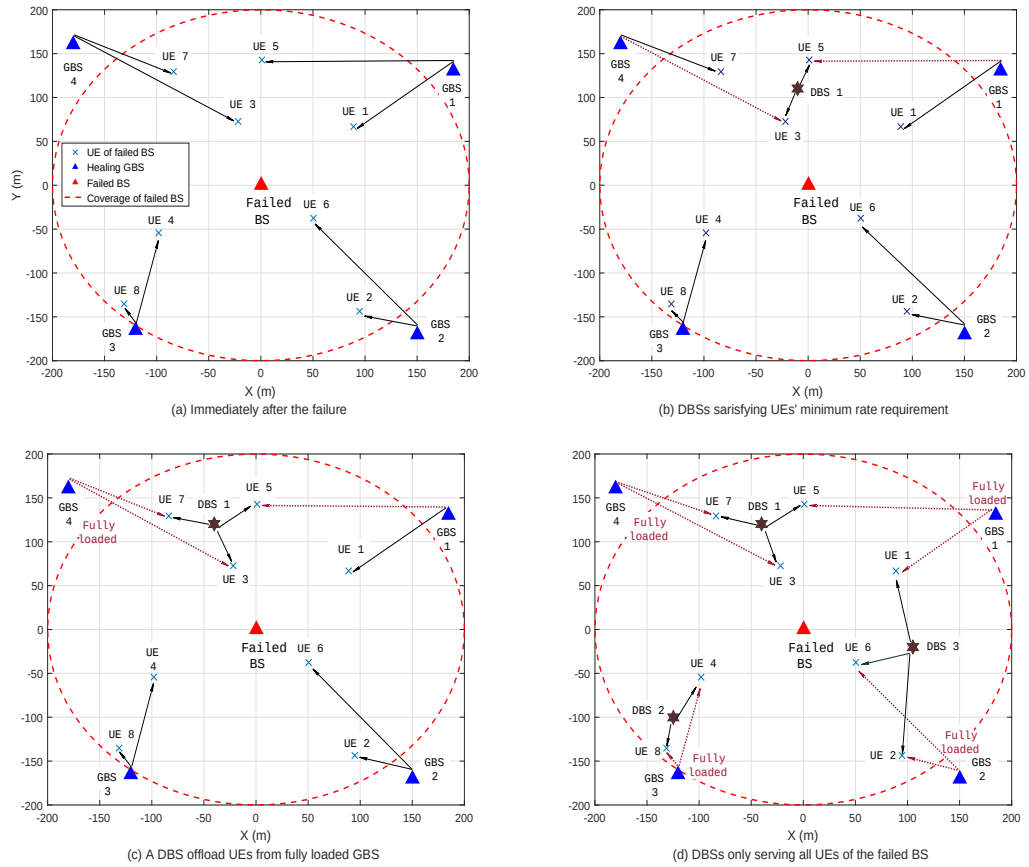

Figure 5.3: Cell outage compensation different scenarios (GBSs COC, hybrid COC and DBSs COC) with 4 DBSs, 4 GBSs and 8 UEs.

Figure 5.3(c) shows the scenario of the proposed hybrid algorithm. In this scenario, GBS 4 is fully loaded with its own UEs, hence, UE 7 will be associated with DBS 1 which is already serving UE 3 and UE 5. If DBS 1 was overloaded, then an additional DBS will be used. Finally, Fig. 5.3(d) shows a scenario where all GBSs are fully loaded. This scenario is subject to feasibility based on the number of available DBSs. It is worth noting that the 4th DBS was not involved in the healing process in all scenarios.

From the simulation results, we can infer that the hybrid COC is converted to the conventional COC approach if the GBSs are having enough extra capacity. If the number of UEs increases, the disadvantage of the conventional approach will start to appear where either the GBS will not serve the target UE or will degrade the rate of its own UE. Using

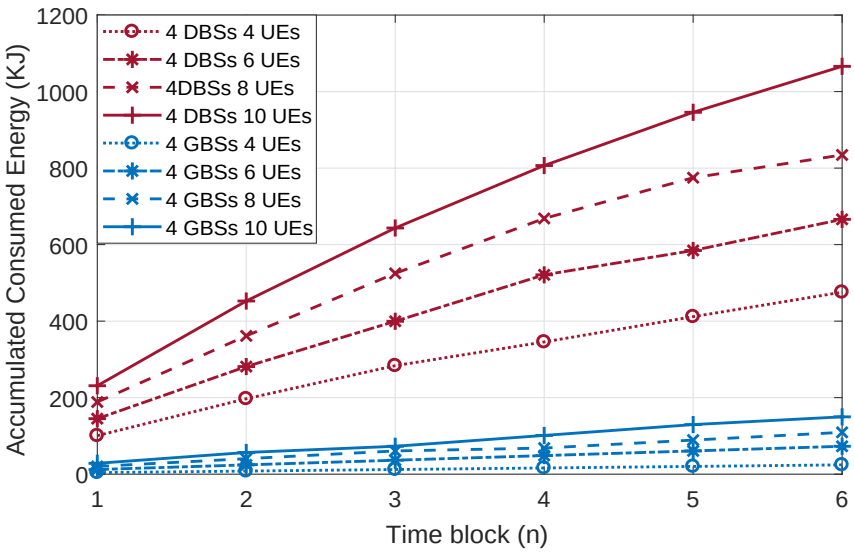

Figure 5.4: Accumulated energy for DBSs and GBSs.

hybrid approach, we can avoid this scenario by using DBSs to serve those UEs.

One of the challenges facing this approach is the movement of a DBS from one location to another which is assumed to happen instantaneously in this proposed model. This challenge can be addressed by adding a velocity constraint to limit the movement of the DBS to its maximum speed.

5.2 Short-term and Long-term Cell Outage Compensation Using UAVs

5.2.1 Introduction

Unmanned Aerial Vehicles (UAVs) enabled communications is considered as a strong candidate to be used in 5G networks. Indeed, UAVs enabled communications offers an encouraging solution to provide wireless connectivity for devices without coverage due to, e.g., severe shadowing by urban or mountainous terrains, unexpected failures, or damage to the communication infrastructure due to malicious or natural causes .

Cellular systems are prone to failures, and the most critical domain for fault management is the radio access network. Operator's revenue losses occurs when at least one BS fails for a short period of time. Longer failures bias users to switch to competitors which results in permanent revenue losses [104].

When a failure occurs to any GBS, the conventional COC technique is to adjust the neighboring BSs' antenna tilt and power to serve the users of the failed BS. This technique is very fast and guarantees minimum Quality of Service (QoS) to the users given a failed BS. However, the disadvantage of this technique is that the users of the neighboring BSs will be affected by the change in their BS's antenna configuration [105; 56].

We propose a solution for this problem that mainly depends on using UAVs as flying BSs. These UAVs are initially co-located with GBSs and ready to fly when needed. When the failure occurs, UAVs will fly to their initial positions to start compensating UEs of the failed BS. During this flying time, the conventional self-healing technique is used to serve those UEs until UAVs reach their predetermined locations. When the UAVs reach these pre-computed locations, the neighboring BSs return to serve their own users only.

Based on the comparison presented in Table 5.1, we propose to use DBSs in healing short-term failures since they have the important feature of instant deployment, especially if the network operator already placed ready-to-fly drones at each cell site. For long-term failures, the helikite is proposed to heal the failed BS since it flies at low altitudes and its

flying power consumption is the lowest compared to other types of UAVs for long flying periods. Weather conditions must be considered when using DBSs. Hence, if weather conditions are not suitable for DBSs to aviate, it is recommended to use helikites even if we are dealing with a short-term failure.

Although there has been a recognized amount of work on using DBSs in cellular networks, using DBSs in self-healing is still at its infancy. The authors in [106] presented a novel idea of offloading the traffic of UEs suffering from degraded service at the GBS cell edge. They jointly optimizing the UAV's trajectory, as well as the user partitioning between the UAV and GBS. In [89], the positioning of aerial relays is discussed to compensate cell outage and cell overload. The authors in [90] show the improvement in coverage by assisting the network with DBSs at a certain altitude during BS failure.

The authors in [107] present a novel COC framework to mitigate the effect of the failure of any BS in 5G networks using both UAVs and GBSs. They showed that their proposed hybrid approach outperforms the conventional COC approach. In [108], a vertical backhaul/fronthaul framework is suggested for transporting the traffic between the access and core networks in a typical HetNet through free space optical links.

5.2.2 System Architecture

We consider a downlink heterogeneous network consisting of a Macro-Base Station overlaying number of Small BSs (SBSs). Fig. 6.1 shows the network architecture during the failure of two SBSs. In this figure we show a short-term failure which is mitigated using three DBSs and a long-term failure which is mitigated using one helikite.

The set $\mathcal{U} = \{1, 2, \ldots, U\}$ denotes the set of active UEs under the failed BS and they are at known locations where the horizontal coordinates of each UE u are fixed at $\mathbf{g}_u = [x_u, y_u]^T \in \mathbb{R}^{2\text{x}1}$, $u \in U$, assuming that all UEs are at zero altitude. The set $\mathcal{D} = \{1, 2, \ldots, D\}$ denotes the set of DBSs used to heal the failed BS where all DBSs are assumed to navigate at a fixed altitude h_d and the horizontal coordinates of DBS d are

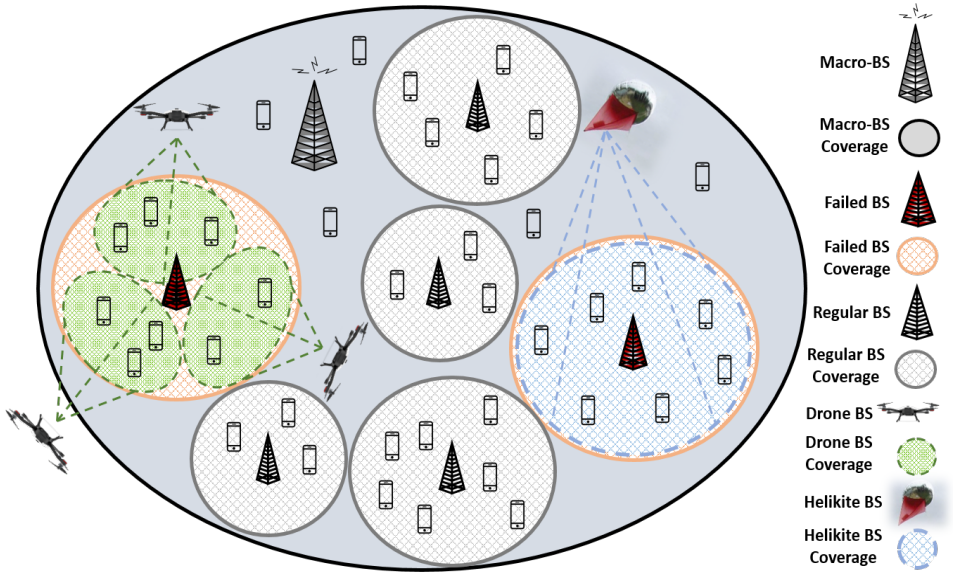

Figure 5.5: System model during failure.

denoted by $\mathbf{J}_d = [x_d, y_d]^T \in \mathbb{R}^{2x1}$.

We denote that DBS d is communicating with UE u using resource block m by the binary variable $\Phi^m_{u,d}$ which acts as a decision variable in our problem formulation. We denote by $\psi_{u,d}$ the binary association between DBS d and UE u.

Assume that the DBS-UE communication channels are dominated by LoS links. Though simplified, the LoS model offers a good approximation for practical Drone-UE channels and enables us to investigate the main objective of the optimization problem presented later. Under the LoS model, the Drone-UE channel power gain follows the free space path loss model which is determined mainly by the DBS-UE distance. Given that $\mathbf{J}_d$ and $\mathbf{g}_u$ are the coordinates of DBS d and UE u in the horizontal plane, respectively, then the distance from DBS d to UE u can be expressed as: $\delta_{u,d} = \sqrt{h_d^2 + ||\mathbf{J}_d - \mathbf{g}_u||^2}$.

5.2.2.1 DBS Channel and Achievable Rate Models

For simplicity, we assume that the communication links DBS-UE are dominated by the LoS links where the channel quality depends only on the distance between the DBS and the

UE. Under this LoS model, the DBS-UE channel power gain mainly follows the free space path loss model which is given as follows:

$$\Gamma_{u,d} = \rho_o(\delta_0/\delta_{u,d})^2 = \rho_o/\left(h^2 + ||\mathbf{J}_d - \mathbf{g}_u||^2\right) \tag{5.33}$$

where ρ_o is a unitless constant that depends on the antenna characteristics and frequency, and is measured at the reference distance $\delta_0 = 1$ m.

Let $\mathcal{M} = \{1, 2, \ldots, M\}$ be the set of sub-channels that each DBS can use during the self-healing process. These sub-channels will be further divided and allocated to the UEs associated with each DBS. Each DBS, d, transmits to each UE, u, with a per sub-channel transmit power $p^m_{u,d}$. If sub-channel m is not assigned to DBS d then $p^m_{u,d}$ will equal to zero. For simplicity, we assume that there is no interference between the DBS tier and the GBS tier which means that each of them is using different sets of sub-channel. However, we consider the interference between different DBSs. Hence, the received Signal to interference plus Noise Ratio between DBS d and UE u per sub-channel m can be expressed as:

$$\gamma^m_{u,d} = \frac{p^m_{u,d}\,\Gamma^m_{u,d}}{\sum\limits_{\substack{i\in\mathcal{U}\\ i\neq u}}\sum\limits_{j\in\mathcal{D}} p^m_{i,j}\Gamma^m_{u,j} + \sigma^2} = \frac{\frac{p^m_{u,d}\ \rho_o}{h^2+||\mathbf{J}_d-\mathbf{g}_u||^2}}{\sum\limits_{\substack{i\in\mathcal{U}\\ i\neq u}}\sum\limits_{j\in\mathcal{D}} \frac{p^m_{i,j}\ \rho_o}{h^2+||\mathbf{J}_j-\mathbf{g}_u||^2} + \sigma^2} \tag{5.34}$$

where σ^2 is the power of the Additive White Gaussian Noise at the receiver. The first term in the denominator of equation (6.2) represents the co-channel interference caused by the transmissions of all other DBSs on the same sub-channel m, respectively.

Accordingly, the achievable per sub-channel downlink rate from DBS d to UE u is given by:

$$R^m_{u,d} = \log_2(1 + \gamma^m_{u,d}) \tag{5.35}$$

5.2.3 UAV Power Model

Since the proposed framework allows different types of UAVs to compensate the failure based on the type of failure (short-term or long-term),two types of UAVs are proposed to

be used in this self-healing framework; Drones and Helikite. The operation power of Drones is very high due to the hovering and hardware power [96]. However, the operation power of Helikites is much lower since its weight is lifted by the helium and additional power is consumed only to sustain the location of the Helikite. From minimizing the consumed power point of view, we assign Drones to short-term healing and Helikites to long-term healing. This is why in the formulated optimization problem we consider minimizing the downlink power $p^m_{u,d}$ of the UAV regardless its type, i.e., Drone or Helikite.

5.2.4 Problem Formulation

In this section, we formulate an optimization problem aiming to maximize the minimum achievable rate of the UEs under the failed GBS and meanwhile minimizing the transmission power of the UAV used, i.e., either the DBS or the helikite. The number of UAVs used to heal a failed GBS is based on the coverage area of the failed GBS and the type of the UAVs used. The optimization problem formulation is given by:

$$(\mathbf{P1}) : \underset{\mathbf{J},\Phi,\Psi,\mathbf{p}}{\text{maximize}} \frac{\Omega}{R^{\text{th}}} - \frac{1}{P^{\max} * |\mathcal{D}|} \sum_d \sum_u \sum_m \psi_{u,d} \Phi^m_{u,d} p^m_{u,d} \tag{5.36a}$$

subject to:

$$\Omega \leq \sum_d \sum_m \psi_{u,d} \Phi^m_{u,d} R^m_{u,d}, \quad \forall\ u \tag{5.36b}$$

$$\sum_d \sum_m \psi_{u,d} \Phi^m_{u,d} R^m_{u,d} \geq R^{\text{th}}, \quad \forall\ u \tag{5.36c}$$

$$\sum_d \sum_m \Phi^m_{u,d} \geq 1, \quad \forall\ u \tag{5.36d}$$

$$\mathbf{J}^{\min}_d \leq \mathbf{J}_d \leq \mathbf{J}^{\max}_d, \quad \forall\ d \tag{5.36e}$$

$$\sum_u \sum_m p^m_{u,d} \leq P^{\max}, \quad \forall\ d \tag{5.36f}$$

$$p^m_{u,d} \geq 0, \quad \forall\ u, d, m \tag{5.36g}$$

$$\sum_d \psi_{u,d} = 1 \quad \forall\ u \tag{5.36h}$$

$$\Phi^m_{u,d} \in \{0, 1\} \quad \forall\ d, \tag{5.36i}$$

Eq. (6.9a) represents the objective function where the first term is maximizing the minimum achievable rate of the UEs originally served by the failed GBS where Ω is an auxiliary continuous variable used to represent the maximization of the minimum achievable rate of the UEs. The second term aims to minimize the sum of the downlink transmission power of all UAVs given that $\Phi_{u,d}^{m}$ is the resource allocation binary variable which will equal to zero if sub-channel m is not used for the downlink transmission between DBS d and UE u. Constraint (5.36b) is the mathematical representation of max-min where we are trying to maximize Ω which is less than or equal the achievable rate of all UEs, i.e., maximizing the minimum rate. Constraint (5.36c) represents the QoS constraint on the rate of each UE, u, where R^{th} is the threshold rate. In constraint (5.36d), each UE is forced to acquire at least one sub-channel. Constraint (5.36e) is used to limit the 2D coordinates of DBS d where $\mathbf{J}_{d}^{\min} = [x_{d}^{\min}, y_{d}^{\min}]^{T}$ and $\mathbf{J}_{d}^{\max} = [x_{d}^{\max}, y_{d}^{\max}]^{T}$. The maximum and minimum power limits are presented in constraints (6.9k) and (5.36g). Constraint (6.9d) enforce each user to associated with only one DBS.

P1 is not easy to solve due to the following: 1) the decision variables $\Phi_{u,d}^{m}$ and $\psi_{u,d}$ are binary and thus the objective function (6.9a) and constraints (5.36b)-(5.36d) involve binary constraints which makes solving it a hard problem. 2) Even if we fixed the decision variables, constraints (5.36b) and (5.36c) are still non-convex with respect to DBS coordinates variable $\mathbf{J}_{d}$ and downlink power, $p_{u,d}^{m}$. Therefore, problem (6.9a) is mixed-integer non-linear non-convex problem, which is difficult to be solved optimally.

To make **P1** more tractable, we reformulate **P1** as follows:

$$(\mathbf{P2}): \underset{\mathbf{J},\Phi,\Psi,\mathbf{p}}{\text{maximize}} \quad \frac{\Omega}{R^{\text{th}}} - \frac{1}{P^{\max} * |\mathcal{D}|} \sum_{d} \sum_{u} \sum_{m} p_{u,d}^{m} \tag{5.37a}$$

subject to:

Constraints (5.36d) - (5.36i)

$$\Omega \geq R^{\text{th}} \tag{5.37b}$$

$$\sum_{d} \sum_{m} \log_2(1 + \frac{p_{u,d}^{m} \, \Gamma_{u,d}^{m}}{\sum\limits_{\substack{i \in \mathcal{U} \\ i \neq u}} \sum\limits_{j \in \mathcal{D}} p_{i,j}^{m} \Gamma_{u,j}^{m} + \sigma^2}) \geq \Omega, \quad \forall \; u \tag{5.37c}$$

$$p_{u,d}^{m} \leq \psi_{u,d} \Phi_{u,d}^{m} P^{\max}, \quad \forall \; u, d, m \tag{5.37d}$$

The main difference between **P2** and **P1** is that we added constraint (5.37d) to **P2** in addition to rewriting constraints (5.36b) and (5.36c). Constraint (5.37d) is used mainly to force $p_{u,d}^{m}$ to equal to zero if $\Phi_{u,d}^{m}$ and/or $\psi_{u,d}$ equal to zero. Consequently, there is no need to multiply the term $\psi_{u,d}\Phi_{u,d}^{m}$ by $p_{u,d}^{m}$ as done in the objective function of **P1**. The same concept apply to constraints (5.36b) and (5.36c) where when $\psi_{u,d}$ or $\Phi_{u,d}^{m}$ equals to zero then $p_{u,d}^{m}$ will equal to zero which consequently will result in $R_{u,d}^{m}$ equals to zero. Similarly, constraint (5.37d) is used to eliminate $\psi_{u,d}$ from constraints (5.36b) and (5.36c). Since Ω main purpose is to maximize the minimum achievable rate, then using the constraint $\Omega \geq R^{\text{th}}$ is doing the same purpose of constraint (5.36c). However in this case, we are guaranteeing that the minimum rate is greater than or equal a certain threshold.

Constraint (5.37d) is non-linear due to the multiplication of the two decision variables $\psi_{u,d}$ and $\Phi_{u,d}^{m}$. This constraint can be exactly linearized, i.e., without any approximation, by replacing it by the following three constraints:

$$p_{u,d}^{m} \leq \psi_{u,d} P^{\max}, \qquad \forall \; u, d, m \tag{5.38a}$$

$$p_{u,d}^{m} \leq \Phi_{u,d}^{m} P^{\max}, \qquad \forall \; u, d, m \tag{5.38b}$$

$$p_{u,d}^{m} \geq (\psi_{u,d} + \Phi_{u,d}^{m} - 1) P^{\max}, \qquad \forall \; u, d, m \tag{5.38c}$$

P2 is still not easy to solve due to the binary variables $\Phi_{u,d}^{m}$ and $psi_{u,d}$ and the non-linearity in constraint (5.37c). In addition, constraint (5.37c) has inside the logarithmic term two variables one in the numerator and the other in the denominator. However, **P2** is more tractable and easier to solve than **P1** given that **P2** is a new version of **P1** without any approximation.

5.2.5 The Proposed Solution

In general, **P2** has no standard method for solving it efficiently. In the following, we propose an efficient iterative algorithm for solving **P2**. Specifically, for a given coordinate $\mathbf{J}_d$, we optimize the decision variables $\Phi_{u,d}^{m}$ and $\psi_{u,d}$ and the continuous variable $p_{u,d}^{m}$ based on the Successive Convex Approximation (SCA) technique [97]. Then for a given resource allocation and power, we find the near optimal coordinates using heuristic iterative technique. Finally, a joint iterative algorithm is proposed to solve **P2** efficiently.

5.2.5.1 UAV Downlink Power and Resource Allocation

For any given coordinates, $\mathbf{J}_d$, the UAV downlink power and resource allocation of **P2** can be optimized by solving the following problem:

$$(\mathbf{P3}): \underset{\Phi_{u,d,m}, p_{u,d,m}}{\text{maximize}} \quad \frac{\Omega}{R^{\text{th}}} - \frac{1}{P^{\max} * |\mathcal{D}|} \sum_{d} \sum_{u} \sum_{m} p_{u,d,m} \tag{5.39}$$

subject to:

Constraints (5.36d), (6.9k) - (5.36i), (5.37b) - (5.37c), (6.11a) - (6.11c)

P3 is a non-convex optimization problem due to the non-convex constraint (5.37c). Based on the mathematical manipulation presented in [98], this constraint can be rewritten as:

$$\sum_{m}\Big(\underbrace{\log_2\big(\sum_{i\in\mathcal{U}}\sum_{j\in\mathcal{D}}p_{i,j}^{m}\Gamma_{u,j}^{m}+\sigma^2\big)}_{\tilde{R}_{u,m}^{1}}-\underbrace{\log_2\big(\sum_{\substack{i\in\mathcal{U}\\ i\neq u}}\sum_{j\in\mathcal{D}}p_{i,j}^{m}\Gamma_{u,j}^{m}+\sigma^2\big)}_{\tilde{R}_{u,m}^{2}}\Big)\geq\Omega,\quad\forall\ u \tag{5.40}$$

From Equation (6.14), it can be noticed that this is a difference of two concave functions, i.e., $\tilde{R}_{u,m}^{1}$ and $\tilde{R}_{u,m}^{2}$, with respect to the UAV downlink power. The difference between two concave functions is not guaranteed to be neither concave nor convex. This motivates us to approximate $\tilde{R}_{u,m}^{2}$. To convert constraint (5.37c) to a convex one, we apply the SCA technique to approximate $\tilde{R}_{u,m}^{2}$ by a linear/convex function in each iteration. Let $p_{u,d}^{m}(r)$ is the given UAV downlink power in the r-th iteration. Since any concave function is globally upper-bounded by its first-order Taylor expansion at any point [98]. Thus, the second term of Eq. (6.14), i.e., $\tilde{R}_{u,m}^{2}$, can be upper bounded as follows:

$$\begin{aligned}\tilde{R}_{u,m}^{2}=&\log_2\big(\sum_{\substack{i\in\mathcal{U}\\ i\neq u}}\sum_{j\in\mathcal{D}}p_{i,j}^{m}\Gamma_{u,j}^{m}+\sigma^2\big)\\ \leq&\sum_{\substack{i\in\mathcal{U}\\ i\neq u}}\sum_{j\in\mathcal{D}}\frac{\log_{\mathrm{e}}\Gamma_{u,j}^{m}}{\sum\limits_{\substack{i\in\mathcal{U}\\ i\neq u}}\sum\limits_{j\in\mathcal{D}}p_{i,j}^{m}(r)\Gamma_{u,j}^{m}+\sigma^2}(p_{u,d}^{m}-p_{u,d}^{m}(r))\\ &+\log_2\big(\sum_{\substack{i\in\mathcal{U}\\ i\neq u}}\sum_{j\in\mathcal{D}}p_{i,j}^{m}(r)\Gamma_{u,j}^{m}+\sigma^2\big)\\ \triangleq&\tilde{\tilde{R}}_{u,m}^{2}\end{aligned} \tag{5.41}$$

Hence, constraint (5.37c) is now convex and it can be written as follows:

$$\sum_{m} \left(\log_2 \left(\sum_{i \in \mathcal{U}} \sum_{j \in \mathcal{D}} p_{i,j}^{m} \Gamma_{u,j}^{m} + \sigma^2 \right) - \tilde{\tilde{R}}_{u,m}^{2} \right) \geq \Omega(r) \tag{5.42}$$

where $\Omega(r)$ is Ω at the r-th iteration. After converting constraint (5.37c) to a convex constraint, **P3** is now a convex optimization problem which can be solved efficiently.

5.2.5.2 UAV Placement

In this subsection, we consider optimizing the UAVs' locations for fixed UAV association, resource and power allocations. Due to the non-convexity of the problem even with fixed association, resource and power allocations, we introduce an efficient algorithm to find the optimal UAVs' placement $\mathbf{J}_d$.

The algorithm starts by dividing the desired area into equal sectors based on the number of the UAVs and each UAV is placed initially in the middle of the sector. Initially, we generate certain number of particles in each sector to identify promising candidates and to form initial populations. Then, it determines the objective function achieved by selected particles by solving **P3**. After that, it finds the particle that provides the highest solution for this iteration. Then, we generate a subset number of particles around this highest solution and calculate the objective function to find the best particle. This procedure is repeated until convergence or reach maximum iteration. To simplify the idea, this algorithm finds a candidate point among a large grid covering the disaster area. Hence, it finetunes by searching among a smaller grid surrounding each candidate point of the large grid until it finally finds the sub-optimal point which is the best point to minimize the objective function of **P3**.

The following algorithm is used to solve **P2** by jointly solving **P3** for fixed coordinates and then finding the sub-optimal placement of the cDBSs.

Algorithm 1 is an iterative efficient algorithm used to solve Problem **P2**. Line 1 initiate the iteration and termination conditions then lines 2-3 solve **P3** for fixed UAVs' location.

Algorithm 2: Joint optimization algorithm

Input: Initial positions for UAVs $\mathbf{J}_d(0)$
Output: $\mathbf{J}_d(r+1)$, $p^m_{u,d}(r+1)$, $\Phi^m_{u,d}(r+1)$

1: **while** Not converged or reach maximum iteration **do**
2: Solve **P3 for the given** $\mathbf{J}_d(r)$
3: **Denote results as** $p^m_{u,d}(r+1)$ **and** $\Phi^m_{u,d}(r+1)$
4: **Generate initial population** $\mathcal{L}$ **composed of** L **particles**
5: **for** $l = 1 \cdots L$ **do**
6: **Compute corresponding objective function of P2 given** $p^m_{u,d}(r+1)$ **and** $\Phi^m_{u,d}(r+1)$
7: **end for**
8: **Find** $(l_d^{\mathbf{r,local}}) = \arg\max_{l,d} \Omega^l - \sum_d \sum_u \sum_m p^m_{u,d}(l)$
9: **Generate a subset of particles around** $l_d^{\mathbf{r,local}}$
10: **Use shrink-and-realign sample spaces process to find the best solution i.e.,** $l_d^{\mathbf{r,sub\text{-}optimal}}$
11: $l_d^{\mathbf{r,local}} = l_d^{\mathbf{r,sub\text{-}optimal}}$, $\forall d$ **and** $\mathbf{J}_d(r+1) = l_d^{\mathbf{r,sub\text{-}optimal}}$
12: **Update r=r+1.**
13: **end while**

By fixing the placement of the UAVs and solving **P3** using successive convex approximation, then lines 4-7 generate particles and compute the objective function at each candidate point. From line 9 to 11 the algorithm finetunes the best placement by searching nearby for the best candidate and this is repeated at each iteration to find $l_d^{\mathrm{r,local}}$ which indicates the index of the best local particle that results in the highest objective function for iteration r.

5.2.5.3 System Model Assumptions

The proposed system model is considering the following assumptions:

- Macro-BSs in dense areas are pre-equipped with at least one DBS which is needed in the healing process.
- DBSs move from one location to another instantaneously. This assumption is used to simplify the optimization problem. Otherwise, a velocity/distance constrain must be added to the optimization problem to limit the distance that the DBS can move based on its maximum velocity.

- The helikite setup time is not considered in this model. In addition, the energy consumed to fill the helikite with helium is not considered.
- The number of UEs associated with the failed BS will not change until the DBSs or the helikite arrive(s) to the failure area.

5.2.6 Numerical Results

In this section, numerical results are provided to investigate the benefits of using UAVs in mitigating GBSs failure in 5G networks. The simulation model consists of 1 failed GBS. We consider short-term and long-term failures in our simulation given one failure at a time; The multiple failures at the same time scenario is considered as a disaster which is a different problem. Under the short-term failure scenario, we initialized 4 standby DBSs to be used in the mitigation process. However, in the long-term failure scenario, we use only one helikite. Simulation was carried out using General Algebraic Modeling System (GAMS) [109]. GAMS is a high-level modeling system for mathematical programming and optimization. It is designed for modeling and solving linear, nonlinear, and mixed-integer optimization problems. It consists of a language compiler and integrated high-performance solvers. GAMS is tailored for complex, large scale modeling applications, and allows to build large maintainable models that can be adapted quickly to new situations.

The simulation area is 400x400 m^2 where the failed BS is centered at the origin and the UEs of the failed BS are distributed randomly over this area. The UEs of the failed BS are static, however, the optimization problem is solved every time the distribution of the UEs is changed. The parameters used in the simulation are presented in Table II. Note that h^s denotes the height of the short-term UAVs, i.e., drones, and h^l denotes the height of the long-term UAVs, i.e., helikites.

In Fig. 5.6, we present the short-term and long-term failure mitigation performance by plotting the achievable downlink rate of all UEs versus the maximum power per DBS/Helikite, i.e., $P^{\max}$, in addition to varying the number of used DBSs in the short-term scenario for

Table 5.4: Simulation parameters (Section 5.2)

Parameter	**Value**	**Parameter**	**Value**
$P^{\max}$ (W)	1	$x_d^{\min}$ (m)	0
R^{th} (bps/Hz)	0.5	$x_d^{\max}$ (m)	400
h^s/h^l (m)	50/80	$y_d^{\min}$ (m)	0
$p_{u,d}^m(r)$ (W)	0.1	$y_d^{\max}$ (m)	400

the same UEs' distribution and the threshold rate, i.e., R^{th}. However intuitively increasing the number of used DBSs consumes more power for hovering and hardware, As $P^{\max}$ increases, the achievable rate of the UEs increases but levels of as the power reaches 1 W. This is because the objective function consists of two parts: 1) maximizing the minimum rate which guarantees fairness among all UEs, and 2) minimizing the downlink power of the DBSs/Helikite. It is worth noting that the excess power is only used to achieve the minimum rate requirement R^{th}.

The long-term scenario using 1 helikite results in the smallest rate. This is because the helikite altitude h^{l} is greater than the DBSs altitude h^{s} which consequently suffers from signal attenuation. Also, in the simulation and for comparison purposes, the maximum power of the helikite is set equal to that of the DBS. In reality, the helikite uses higher power levels, hence achieving higher rates.

Table III shows the association and UE power for both short-term and long-term scenarios. In case of long-term failure, the maximum power, $P^{\max}$, assigned to the helikite is 2.25 W. Since in this scenario we are using only one helikite, it is obvious that there is a high variety in power levels among different UEs. For example, UE3 has the least power, 0.108 W, and this implies that this UE is near to the helikite. Furthermore, UE8 and UE2 use around 40% of the helikite maximum power and this only happens in the case of the long-term failure since the helikite is covering the whole area of the failed GBS, hence satisfying the minimum rate of the far located UEs by increasing their transmission power. It is worth noting that the helikite is using its maximum power to serve its users. This implies

that although minimizing the power as one of the objectives of the optimization problem, the helikite still must satisfy the minimum rate requirements of all UEs where the main objective of the optimization problem is to find the best location that helps in satisfying the rate constraint of the UEs by using the minimum power.

In case of short-term failure, although there are 4 DBSs available/standby, only GBS1, GBS2 and GBS4 are used to serve all UEs as shown in Table III. Given that the maximum power for each DBS is 1 W, DBS1 and DBS2 utilize less than 50% of their maximum power since in this scenario not all UEs are associated with one UAV compared to the long-term scenario. The remaining power is not used since the minimum rate is already achieved beside the power minimization term used in the objective of the optimization problem. On the other hand, DBS4 utilized around 95% of its maximum power. The reason for that is that half of the UEs are associated with this DBS. If the number of UEs increased or if the threshold rate is raised, then the last DBS, i.e., DBS3, will start to be involved and then the optimization problem will be solved again.

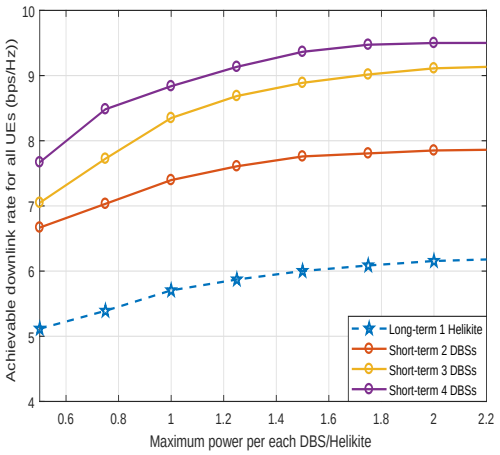

Figure 5.6: Achievable downlink rate for all UEs.

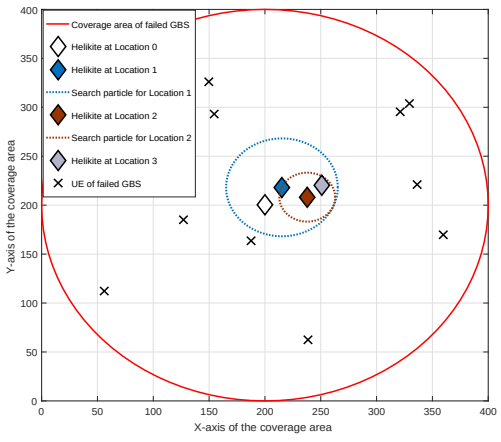

Figure 5.7: UAV placement algorithm with fine-tuning.

Finally, Fig. 5.7 investigates the long-term failure and its mitigation using one helikite. As shown in Algorithm 1, the initial position of the helikite is chosen to be in the center

Table 5.5: Association and power for 10 UEs

UEs	**Short-term**		**Long-term**	
	Association	$p_{u,d}$ (W)	**Association**	$p_{u,d}$ (W)
UE1	GBS4	0.156	Helikite	0.176
UE2	GBS1	0.147	Helikite	0.397
UE3	DBS4	0.105	Helikite	0.108
UE4	GBS2	0.197	Helikite	0.203
UE5	DBS4	0.130	Helikite	0.239
UE6	GBS1	0.132	Helikite	0.115
UE7	GBS4	0.171	Helikite	0.279
UE8	GBS2	0.121	Helikite	0.451
UE9	DBS4	0.164	Helikite	0.153
UE10	GBS1	0.139	Helikite	0.129

which is called location 0. Then the algorithm will find the best candidate location from l locations which is named as location 2. A new search area of radius 50m centered at location 2 is used to find the best candidate location and the same approach repeated to find the finetuned location, i.e., location 3, which is considered to be the near optimal placement of the helikite.

5.3 Chapter Summary

In this chapter, we presented two cell outage mitigation frameworks using flying BSs.

In the first framework, we proposed a novel cell outage compensation (COC) approach for 5G networks assisted by Drone Base-Stations (DBSs). The objective is to minimize the total energy consumption of the DBSs and Ground BSs (GBSs) while maintaining the minimum quality of service requirements of users originally served by the failed BS. DBSs are optimally managed in order to serve the users that can not be served by GBSs while considering DBSs consumed energy. The simulation results show how this hybrid COC approach outperforms the conventional COC approach. The proposed hybrid approach

shows significant impacts on ensuring connectivity of the users originally served by the failed BS while minimizing the number of used DBSs.

In the second framework, we proposed a novel self-healing framework for 5G networks assisted by two different types of UAVs to mitigate or at least alleviate the effect of any Ground base station (GBS) failure either if it is long-term or short-term failure. An optimization problem is formulated where its objective is to maximize the minimum achievable rate of the UEs under the failed BS by finding the optimal 2D placement of the UAVs in addition to minimizing the UAVs' downlink power. The UEs are served immediately after failure detection by the conventional self-healing technique until UAVs arrive to their initial positions.

Results show that the minimum rate requirement is guaranteed for each UE under the failed BS. In addition, fairness is guaranteed among them where the minimum achievable rate is maximized for all UEs. The behavior of UAVs shows that each UAV is detecting its 2D location to serve its UEs based on the minimum rate requirement, i.e., R^{th}. These results show the ability of self-healing framework to mitigate either long-term or short-term failures of any GBS in the upcoming 5G networks. Addressing multi-GBS failures and using realistic channel model which considers the probability of line-of-site are an interesting future research direction.

CHAPTER 6. POST-DISASTER 4G/5G NETWORK REHABILITATION USING DRONES

6.1 Introduction

Natural disasters always cause massive unpredictable loss to life and property. Various types of natural disasters, such as geophysical (earthquake), hydrological (flash-floods), climatological (wildfire) and meteorological (tropical storm), among others, have caused losses of many lives in addition to increase in material losses. This is why the occurrence of natural disasters is a terrible problem irritating the whole world including both developed and developing countries [110].

Currently, efforts are being made in three directions: 1) pre-disaster preparedness 2) disaster assessment 3) post-disaster response and recovery. The first two directions mainly depend on the recognition and forecast monitoring. The post-disaster stage mainly focuses on the rescue operation and facilitates the first responders' mission. In the USA, the Drone Integration Pilot Program was launched in November 2017 under presidential memorandum from the White House [111] to maximize the benefits of Unmanned Aerial Vehicles (UAVs) technologies for mitigating risks to public safety and security. This memorandum was issued after the successful mission of drones during the last two disasters: hurricane Irma in Florida and the wildfires in California. In Europe, ABSOLUTE project is aiming to use flying drones to enhance the ground network, especially for public safety and emergency situations [112].

Drone-based communications is considered as a strong candidate to be used regularly in 5G. Moreover, 3GPP is planning to support non-terrestrial networks, i.e., drones and

UAVs, in the second phase of the 5G new radio standard which is expected to appear in the 3GPP Rel-16 by mid-2019. Drone-based communications offers encouraging solutions to providing wireless connectivity for devices without infrastructure coverage due to, e.g., unexpected failures, or damage to the communication infrastructure caused by malicious actions or natural disasters [100].

There are two major ways to practically implement Drone BSs (DBSs) or relays; tethered and untethered DBSs. A tethered DBS means that a drone is connected by a cable that provides power and/or backhauling. Although it may sound uncanny for a drone to be tethered by a cable, this has many advantages such as a stable power source and hence unlimited flying time and ultra-high speed backhaul. All these advantages have encouraged well-known companies to test tethered DBSs, such as Facebook's "tether-Tenna", AT&T's "Flying Cell-On Wings (COWS)", and EE's, UK's largest cellular operator, "Air Masts" [113]. Such a tethering feature also limits the operations of DBSs to taking off, hovering and landing only which in some cases is useful as proposed later in this chapter.

On the other hand, untethered DBSs rely on the onboard battery for powering up the platform. Although untethered DBSs have limited flying time, they have fully controllable mobility in 3D space. Also, untethered DBS can adjust its placement based on users distribution [114]. In this chapter, we will show an effective way to overcome the limited battery of the untethered DBS.

In emergency zones, where the disaster causes total loss to the cellular infrastructure, the network has to be rapidly rehabilitated to facilitate and support the rescue operations of the first responders. We propose to use a grid of DBSs to cover the affected area to provide an alternate connectivity solution. By using the mentioned grid of DBSs, the main technical challenges to face are the difficulty to charge and backhaul these DBSs. Our proposed solution for the limited DBS battery issue is to use another drone to charge the DBSs on the fly. This special drone, we call it Powering Drone (PD), has on its platform a large capacity battery which is used to charge the DBSs on the fly. For solving the

backhaul issue, we propose to use a tethered Backhaul Drone (tBD) which is powered and backhauled via cabling. This tBD is used to provide backhauling to the DBSs grid via Free Space Optics (FSO)/RF hybrid link. In addition to solving these challenges, we introduce an optimization problem to minimize the energy consumption of the DBSs' network.

6.1.1 Literature Review

Coexistence of drone grid with a totally inactive cellular network in a post-disaster situation has not been sufficiently investigated especially the unexplored issues: battery recharging and backhauling.

The authors in [115] used UAVs in disaster-resilience where they present a disaster-struck scenario where all terrestrial BSs are inactive. They used two UAVs to cover 50 users. They presented the trade-off between the altitude, beamwidth angles and the coverage area of the UAVs. However, the authors in [117] are using drones to manage disasters via various tasks. They use drones to capture a full up-to-date 3D terrain elevation model of the affected area. They also use drones to place sensors in that area to create an efficient wireless sensor network to aid first responders.

The authors in [107] present a novel framework to mitigate the effect of the failure of any BS in 5G networks using both DBSs and ground BSs. They showed that their proposed hybrid approach outperforms the conventional BS failure approach. In [108], a vertical backhaul/fronthaul framework is suggested for transporting the traffic between the access and core networks in a typical HetNet through FSO links. 3D placements of drone-BSs are considered as one of the important problems to design and implement drone-BS enabled HetNets.

6.2 System Architecture

We consider a geographical area that experienced a natural disaster where 100% of its terrestrial cellular network is out of service. A grid of drones is used to provide cellular

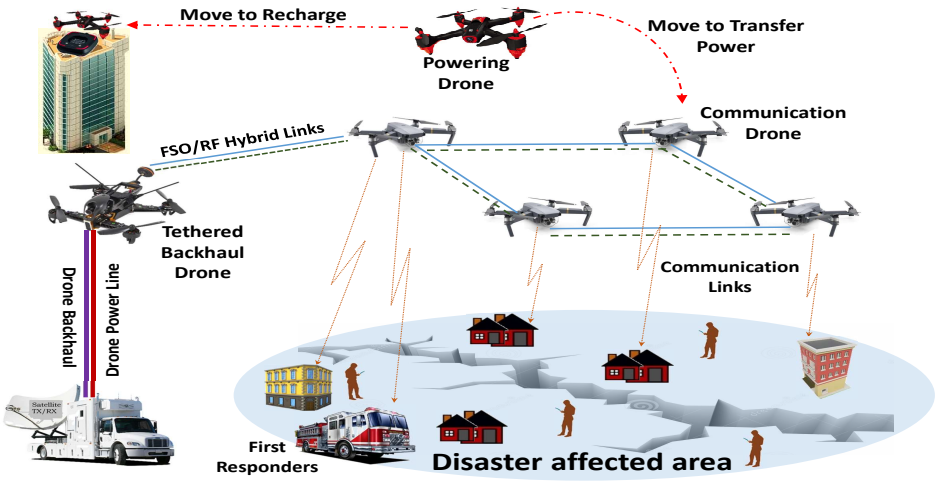

Figure 6.1: System model during post-disaster rehabilitation.

coverage to the affected area where drones are connected to each other using hybrid FSO/RF links and one of the DBSs acquires the backhaul connection from a post-disaster tBD installed hundred of meters from the disaster area [116].

Fig. 6.1, shows the topology of the network during the post-disaster period. Upon the failure of the terrestrial BSs, the DBSs will fly to their initial positions to cover the whole footprint of the affected area. There are three types of drones: 1) tethered Backhaul Drone (tBD), 2) Powering Drone (PD), and 3) communication Drone BSs. The tBD provides the connectivity to the core network to the whole flying network via hybrid FSO/RF links. It also co-locates a central controller to manage and control this flying cellular network. The PD is mainly used to charge the cDBSs on the fly. This means that the cDBSs do not have to leave their locations to recharge their batteries. Finally, the cDBSs are used mainly to construct the flying cellular network to provide connectivity to first responders and users in the disaster area [116].

6.2.1 cDBSs Backhauling

During and post-disaster and especially when the whole cellular infrastructure is destroyed, the only available backhaul connection can be acquired from the satellite. However, in drone-based communications, it is impossible to equip the drone platform with satellite transceiver equipment. In our proposed solution and as it appears in Fig. 6.1, we propose using a tBD which is powered and backhauled using a cable and this cable is connected to a special truck which is pre-equipped with satellite transceiver equipment to connect the drone cellular infrastructure to the core network. Also, this truck acts as a power supply which provides unlimited flying time to the tBD.

The tBD provides backhauling to the DBSs grid via FSO/RF hybrid link. FSO has been constantly claimed to be the alternative wireless technology of the future that provides unlimited bandwidth. However, FSO is sensitive to atmospheric conditions apart from precipitation. A solution to such a problem is to introduce a secondary wireless channel which is less affected by such conditions like radio frequency (RF) transmission. Commercial hybrid FSO/RF systems have already made their presence using a combination of millimeter Wave (mmW) and laser-based FSO that allows more than 1 Gbps data transmission over many kilometers of distance.

Reference [118] analyze the performance of the FSO/RF systems. In [108], the authors investigate the feasibility of a novel vertical backhaul framework where the UAVs transport the backhaul traffic between the access and core networks via FSO links. Simulations have shown that the performance can be improved significantly and rates in the order of multi Gbits/s can be achieved by a careful design of the FSO framework.

6.2.2 Drones Battery Charging

From Fig. 6.1, it can be noticed that we have three type of drones: 1) tethered Backhaul Drone (tBD), 2) untethered PD and 3) untethered cDBS. The tBD is power supplied directly from the ground using a cable which allow it to fly 24/7 continuously. The PD carries a large

capacity battery, usually double the capacity of cDBS. This battery is used mainly to charge the untethered cDBSs whenever their batteries' charge is less than a certain threshold. The PD returns to its docking station to charge its battery while a replacement PD takes over the charging role so that the charging process will be available without any discontinuity. Finally, the untethered cDBS will have unlimited flying time due to the charge on the fly property provided by the PD. It is worth noticing that the charging process can be 1) wired charging and 2) inductive wireless charging. The wired charging has very high efficiency but it still needs special alignment technology between drones on the fly. The inductive wireless charging does not require physical contact since it can achieve an efficiency of 75% given that the distance is within few inches. Hence, we consider the wired charging using advanced alignment techniques due to its high efficiency (almost 100%).

6.3 Problem Formulation

In this architecture, a set $\mathcal{D} = \{1, 2, \ldots, D\}$ of cDBSs are used to provide the needed coverage to the affected area. These cDBSs can dynamically move, when needed, to effectively mitigate the effect of the cellular infrastructure failure. The set $\mathcal{U} = \{1, 2, \ldots, U\}$ denotes the set of active UEs within the affected area and they are at known locations where the horizontal coordinate of each UE u is fixed at $\mathbf{g}_u = [x_u, y_u]^T$, $u \in U$. All DBSs are assumed to navigate at a fixed altitude h and the horizontal coordinate of DBS, d, at discrete time block n where $n = 1, ..., N$ is denoted by $\mathbf{J}_d^n = [x_d^n, y_d^n]^{\mathrm{T}}$ where N is a total discrete period where n are time blocks of equal duration T_n and the total time is given by T. The time blocks are relatively long as compared to the channel coherence time, hence we are dealing with minutes not seconds.

Assume that the DBS-UE communication channels are dominated by Line-of-Site (LoS) links. Though simplified, the LoS model offers a good approximation for practical Drone-UE channels. Under the LoS model, the Drone-UE channel power gain follows the free space path loss model which is determined mainly by the DBS-UE distance. Given that $\mathbf{J}_d^n$ and

$\mathbf{g}_u$ are the coordinates of DBS, d, and UE u in the horizontal plane, respectively, then the distance from DBS, d, to UE u during time block n is given as $\delta^n_{u,d} = \sqrt{h^2 + ||\mathbf{J}^n_d - \mathbf{g}_u||^2}$.

6.3.1 cDBS Channel and Achievable Rate Models

The DBS-UE channel power gain mainly follows the free space path loss model which is given as follows:

$$\Gamma^n_{u,d} = \rho_o(\delta_0/\delta^n_{u,d})^2 = \frac{\rho_o}{h^2 + ||\mathbf{J}^n_d - \mathbf{g}_u||^2} \tag{6.1}$$

where ρ_o is a unitless constant that depends on the antenna characteristics and frequency, and is measured at the reference distance $\delta_0 = 1$ m and $\delta^n_{u,d})^2$ is the square of the Euclidean distance between cDBS d and user u.

Let $\mathcal{M} = \{1, 2, \ldots, M\}$ be the set of sub-channels that each DBS can use during the rehabilitation process. These sub-channels will be further divided and allocated to the UEs associated with each DBS. Each DBS, d, transmits to each UE, u, with a per sub-channel transmit power $p^n_{u,d,m}$. If sub-channel m is not assigned to DBS, d, then $p^n_{u,d,m}$ will equal to zero. We consider the interference between different DBSs. Hence, the SINR between DBS, d, and UE u per sub-channel m during time block n can be expressed as:

$$\begin{aligned}\gamma^n_{u,d,m} &= \frac{p^n_{u,d,m}\,\Gamma^n_{u,d}}{\sum\limits_{\substack{i\in\mathcal{U}\\ i\neq u}}\sum\limits_{j\in\mathcal{D}} p^n_{i,j,m}\Gamma^n_{u,j} + \sigma^2} \\ &= \frac{\frac{p^n_{u,d,m}\ \rho_o}{h^2+||\mathbf{J}^n_d-\mathbf{g}_u||^2}}{\sum\limits_{\substack{i\in\mathcal{U}\\ i\neq u}}\sum\limits_{j\in\mathcal{D}} \frac{p^n_{i,j,m}\ \rho_o}{h^2+||\mathbf{J}^n_j-\mathbf{g}_u||^2} + \sigma^2}\end{aligned} \tag{6.2}$$

where σ^2 is the power of the Additive White Gaussian Noise at the receiver. The first term in the denominator of equation (6.2) represents the co-channel interference caused by the transmissions of all other DBSs on the same sub-channel m, respectively.

Accordingly, the achievable downlink rate from DBS, d, to UE, u, is given by:

$$R^n_{u,d,m} = \log_2(1 + \gamma^n_{u,d,m}) \tag{6.3}$$

6.3.2 Drone Battery Energy Consumption Model

In our proposed solution we have two types of untethered drones: 1) PD and 2) cDBS. Both of them consume hovering and hardware powers. We denote that the speed of the DBS d in time block n denoted by v_d^n. The hovering and hardware drone energy levels, denoted by E_{hov} and $E_{\text{har},d}^n$, can be expressed, respectively, as [96]:

$$E_{\text{har},d}^n = \left[\frac{P_{\text{full}} - P_{\text{idle}}}{v_{\max}} v_d^n + P_{\text{idle}}\right](T_{\text{move}}) \tag{6.4}$$

$$E_{\text{hov}} = \sqrt{\frac{(m_{\text{tot}} g)^3}{2\pi r_p^2 n_p \rho}}\ (T - T_{\text{move}}) \tag{6.5}$$

where m_{tot}, g, and ρ are the drone mass in (Kg), earth gravity in (m/s^2), and air density in (Kg/m^3), respectively. r_p and n_p are the radius and the number of the drone's propellers, respectively. $v_{\max}$ is the maximum speed of the drone. P_{full} and P_{idle} are the hardware power levels when the drone is moving at full speed and when the drone is in idle mode, respectively. T_{move} is the time used by cDBS to move from one location to another.

Hence, the total energy consumed by all the untethered cDBSs is the total transmission energy added up with the hovering and hardware energies which is given as:

$$E = \sum_d \sum_u \sum_m \sum_n p_{u,d,m}^n\ T + \sum_d \sum_n \left[E_{\text{har},d}^n + E_{\text{hov}}\right] \tag{6.6}$$

Given that the initial battery level DBS, d, is B_0, hence, the battery level of DBS, d, at time block n is given by:

$$\begin{aligned} B_d^n = B_0 - \sum_{i=1}^{n} \left[E_{\text{har},d}^i + E_{\text{hov}} + \sum_u \sum_m p_{u,d,m}^i\ T\right] \\ + \sum_d \sum_{i=1}^{n} \beta_d^i (B_{\text{charge}}) \end{aligned} \tag{6.7}$$

where β_d^n is a decision variable indicating whether PD is going to charge DBS, d, during time block n or not. B_{charge} represents the amount of charge that DBS, d, will receive from PD during one time block.

The PD battery model is different since it is not used for communication. Hence, it is given by:

$$B^n_{\text{PD}} = B_{00} - \sum_{i=1}^{n} \left[E^i_{\text{har},d} + E_{\text{hov}}\right] - \sum_{d} \sum_{i=1}^{n} \beta^i_d(B_{\text{charge}}) \tag{6.8}$$

where B_{00} is the initial battery charge of PD. The term $\sum_d \sum_{i=1}^{n} \beta^i_d(B_{\text{charge}})$ represents the consumed energy up to time block n used to charge the cDBSs given that at most one cDBS is charged in each time block. Note that m_{tot} in case of PD is greater than that of cDBS because PD is carrying a large capacity battery.

6.4 The Optimization Problem

In emergency zones, where the disaster causes total loss to the cellular infrastructure, the network has to be rapidly rehabilitated to facilitate and support the rescue operations of the first responders. This is the motivation behind formulating an optimization problem that will maintain the operation of the flying cellular infrastructure.

To mitigate or at least alleviate the effect of the disaster and facilitate the mission of the first responders, We formulate an optimization problem which mainly have three types of drones; PD, tBD, and cDBSs, aiming to construct a flying cellular infrastructure capable of operating for extended period of time or until the ground cellular network is maintained and ready to serve its users. The extended operation of the flying cellular infrastructure is guaranteed by minimizing the network's energy consumption during n time blocks. Energy minimization metric reduces at maximum the use of untethered DBSs and hence send them only when needed.

We assume that initially the battery of the PD or the DBS is fully charged. We also assume that the PD can be replaced with another PD at the docking/charging station. This means that the PD is always available to charge cDBSs. Defining the decision variables: $\psi^n_{u,d}$ as the user association between user u and cDBS d during time block n and $\Phi^n_{u,d,m}$ as the resource m allocation to user u by cDBS d during time block n. Hence, the optimization

problem which aims to minimize the total energy consumption of the untethered cDBSs while maintaining a minimum quality of service, i.e., minimum rate, for the users in the disaster area is given as:

$$(\mathbf{P1}): \underset{\mathbf{v},\mathbf{J},\Phi,\Psi,\mathbf{p}}{\text{minimize}} \sum_{d}\sum_{u}\sum_{m}\sum_{n} \psi^n_{u,d}\ \Phi^n_{u,d,m}\ p^n_{u,d,m}\ T + \sum_{d}\sum_{n}\left[E^n_{\text{har},d} + E_{\text{hov}}\right] \tag{6.9a}$$

subject to:

$$\sum_{d}\sum_{m} \psi^n_{u,d}\Phi^n_{u,d,m}R^n_{u,d,m} \geq R^{\text{th}}, \qquad \forall\ u,n \tag{6.9b}$$

$$\sum_{u}\sum_{d}\sum_{m} \psi^n_{u,d}\Phi^n_{u,d,m}R^n_{u,d,m} \leq R^{\text{BH}}, \quad \forall\ n \tag{6.9c}$$

$$\sum_{d} \psi^n_{u,d} = 1, \qquad \forall\ u,n \tag{6.9d}$$

$$\sum_{d}\sum_{m} \Phi^n_{u,d,m} \geq 1, \qquad \forall\ u,n \tag{6.9e}$$

$$\beta^n_d \geq \frac{B^{\text{th}} - B^n_d}{Q}, \qquad \forall\ d,n \tag{6.9f}$$

$$\beta^n_d \leq \frac{B^{\text{th}}}{B^n_d}, \qquad \forall\ d,n \tag{6.9g}$$

$$\mathbf{J}^{\min}_d \leq \mathbf{J}^n_d \leq \mathbf{J}^{\max}_d, \qquad \forall\ d,n \tag{6.9h}$$

$$||\mathbf{J}^n_d - \mathbf{J}^{n-1}_d|| = v^n_d\ T_{\text{move}}, \qquad \forall\ d,n \tag{6.9i}$$

$$0 \leq v^n_d \leq v^{\max}, \qquad \forall\ d,n \tag{6.9j}$$

$$\sum_{u}\sum_{m} p^n_{u,d,m} \leq P^{\max}, \qquad \forall\ d,n \tag{6.9k}$$

$$p^n_{u,d,m} \geq 0, \qquad \forall\ u,d,m \tag{6.9l}$$

$$\psi^n_{u,d},\ \Phi^n_{u,d,m}\ , \beta^n_d \in \{0,1\} \qquad \forall\ u,d,m,n \tag{6.9m}$$

Constraint (6.9b) represents the QoS constraint on the rate of each use, u, where R^{th} is the threshold rate. In constraint (6.9c), we are ensuring that the total rate of all users is less than or equal the backhaul capacity of the tBD. Constraint (6.9d) is limiting the association of each user to one cDBS only during each time block where $\psi^n_{u,d}$ is the association between cDBS d and user u during time block n. Constraint (6.9e) guarantees that each user is

getting at least one resource block. Constraints (6.9f) and (6.9g) together are enforcing β_d^n to equal to 1 if the PD is going to charge cDBS, d, during time block, n where Q is a very large number. This enforcement occurs if $B_d^n \leq B^{\text{th}}$ where B^{th} is a certain battery level at which cDBS needs to be charged. Constraint (6.9h) is limiting all cDBSs to fly within the disaster region. However, constraint (6.9i) controls the velocity of cDBS d based on the displacement of this cDBS. Then constraint (6.9j) is limiting the velocity of the cDBSs. Finally, constraints (6.9k) and (6.9l) provides the minimum and maximum power limits of each cDBS.

P1 is not easy to solve due to the following: 1) the decision variables $\Phi_{u,d}^m$, $\psi_{u,d}$ and β_d^n are binary and thus the objective function (6.9a) and constraints (6.9b)-(6.9g) involve binary constraints which makes solving it a hard problem. 2) Even if we fixed the decision variables, objective function (6.9a), constraints (6.9b) and (6.9c) are still non-convex with respect to cDBS coordinates variable $\mathbf{J}_d$ and downlink power, $p_{u,d}^m$. Therefore, problem (6.9a) is mixed-integer non-linear non-convex problem, which is difficult to be solved optimally.

To make **P1** more tracktable, we propose to add the following constraint to **P1**:

$$p_{u,d}^m \leq \psi_{u,d} \Phi_{u,d}^m P^{\max}, \quad \forall\ u, d, m \tag{6.10}$$

Constraint (6.10) is used mainly to force $p_{u,d,m}^n$ to equal to zero if $\Phi_{u,d,m}^n$ and/or $\psi_{u,d}^n$ equal to zero. Consequently, there is no need to multiply the term $\psi_{u,d}^n \Phi_{u,d,m}^n$ by $p_{u,d,m}^n$ as done in the objective function. The same concept applies to constraints (6.9b) and (6.9c) where when $\psi_{u,d}$ or $\Phi_{u,d}^m$ equals to zero then $p_{u,d}^m$ will equal to zero which consequently will result in $R_{u,d}^m$ equals to zero.

Although adding constraint (6.10) to **P1** will remove the non-linearity from the objective function, (6.9a), the constraint itself is non-linear which will increase the complexity of the problem. But fortunately, this constraint can be linearized since the non-linearity is coming from multiplying three variables, one of them is continuous and the other two are binary. The lumbarization process will result in three linear constraints which are equivalent to

the original non-linear constraint. Note that this is exactl linearized, i.e., without any approximation. this is done by replacing the non-linear constraint by the following three constraints:

$$p^n_{u,d,m} \leq \psi^n_{u,d}\ P^{\max}, \qquad \forall\ u,d,m,n \tag{6.11a}$$

$$p^n_{u,d,m} \leq \Phi^n_{u,d,m}\ P^{\max}, \qquad \forall\ u,d,m,n \tag{6.11b}$$

$$p^n_{u,d,m} \geq (\psi^n_{u,d} + \Phi^n_{u,d,m} - 1)\ P^{\max}, \qquad \forall\ u,d,m,n \tag{6.11c}$$

After adding the new constraints and eliminating the non-linearity from the objective function of **P1** and eliminating $\psi^n_{u,d}$ and $\Phi^n_{u,d,m}$ from constraints (6.9b) and (6.9c) and expanding $R^n_{u,d,m}$, we introduce **P2** which is a modified, non approximated, version of **P1** which is given as follows:

$$(\mathbf{P2}): \underset{\mathbf{v},\mathbf{J},\Phi,\Psi,\mathbf{p}}{\text{minimize}} \sum_d \sum_u \sum_m \sum_n p^n_{u,d,m}\ T + \sum_d \sum_n \left[E^n_{\text{har},d} + E_{\text{hov}}\right] \tag{6.12a}$$

subject to:

Constraints (6.9d) - (6.9m), (6.11a)-(6.11c)

$$\sum_d \sum_m \log_2\Big(1 + \frac{p^n_{u,d,m}\ \Gamma^n_{u,d}}{\sum\limits_{\substack{i\in\mathcal{U}\\ i\neq u}} \sum\limits_{j\in\mathcal{D}} p^n_{i,j,m}\Gamma^n_{u,j} + \sigma^2}\Big) \geq R^{\text{th}}, \qquad \forall\ u,n \tag{6.12b}$$

$$\sum_u \sum_d \sum_m \log_2\Big(1 + \frac{p^n_{u,d,m}\ \Gamma^n_{u,d}}{\sum\limits_{\substack{i\in\mathcal{U}\\ i\neq u}} \sum\limits_{j\in\mathcal{D}} p^n_{i,j,m}\Gamma^n_{u,j} + \sigma^2}\Big) \leq R^{\text{BH}}, \forall\ n \tag{6.12c}$$

P2 is still not easy to solve due to the binary variables $\Phi^m_{u,d}$ and $\psi_{u,d}$ and the non-linearity in constraints (6.12b) and (6.12c). In addition, these two constraints have inside the logarithmic term two variables, $p^n_{u,d,m}$ and J^n_d, one in the numerator and the other in the denominator.

For simplicity and given that the tBD has high speed backhaul wired link, we will consider that the backhaul rate is always greater than the sum rate of all users.

This simplicity assumption is supported by the simulation results from [108] which have shown that rates in the order of multi Gbits/s can be achieved by a careful design of the FSO

framework. In addition, we claim that post-disaster users are not using high bandwidth application(s) during this hard situation. Hence, we can ignore constraint (6.12c).

6.5 The Proposed Solution

In general, **P2** has no standard method for solving it efficiently. In the following, we propose an efficient iterative algorithm for solving **P2**. Specifically, for a given coordinate $\mathbf{J}_d$, we optimize the decision variables β_d^n, $\Phi_{u,d}^m$ and $\psi_{u,d}$ and the continuous variable $p_{u,d,m}^n$ based on the Successive Convex Approximation (SCA) technique [97]. Then for a given decision variables and power, we find the cDBSs coordinates using the same technique. Finally, a joint iterative algorithm is proposed to solve **P2** efficiently.

6.5.1 Solving for cDBS Power and Decision Variables

For any given coordinates, $\mathbf{J}_d$, the cDBS downlink power and decision variables of **P2** can be optimized by solving the following problem:

$$(\mathbf{P3}): \underset{\mathbf{v},\Phi,\Psi,\mathbf{p}}{\text{minimize}} \sum_{d}\sum_{u}\sum_{m}\sum_{n} p_{u,d,m}^{n}\ T + \sum_{d}\sum_{n}\left[E_{\text{har},d}^{n} + E_{\text{hov}}\right] \tag{6.13}$$

subject to:

Constraints (6.9d) - (6.9m), (6.11a) - (6.11c), (6.12b)

P3 is a non-convex optimization problem due to constraint (6.12b) which is non-convex. Based on the mathematical manipulation presented in [98], this constraint can be rewritten as:

$$\sum_{m}\Big[\underbrace{\log_2\big(\sum_{i\in\mathcal{U}}\sum_{j\in\mathcal{D}} p_{i,j,m}^{n}\Gamma_{u,j}^{n}+\sigma^2\big)}_{\tilde{R}_{u,m,n}^{1}} - \underbrace{\log_2\big(\sum_{\substack{i\in\mathcal{U}\\ i\neq u}}\sum_{j\in\mathcal{D}} p_{i,j,m}^{n}\Gamma_{u,j}^{n}+\sigma^2\big)}_{\tilde{R}_{u,m,n}^{2}}\Big] \geq R^{\text{th}}, \quad \forall\ u \tag{6.14}$$

From constraint(6.14), it can be noticed that this is a difference of two concave functions, with respect to the cDBS downlink power. The difference between two concave functions is not guaranteed to be neither concave nor convex. This motivates us to approximate $\tilde{R}^2_{u,m}$. To convert constraint (6.14) to a convex one, we apply the SCA technique to approximate $\tilde{R}^2_{u,m,n}$ by a linear function in each iteration. Let $p^n_{u,d,m}(r)$ is the given cDBS power in the r-th iteration. Since any concave function is globally upper-bounded by its first-order Taylor expansion at any point [98]. Thus, the second term of Eq. (6.14), can be upper bounded as follows:

$$\begin{aligned}\tilde{R}^2_{u,m,n} =& \log_2\Big(\sum_{\substack{i\in\mathcal{U}\\ i\neq u}}\sum_{j\in\mathcal{D}} p^n_{i,j,m}\Gamma^n_{u,j}+\sigma^2\Big)\\ \leq& \sum_{\substack{i\in\mathcal{U}\\ i\neq u}}\sum_{j\in\mathcal{D}} \frac{\log_{\mathrm{e}}\Gamma^n_{u,j}\ (p^n_{u,d,m}-p^n_{u,d,m}(r))}{\sum\limits_{\substack{i\in\mathcal{U}\\ i\neq u}}\sum\limits_{j\in\mathcal{D}} p^n_{i,j,m}(r)\Gamma^n_{u,j}+\sigma^2}\\ &+\log_2\Big(\sum_{\substack{i\in\mathcal{U}\\ i\neq u}}\sum_{j\in\mathcal{D}} p^n_{i,j,m}(r)\Gamma^n_{u,j}+\sigma^2\Big) \triangleq \tilde{\tilde{R}}^2_{u,m,n}\end{aligned} \tag{6.15}$$

Constraint (6.12b) is now convex and it can be rewritten as:

$$\sum_m \Big(\log_2\Big(\sum_{i\in\mathcal{U}}\sum_{j\in\mathcal{D}} p^n_{i,j,m}\Gamma^n_{u,j}+\sigma^2\Big)-\tilde{\tilde{R}}^2_{u,m,n}\Big)\geq R^{\mathrm{th}}(r) \tag{6.16}$$

where $R^{\mathrm{th}}(r)$ is R^{th} at the r-th iteration. After converting constraint (6.12b) to a convex constraint, **P3** is now a convex which can be solved efficiently.

6.5.2 Solving for cDBS Coordinates

For any given decision variable, the DBS coordinates $\mathbf{J}^n_d$ can be optimized by solving the following problem:

$$(\mathbf{P4}): \underset{\mathbf{J}}{\text{minimize}} \sum_{d}\sum_{u}\sum_{m}\sum_{n} p^{n}_{u,d,m}\ T + \sum_{d}\sum_{n}\left[E^{n}_{\text{har},d} + E_{\text{hov}}\right] \tag{6.17}$$

subject to:

$$\sum_{d}\sum_{m}\log_2\Big(1+\frac{\frac{p^{n}_{u,d,m}\ \rho_o}{h^2+||\mathbf{J}^{n}_{d}-\mathbf{g}_u||^2}}{\sum\limits_{\substack{i\in\mathcal{U}\\ i\neq u}}\sum\limits_{j\in\mathcal{D}}\frac{p^{n}_{i,j,m}\ \rho_o}{h^2+||\mathbf{J}^{n}_{j}-\mathbf{g}_u||^2}+\sigma^2}\Big) \geq R^{\text{th}}, \qquad \forall\ u,n \tag{6.18}$$

$$\mathbf{J}^{\min}_{d} \leq \mathbf{J}^{n}_{d} \leq \mathbf{J}^{\max}_{d}, \qquad \forall\ d,n \tag{6.19}$$

The objective function and constraint (6.19) are convex. However constraint (6.18) is neither concave nor convex with respect to the DBSs' coordinates. Using SCA in this case is not optimally efficient since we have to linearize both logarithmic functions if we expanded (6.19) in the same way of constraint (6.14). It is proved in [98] that linearizing/convexifying this constraint is not an easy in general. This motivates us to find the cDBSs' coordinates using the following heuristic approach.

Due to the non-convexity of the problem even with fixed decision variables and downlink power, we introduce an efficient algorithm to find the optimal cDBSs' coordinates, $\mathbf{J}_d$.

The algorithm starts by dividing the desired area into equal sectors based on the number of the cDBSs and each cDBS is placed initially in the middle of the sector. Then we generate certain number of particles in each sector to identify promising candidates and to form initial populations. Then, it determines the objective function achieved by selected particles by solving **P3**. After that, it finds the particle that provides the highest solution for this iteration. Then, we generate a subset number of particles around this highest solution and calculate the objective function to find the best particle. This procedure is repeated until convergence or reach maximum iteration.

Algorithm 1 is an iterative efficient algorithm used to solve Problem **P2**. Line 1 initiate the iteration and termination conditions. Lines 2-4 used to replace PD if its battery level is below the threshold then lines 5-7 make sure that the PD is charging only 1 DBS at each time block. Lines 8-9 solve **P3** for fixed cDBSs' location. By fixing the coordinates of

Algorithm 3: Joint optimization algorithm

Input: Initial positions for UAVs $\mathbf{J}_d^n(0)$

Output: $\mathbf{J}_d^n(r+1)$, $\psi_{u,d}^n(r+1)$, $\Phi_{u,d,m}^n(r+1)$, $\beta_d^n(r+1)$, $p_{u,d,m}^n(r+1)$, $v_d^n(r+1)$

1: **while** Not converged or reach maximum iteration **do**
2: **if** $B_{\text{PD}}^n \leq B_{\text{PD}}^{\text{th}}$ **then**
3: Replace PD
4: **end if**
5: **if** $\sum_d \beta_d^n \geq 2$ **then**
6: Choose cDBS d randomly to be charged
7: **end if**
8: Solve **P3 for the given** $\mathbf{J}_d^n(r)$
9: **Denote results as** $p_{u,d,m}^n(r+1)$ **and** $\Phi_{u,d,m}^n(r+1)$
10: **Generate initial population** $\mathcal{L}$ **composed of** L **particles**
11: **for** $l = 1 \cdots L$ **do**
12: **Compute corresponding objective function of P4 given** $\psi_{u,d}^n(r+1)$, $\Phi_{u,d,m}^n(r+1)$, $\beta_d^n(r+1)$, $p_{u,d,m}^n(r+1)$, $v_d^n(r+1)$
13: **end for**
14: **Find** $(l_d^{\mathbf{r,local}}) = \arg\min_{l,d} \sum_d \sum_u \sum_m \sum_n p_{u,d,m}^n \, T + \sum_d \sum_n \left[E_{\mathbf{har},d}^n + E_{\mathbf{hov}}\right]$
15: **Generate a subset of particles around** $l_d^{\mathbf{r,local}}$
16: **Use shrink-and-realign sample spaces process to find the best solution i.e.,** $l_d^{\mathbf{r,sub\text{-}optimal}}$
17: $l_d^{\mathbf{r,local}} = l_d^{\mathbf{r,sub\text{-}optimal}}$, $\forall d$ **and** $\mathbf{J}_d^n(r+1) = l_d^{\mathbf{r,sub\text{-}optimal}}$
18: **Update r=r+1.**
19: **end while**

the cDBSs and solving **P3** using SCA, then lines 10-13 generate particles and compute the objective function at each candidate point. From line 15 to 17 the algorithm finetunes the best placement by searching nearby particles for the best candidate coordinate and this is repeated at each iteration to find $l_d^{\text{r,local}}$ which indicates the index of the best local particle that results in the highest objective function for iteration r.

6.5.3 System Model Assumptions

The proposed system model is considering the following assumptions:

- The tBD is capable of flying continuously without landing given that it has an unlimited source of power.
- The cellular users in the disaster area are not assumed to use high bandwidth consuming applications. Hence, the backhaul constraint can be ignored.

Table 6.1: Simulation parameters (Section 6.6)

Parameter	Value	Parameter	Value	Parameter	Value
$P_{\max}$ (W)	1	$x_d^{\min}$ (m)	-400	T (minute)	48
$P^n_{u,d,m}(r)$ (W)	0.1	$x_d^{\max}$ (m)	400	T_n (minute)	8
R^{th} (bps/Hz)	0.5	$y_d^{\min}$ (m)	-400	T_{move} (sec)	30
R^{BH} (bps/Hz)	10	$y_d^{\max}$ (m)	400	B_0 (kJ)	200
N	6	h (m)	100	B_{00} (kJ)	400
ρ_o	0.01	$v^{\max}$ (m/s)	20	B_{charge} (kJ)	25%B_0
Q	10^6	B^{th} (kJ)	100	$B^{\text{th}}_{\text{PD}}$(kJ)	100

- The special alignment needed for the on-the-fly charging process between PD and cDBS is assumed to be done instantaneously.
- The PD is not carrying any cellular equipment, however, it carries simple transceiver to communicate with cDBSs for the charging process coordination.

6.6 Numerical Results

In this section, numerical results are provided to investigate the benefits of using cDBSs in mitigating disaster effects. The simulation area is 800x800 m^2 where the users are distributed randomly over this area given that all terrestrial ground BSs are inactive. Under the post-disaster scenario, we initialized 4 standby cDBSs to be used in the mitigation process. We use two PD where one is active and the other is standby in case its battery is depleted. Simulation was carried out using General Algebraic Modeling System (GAMS) https://www.gams.com/. GAMS is a high-level modeling system for mathematical programming and optimization. It is designed for modeling and solving linear, nonlinear, and mixed-integer optimization problems. It is tailored for complex, large scale modeling problems, and allows to build large models. The parameters used in the simulation are presented in Table II. Also, the parameters of E_{hov} and E_{har} can be found in [96] given that m_{tot} for PD is double that of cDBS.

The battery specifications of cDBS and PD are taken from a real market specifications. For cDBS it has 3cell battery with 11.1 volts, 5000 mAh and 55.5 Wh. The PD has a double battery capacity specifications where it has 6 cells with 22.2 volts, 10,000 mAh and 222 Wh.

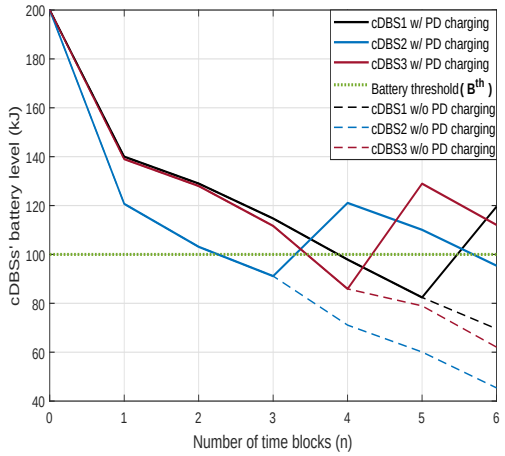

Figure 6.2: cDBSs' battery levels with and without the PD.

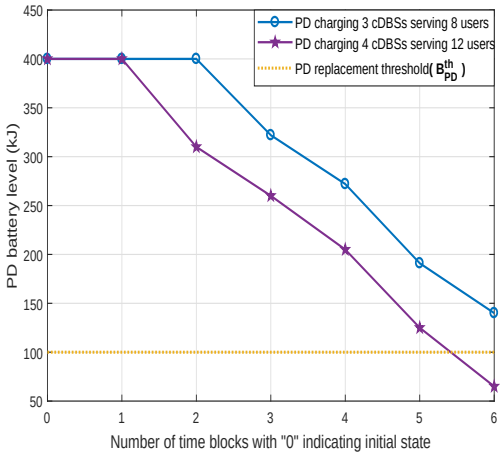

Figure 6.3: PD's battery level for 3 cDBSs (8 users) and 4 cDBSs (12 users).

Fig. 6.2 shows the battery level of each cDBS for time blocks from 0 to 6 where time block 0 is considered to be the initial state where all drones fly to reach the disaster area. Given that all cDBSs are initialized with a battery capacity of 200 kJ, the cDBSs are consuming their battery in hovering ,E_{hov}, moving, E_{har}, and in downlink transmission. From time block 0 to 1, all cDBSs are consuming high energy since they are crossing long distance to reach the disaster area. The solid lines represent the scenario where the PD is used. As it can be observed from the figure, all cDBSs are charged whenever their batteries' level is lower than B^{th}. At time block 4, cDBSs 1 and 3 curves are lower than B^{th} although the lower battery were charged, the PD is choosing it randomly. If PD is not used, dashed curves, the cDBSs' grid will not be able to serve the disaster affected users more than 48 minutes. It can be inferred from Fig. 6.2 that the PD was not used until time block 3 and most of the cDBSs' battery level went near to the threshold level after time block 3, this

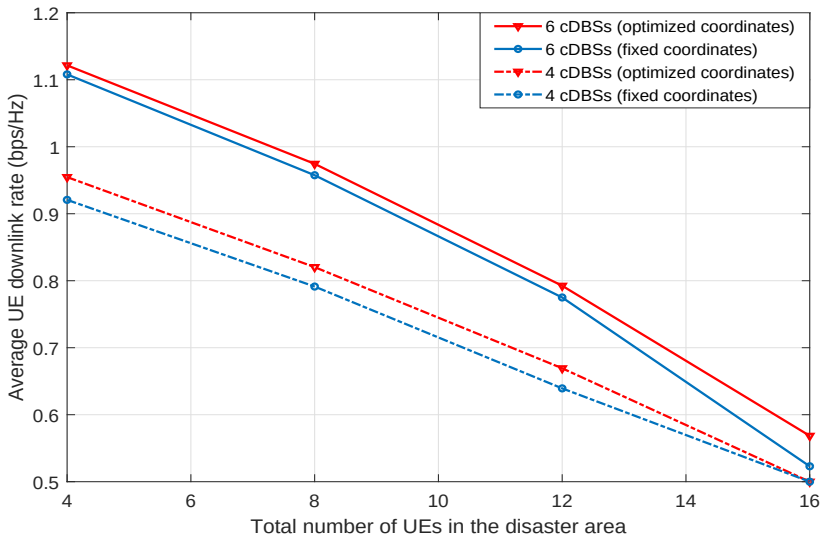

Figure 6.4: Average UE download rate versus the number of UEs for fixed and optimized cDBSs coordinates.

motivates us to consider using an adaptive threshold level, B^{th}, which decreases as the time increases.

Fig. 6.3 shows the battery level of the PD versus the number of time blocks for 3 cDBSs/8 users and 4 cDBSs/12 users. For the PD serving 3 cDBSs which is related to the results in Fig. 6.2, the PD left its docking station with full battery towards cDBS 2 to charge it. During each time block the PD is charging the targeted cDBS with 50 kJ. For the 4 cDBS scenario, the battery level of the PD crossed the threshold level $B_{\text{PD}}^{\text{th}}$ in this case and based on our model, this PD will be replaced with a fully charged PD to take over the charging process and the depleted PD will return back to the docking station to charge its battery. This process will allow unlimited fly time for the flying cellular infrastructure. Note that if we provided 4 cDBSs to the scenario which is having 8 users, only three cDBSs will be used since the objective of the optimization problem is to minimize the consumed energy of all cDBSs.

In Fig. 6.4, the optimization problem is solved with and without optimizing the cDBSs coordinates variable, $\mathbf{J}$, while increasing the number of cDBSs from 4 to 6. By fixing the

cDBSs coordinates variable, the optimization problem will become more tractable and easier to solve. As it can be noticed from the figure, the gap between the optimized coordinates and fixed coordinates approaches decreases by increasing the number of cDBSs except when the number of UEs equals to 16 which is explained below. It is worth noting that for the optimized coordinates approach, the cDBSs tend to stay at the same location even if a user changed his location. For example, if user a changed his location to another location the cDBS will not change its location as far as the minimum rate requirement is satisfied. If this rate is not satisfied, the optimization problem associates user a with another cDBS in order to avoid the movement of one of the cDBSs since this movement will consume more energy than just associating this user with another cDBS.

Finally, when the number of UEs in the disaster area is 16 and considering the 4 cDBSs scenario, we can observe that both optimized and fixed coordinates approaches are achieving 0.5 bps/Hz. Although the optimized coordinates approach always outperforms the fixed coordinates approach, the optimization problem enforces the minimum rate to be greater than or equal to R^{th} based on constraint 6.9b. Given the simulation parameters' values in this section, R^{th} is set to be 0.5 bps/Hz. For the other scenario, i.e., 6 cDBSs and 16 UEs, the fixed coordinates approach has poor performance, however, it is still satisfying the UEs' minimum rate.

6.7 Chapter Summary

In this chapter, we proposed a novel post-disaster rehabilitation framework for 4G/5G networks assisted by three different types of drones: 1) tethered Backhaul Drone (tBD) 2) untethered Powering Drone (PD) 3) untethered communication Drone Base-station (cDBS). This framework provides an unconstraint flying cellular infrastructure to the disaster area. An optimization problem is formulated where its objective is to minimize the consumed energy of the cDBSs. The optimization problem guarantees a minimum rate for each user in addition to finding the sub-optimal placement of the cDBSs and the time block to charge

the cDBSs using PD. Results show that the minimum number of cDBSs is used given that the users' minimum rate is satisfied. Also, the cDBSs are able to serve the users continually without the need to leave their location to charge their batteries due to the presence of the PD which is capable of charging cDBSs on the fly. Using an adaptive threshold level for charging the cDBSs will be considered in the future extension of this work to avoid charging most of the cDBSs during certain time blocks.

CHAPTER 7. CONCLUSIONS AND FUTURE WORK

7.1 Conclusions and Summary of Contributions

This thesis focused on proposing and analyzing outage compensation models for wireless communication systems. A brief summary of the main contributions of this thesis is outlined.

- Chapter 3 proposed two schemes for healing backhaul/fronthaul links for 4G/5G networks. In the first scheme, we proposed using a new radio to mitigate the fronhaul failures beside adapting software defined networking and cognitive radio networks. Performance was evaluated using system simulation and it shows that at least 20% of the fronthauling rate can be guaranteed during the fronthaul failure of any cell site type. In the second scheme, the backhaul of 5G networks is considered with the integration of 5G new radio. The concept of self-backhauling is presented with more focus on the challenges of this technology and ways to overcome it. Then, an optimization problem is formulated to maximize the minimum rate of the users affected by the failed backhaul link. The simulation results show that the used scheme can heal the network in the presence of backhaul failures for single and multiple failures up-to two concurrent failures.

- Chapter 4 proposed a novel scheme named Self-healing of Users equipment by Rf Energy transfer (SURE) in order to heal battery starved users using on demand RF energy transfer. We formulated a Mixed Integer Non Linear Programming (MINLP) optimization problem for the SURE scheme to maximize the sum rate and mean-

while minimize the UL power of the target UE. To achieve better scalability, we used three different heuristic algorithms to solve the problem named Interior Point OPTimizer (IPOPT), Solving Constraint Integer Programs (SCIP) and Basic Open-source Nonlinear Mixed Integer Programming (BONMIN). The simulation results show that BONMIN is the best solver for this problem. Also, it is recommended that the SURE scheme starts with at least four cooperative UEs beside the cooperative BSs in order to charge the target UE's battery with 5% (at least) of its full capacity.

- Chapter 5 proposed two cell outage compensation frameworks for 4G/5G network supported by dynamic Drone Base-stations (DBSs). In the first framework, we proposed a novel cell outage compensation (COC) approach for 5G networks assisted by Drone Base-Stations (DBSs). The objective is to minimize the total energy consumption of the DBSs and Ground BSs (GBSs) while maintaining the minimum quality of service requirements of users originally served by the failed BS. The simulation results show how this hybrid COC approach outperforms the conventional COC approach. The proposed hybrid approach shows significant impacts on ensuring connectivity of the users originally served by the failed BS while minimizing the number of used DBSs. In the second framework, we proposed a novel self-healing framework for 5G networks assisted by two different types of UAVs to mitigate or at least alleviate the effect of any Ground base station (GBS) failure either if it is long-term or short-term failure. An optimization problem is formulated where its objective is to maximize the minimum achievable rate of the UEs under the failed BS. Results show that the minimum rate requirement is guaranteed for each UE under the failed BS.

- Chapter 6 proposed a novel post-disaster rehabilitation framework for 4G/5G networks assisted by three different types of drones: 1) tethered Backhaul Drone (tBD) 2) untethered Powering Drone (PD) 3) untethered communication Drone Base-station (cDBS). This framework provides an unconstrained flying cellular infrastructure for the disaster area. An optimization problem is formulated where its objective is to

minimize the consumed energy of the cDBSs. Results show the minimum required number of cDBSs in order to satisfy the users' minimum rate. Also, the cDBSs are able to serve the users continually without the need to leave their location to charge their batteries due to the presence of the PD which is capable of charging cDBSs on the fly.

7.2 Directions for Future Research

The future research directions will include future research efforts that can improve our work and lead to better performance.

The future and ongoing works of this thesis will deal with new research directions that can improve our work and lead to better performance

7.2.1 Self Healing Assisted with Advanced Machine Learning

The rapid uptake of mobile devices and the rising popularity of mobile applications and services pose unprecedented demands on mobile and wireless networking infrastructure. Upcoming 5G systems are evolving to support exploding mobile traffic volumes, agile management of network resource to maximize user experience, and extraction of fine-grained realtime analytics. Fulfilling these tasks is challenging, as mobile environments are increasingly complex, heterogeneous, and evolving. One potential solution is to resort to advanced machine learning techniques to help managing the rise in data volumes and algorithm-driven applications. The recent success of deep learning underpins new and powerful tools that tackle problems in this space.

Embedding deep learning into the 5G mobile and wireless networks is well justified. In particular, data generated by mobile environments are heterogeneous as these are usually collected from various sources, have different formats, and exhibit complex correlations [120]. This data can facilitate the self-healing procedures if usefull information are extracted from it. Traditional ML tools require expensive hand-crafted feature engineering

to make accurate inferences and decisions based on such data. Deep learning eliminates domain expertise as it employs hierarchical feature extraction, by which it efficiently distills information and obtains increasingly abstract correlations from the data, while minimizing the data pre-processing effort. Graphics Processing Unit (GPU)-based parallel computing further enables deep learning to make inferences within milliseconds. This facilitates network analysis and management with high accuracy and in a timely manner, overcoming the runtime limitations of traditional mathematical techniques (e.g. convex optimization, game theory, meta heuristics).

A key advantage of deep learning is that it can automatically extract high-level features from data that has complex structure and inner correlations. The learning process does not need to be designed by a human, which tremendously simplifies prior feature handcrafting [121]. The importance of this is amplified in the context of mobile networks, as mobile data is usually generated by heterogeneous sources, is often noisy, and exhibits non-trivial spatial and temporal patterns [120], whose otherwise labeling would require outstanding human effort.

7.2.2 Empowering SON with Big Data for 5G

While the SON paradigm has evolved over the past decade to automate 3G, and 4G, it may not meet the requirements of 5G, mainly, because of its intrinsically reactive design approach and lack of end-to-end knowledge of the network. To address these problems, a vision for empowering SON with big data must be considered.

The exact definition of big data is context-specific. In the context of cellular networks, a huge amount of diverse data can be available from different levels of the network. for example, subscriber-level, cell-level, core network level. Given its volume, variety, velocity, and veracity, this data as a whole is big in the context of mobile networks. In the following bullets, we further delineate key elements and sources of big data in the mobile network by discussing their potential utilities.

• **Subscriber-Level Data**: It contains control data and contextual data, which not only can be exploited to optimize, configure, and plan network-centric operations, but is equally useful for supporting key business processes such as customer experience and retention enhancement. However, conventional approaches relying on offline analysis of individual metrics from these data streams are unable to accurately estimate user experience and create a holistic picture of the network.

• **Cell-Level Data**: provides the physical layer measurements that are reported by a base station and all user equipment (UE). An example of these data streams is the Minimization of Drive Test Data (MDT). The MDT reporting schemes have been defined in LTE Release 10 specification [77]. The release proposes to construct a data base of MDT reports from the network using Immediate or Logged MDT reporting conguration. The release proposes to construct a data base of MDT reports from the network using Immediate and/or Logged MDT reports from UEs. The measurements including Reference Signal Received Power and quality of serving BS as well as of the three strongest neighboring BSs and the Channel Quality Indicator. The same measurements can also be exploited to develop automated fault detection and localization solutions for identifying coverage holes, sleeping cells, or cells in outage.

• **Core-Network-Level Data**: Data from these streams can be used to fully automate the fault detection and troubleshoot network level problems. Today such information is only dealt with independently and therefore fails to capture the overall network behavior. The complexity of identifying problems in a core network is increased manifold. Such problems again advocate the need to share the data from all potential sources at various levels of network operation into a single database, big data. An up-to-date picture of a network's behavior with fine temporal granularity can only be gathered if information from the subscriber, cell, and core network levels is combined with additional sources of potentially useful data.

Therefore, the next task is to develop a framework to implement big data empowered SON with big data for 5G. The core idea is to develop end-to-end visibility of the network by extracting intelligence from big data. The three main features that will make this framework distinct from state-of-the-art SON are; 1) Full intelligence of the current network status, 2) Capability of predicting user behavior and 3) Capability of dynamically associating the network response with the network parameters. These three capabilities can go a long way to design SON that can meet 5G requirements.

BIBLIOGRAPHY

[1] J. G. Andrews et al., "What Will 5G Be?," in IEEE Journal on Selected Areas in Communications, vol. 32, no. 6, pp. 1065-1082, June 2014.

[2] J. Ramiro, K. Hamied,"Self-Organizing Networks (SON): Self-Planning, Self-Optimization and Self-Healing for GSM, UMTS and LTE", John Wiley and Sons, Ltd, ISBN: 978-0-470-97352-3, 2011.

[3] SOCRATES Project, "http://www.fp7-socrates.eu".

[4] Rui Wang; Honglin Hu; Xiumei Yang, "Potentials and Challenges of C-RAN Supporting Multi-RATs Toward 5G Mobile Networks", IEEE Access, vol.2, no., pp.1187,1195, 2014.

[5] P. Heino, et al., "WINNER+Final Channel Models", CELTIC CP5-026 WINNER+Project, Deliverable D5.3, v1.0, 2010.

[6] O. Aliu, A. Imran, M. Imran, B. Evans, "A Survey of Self Organisation in Future Cellular Networks," IEEE Comm. Surveys & Tutorials, vol.15, no.1, pp.336-361, 2013.

[7] A. Imran, A. Zoha, "Challenges in 5G: how to empower SON with big data for enabling 5G," Network, IEEE , vol.28, no.6, pp.27,33, Nov.-Dec. 2014.

[8] Qi Liao, M. Wiczanowski, S. Stanczak,, "Toward cell outage detection with composite hypothesis testing," Communications (ICC), 2012 IEEE International Conference on , vol., no., pp.4883,4887, 10-15 June 2012.

[9] Wei Wang, Jin Zhang, Qian Zhang, "Cooperative cell outage detection in Self-Organizing femtocell networks," INFOCOM, 2013 Proceedings IEEE , vol., no., pp.782,790, 14-19 April 2013.

[10] Wei Wang, Qing Liao, Qian Zhang, "COD: A Cooperative Cell Outage Detection Architecture for Self-Organizing Femtocell Networks," Wireless Communications, IEEE Transactions on , vol.13, no.11, pp.6007,6014, Nov. 2014.

[11] Wenqian Xue, Mugen Peng, Yu Ma, Hengzhi Zhang, "Classification-based approach for cell outage detection in self-healing heterogeneous networks," Wireless Communications and Networking Conference (WCNC), 2014 IEEE , vol., no., pp.2822,2826, 6-9 April 2014.

[12] O. Onireti, A. Imran; M. Imran, R. Tafazolli, "Cell Outage Detection in Heterogeneous Networks with Separated Control and Data Plane," European Wireless 2014; 20th European Wireless Conference; Proceedings of , vol., no., pp.1,6, 14-16 May 2014.

[13] M. Amirijoo, L. Jorguseski, T. Kurner, R. Litjens, M. Neuland, L. Schmelz, U. Turke, "Cell outage management in LTE networks," Wireless Communication Systems "ISWCS", vol., no., pp.600,604, 7-10 Sept. 2009.

[14] M. Amirijoo, L. Jorguseski, R. Litjens, L. Schmelz, "Cell Outage Compensation in LTE Networks: Algorithms and Performance Assessment," Vehicular Technology Conference (VTC Spring), 2011 IEEE 73rd , vol., no., pp.1,5, 15-18 May 2011.

[15] A. Saeed, O. Aliu, M. Imran, "Controlling self healing cellular networks using fuzzy logic," Wireless Communications and Networking Conference (WCNC), 2012 IEEE , vol., no., pp.3080,3084, 1-4 April 2012.

[16] Moysen, J.; Giupponi, L., "A Reinforcement Learning Based Solution for Self-Healing in LTE Networks," Vehicular Technology Conference (VTC Fall), 2014 IEEE 80th , vol., no., pp.1,6, 14-17 Sept. 2014.

[17] O. Onireti, A. Zoha, J. Moysen, A. Imran, L. Giupponi, M. Imran, A. Abu Dayya, "A Cell Outage Management Framework for Dense Heterogeneous Networks," Vehicular Technology, IEEE Transactions on , vol.no.99, May 2015.

[65] S. Fan, H. Tian, "Cooperative Resource Allocation for Self-Healing in Small Cell Networks," Communications Letters, IEEE , vol.19, no.7, pp.1221,1224, July 2015.

[19] M. Selim, A. E. Kamal, K. Elsayed, H. M. Abdel-Atty and M. Alnuem, "Fronthaul cell outage compensation for 5G networks," IEEE Communications Magazine, vol. 54, no. 8, pp. 169-175, Aug. 2016.

[20] J. Robson, L. Hiley, "Easy small cell backhaul: an analysis of small cell backhaul requirements and comparison of solution", White Paper. Cambridge Broadband Networks Limited 2012.

[21] A. Jafari, D. Lpez-Prez, H. Song, H. Claussen, L. Ho, J. Zhang, "Small cell backhaul: challenges and prospective solutions", EURASIP Journal on Wireless Communications and Networking, Aug. 2015.

[22] R. Gupta and S. Kalyanasundaram, "Resource allocation for self-backhauled networks with half-duplex small cells," 2017 IEEE International Conference on Communications Workshops (ICC Workshops), Paris, 2017

[23] C. Dehos, J. Gonzlez, A. Domenico, D. Ktnas, L. Dussopt, "Millimeter-wave access and backhauling: the solution to the exponential data traffic increase in 5G mobile communications systems?," IEEE Communications Magazine, vol. 52, no. 9, Sept. 2014.

[24] M. Islam, S. Subramanian, A. Sampath, "Integrated Access Backhaul in Millimeter Wave Networks," 2017 IEEE Wireless Communications and Networking Conference (WCNC), San Francisco, CA, 2017.

[63] H. Li, J. Xu, R. Zhang, and S. Cui, "A general utility optimization framework for energy-harvesting-based wireless communications", IEEE Communications Magazine, vol. 53, no. 4, pp. 7985, Apr. 2015.

[26] V. Marian, B. Allard, C. Vollaire, and J. Verdier, "Strategy for microwave energy harvesting from ambient field or a feeding source", IEEE Transaction on Power Electron., vol. 27, no. 11, pp. 44814491, Nov. 2012.

[27] H. Nishimoto, Y. Kawahara, and T. Asami, "Prototype implementation of ambient RF energy harvesting wireless sensor networks", IEEE Sensors, pp. 12821287, Nov. 2010.

[28] A. H. Sakr and E. Hossain, "Analysis of K -Tier Uplink Cellular Networks With Ambient RF Energy Harvesting," IEEE Journal on Selected Areas in Communications, vol. 33, no. 10, pp. 2226-2238, Oct. 2015.

[29] A. Bhowmick, S. D. Roy and S. Kundu, "Performance of secondary user with combined RF and non-RF based energy-harvesting in cognitive radio network," IEEE International Conference on Advanced Networks and Telecommuncations Systems (ANTS), Kolkata, 2015.

[30] A. H. Sakr and E. Hossain, "Cognitive and Energy Harvesting-Based D2D Communication in Cellular Networks: Stochastic Geometry Modeling and Analysis," in IEEE Transactions on Communications, vol. 63, no. 5, pp. 1867-1880, May 2015.

[31] S. Rohde and C. Wietfeld, "Interference aware positioning of aerial relays for cell overload and outage compensation," in Proc. of the IEEE Vehicular Technology Conference (VTC Fall), Quebec, QC, Canada, Sept. 2012.

[32] P. Zhan, K. Yu, and A. L. Swindlehurst, "Wireless relay communications using an unmanned aerial vehicle," in IEEE Workshop on Signal Processing Advances in Wireless Communications, Cannes, France, July 2006.

[33] J. Komerl and A. Vilhar, "Base stations placement optimization in wireless networks for emergency communications,", June 2014.

[34] Z. Han, A. L. Swindlehurst, and K. J. R. Liu, "Optimization of MANET connectivity via smart deployment/movement of unmanned air vehicles," IEEE Transactions on Vehicular Technology, vol. 58, Sept. 2009.

[35] I. Bekmezci, M. Ermis, and S. Kaplan, "Connected multi UAV task planning for flying ad hoc networks," in Proc. of the IEEE International Black Sea Conference on Communications and Networking (BlackSeaCom), Odessa, Ukraine, May 2014.

[36] J. Scherer and B. Rinner, "Persistent multi-UAV surveillance with energy and communication constraints," in Proc. of the IEEE International Conference on Automation Science and Engineering (CASE), Fort Worth, TX, USA, Aug. 2016.

[37] T. Schouwenaars, J. How, and E. Feron, "Receding horizon path planning with implicit safety guarantees," in Proc. of the American Control Conference, Boston, MA, USA, June 2004.

[38] M. Mozaffari, W. Saad, M. Bennis, and M. Debbah, "Drone small cells in the clouds: Design, deployment and performance analysis," in Proc. of the IEEE Global Communications Conference (GLOBECOM), San diego, CA, USA, Dec. 2015.

[39] Q. Feng, E. K. Tameh, A. R. Nix, and J. McGeehan, "Modelling the likelihood of line-ofsight for air-to-ground radio propagation in urban environments," in Proc. of the IEEE Global Communications Conference (GLOBECOM), San Francisco, CA, USA, Nov.- Dec 2006.

[40] Q. Feng, J. McGeehan, E. K. Tameh, and A. R. Nix, "Path loss models for air-to-ground radio channels in urban environments," in Proc. of the 63rd IEEE Vehicular Technology Conference (VTC Spring), Melbourne, VIC, Australia, May 2006.

[93] A. Al-Hourani, S. Kandeepan, and A. Jamalipour, "Modeling air-to-ground path loss for low altitude platforms in urban environments," in Proc. of the IEEE Global Communications Conference (GLOBECOM), Austin, TX, USA, Dec. 2014.

[42] J. Bartelt, P. Rost, D. Wubben, J. Lessmann, B. Melis, G. Fettweis, "Fronthaul and backhaul requirements of flexibly centralized radio access networks", IEEE Wireless Communications Magazine, vol.22, no.5, pp.105-111, Oct. 2015.

[43] K. Zheng, L. Zhao, J Mei, M. Dohler, W. Xiang, Y. Peng, "10 Gb/s hetsnets with millimeter-wave communications: access and networking - challenges and protocols," IEEE Communications Magazine, vol.53, no.1, pp.222-231, Jan. 2015.

[44] 0. Al-Kofahi and A. E. Kamal, " Survivability Strategies in Multihop Wireless Networks", IEEE Wireless Communications, Vol. 17, No. 5, Oct. 2010, pp.71-80.

[45] M. Selim, A. Kamal, K. Elsayed, H. Abd-El-Atty, M. Alnuem, "A Novel Approach for Back-haul Self Healing in 4G/5G HetNets". IEEE International Conference on Communications (ICC), June 2015.

[46] J. Bartelt, G. Fettweis, D. Wubben, M. Boldi, B. Melis "Heterogeneous Backhaul for Cloud-Based Mobile Networks", 78th IEEE VTC Fall, Sept. 2013.

[47] A. Oliva, X. Perez, A. Azcorra, A. Giglio, F. Cavaliere, D. Tiegelbekkers, J. Lessmann, T. Haustein, A. Mourad, P. Iovanna, "Xhaul: toward an integrated fronthaul/backhaul architecture in 5G networks," IEEE Wireless Communications, vol.22, no.5, pp.32-40, Oct. 2015.

[48] J. Singh, S. Ramakrishna, "On the feasibility of beamforming in millimeter wave communication systems with multiple antenna arrays", IEEE Global Communications Conference (GLOBECOM), Dec. 2015.

[49] ETSI TR 101 534 V1.1.1, "Broadband Radio Access Networks (BRAN); Very high capacity density BWA networks; System architecture, economic model and derivation of technical requirements," 2012.

[50] S. Ghafoor, et al. "Cognitive radio for disaster response networks: survey, potential, and challenges," in IEEE Wireless Communications, vol. 21, no. 5, pp. 70-80, Oct. 2014.

[51] C. Bernardos, et al. "An architecture for software defined wireless networking," IEEE Wireless Comm. Magazine, vol.21, no.3, pp.52-61, Jun. 2014.

[52] F. Boccardi, R. W. Heath, A. Lozano, T. L. Marzetta and P. Popovski, "Five disruptive technology directions for 5G," in IEEE Communications Magazine, vol. 52, no. 2, pp. 74-80, February 2014.

[53] Small Cell Forum, https://www.smallcellforum.org/

[104] 3GPP TR 38.874, "NR; Study on integrated access and backhaul", Tech. Rep., 2017.

[55] H. Holma; A. Toskala, "Self Organizing Networks (SON)," in LTE for UMTS:Evolution to LTE-Advanced , 1, Wiley Telecom, 2011

[56] M. Selim, A. Kamal, K. Elsayed, H. Abd-El-Atty, M. Alnuem, Book Chapter: "Self-Healing in 5G HetNets". Book: 5G Networks: A Research and Development Perspective, April 5, 2016 by CRC Press, ISBN 9781498739542.

[57] M. Akdeniz, Y. Liu, M. Samimi, S. Sun, S. Rangan, T. Rappaport, E. Erkip, "Millimeter Wave Channel Modeling and Cellular Capacity Evaluation", Available Online at: "https://arxiv.org/abs/1312.4921".

[58] Gabriel Brown, "Exploring 5G New Radio: Use Cases, Capabilities and Timeline", Qualcomm White Paper, Sept. 2016.

[59] Mediatek Inc., "5G New Radio: A New Era For Enhanced Mobile Broadband", White Paper, 2018.

[60] S. Lien, S. Shieh, Y. Huang, B. Su, Y. Hsu, H. Wei, "5G New Radio: Waveform, Frame Structure, Multiple Access, and Initial Access," in IEEE Communications Magazine, vol. 55, no. 6, 2017.

[61] A. Asghar, H. Farooq, A. Imran, "Self-Healing in Emerging Cellular Networks: Review, Challenges and Research Directions," IEEE Communications Surveys & Tutorials, Apr. 2018.

[62] M. Selim, A. E. Kamal, K. Elsayed, H. M. Abdel-Atty and M. Alnuem, "Fronthaul cell outage compensation for 5G networks," IEEE Communications Magazine, vol. 54, no. 8, Aug. 2016.

[63] W. Li, P. Yu, M. Yin, L. Feng, X. Qiu, "Automated cell outage compensation mechanism based on downtilt adjustments in cellular networks," 16th International Symposium on Communications and Information Technologies, Sept. 2016.

[64] I. Bandera, P. Muoz, I. Serrano, R. Barco, "Adaptive Cell Outage Compensation in Self-Organizing Networks," IEEE Transactions on Vehicular Technology, vol. 67, no. 6, Jun. 2018.

[65] S. Fan, H. Tian, "Cooperative resource allocation for self-healing in small cell networks", IEEE Communications Letters, vol. 19, no. 7, pp. 12211224, 2015.

[66] 3GPP Release 15 standard, available online at: http://www.3gpp.org/release-15.

[67] M. Jaber, M. Imran, R. Tafazolli, A. Tukmanov, "5G Backhaul Challenges and Emerging Research Directions: A Survey", IEEE Access, 2016.

[68] T. S. Rappaport, G. R. MacCartney, M. K. Samimi and S. Sun, "Wideband Millimeter-Wave Propagation Measurements and Channel Models for Future Wireless Communication System Design," in IEEE Transactions on Communications, vol. 63, no. 9, Sept. 2015.

[69] Mohamed Y. Selim, Ahmad Alsharoa, Ahmed E. Kamal, "Short-term and Long-term Cell Outage Compensation Using UAVs in 5G Networks", to appear in the proceedings of IEEE GLOBECOM 2018. Available online at: https://arxiv.org/abs/1807.08615.

[70] R. Thakur, S. N. Swain and C. S. R. Murthy, "An Energy Efficient Cell Selection Framework for Femtocell Networks With Limited Backhaul Link Capacity," in IEEE Systems Journal, vol. 12, no. 2, pp. 1969-1980, June 2018.

[71] A. Abdelhadi and C. Clancy, "An optimal resource allocation with joint carrier aggregation in 4G-LTE," 2015 International Conference on Computing, Networking and Communications (ICNC), Garden Grove, CA, 2015.

[72] A. Abdel-Hadi and C. Clancy, "A utility proportional fairness approach for resource allocation in 4G-LTE," 2014 International Conference on Computing, Networking and Communications (ICNC), Honolulu, HI, 2014.

[73] Steven Percy, Chris Knight, Francis Cooray, Ken Smart, "Supplying the Power Requirements to a Sensor Network Using Radio Frequency Power Transfer", Sensor Network Journal, Vol. 12, no. 7, pp. 8571-8585, June 2012.

[74] D. Mishra, S. De, S. Jana, S. Basagni, K. Chowdhury and W. Heinzelman, "Smart RF energy harvesting communications: challenges and opportunities," IEEE Communications Magazine, vol. 53, no. 4, pp. 70-78, Apr. 2015.

[75] M. Tehrani, M. Uysal, H. Yanikomeroglu, "Device-to-device communication in 5G cellular networks: Challenges, solutions, and future directions", IEEE Communications Magazine, vol. 52, no. 5, pp. 86-92, May 2014.

[76] Baumann, Daniel. "Minimization of drive tests (MDT) in mobile communication networks." Proceeding zum Seminar Future Internet (FI) und Innovative Internet Technologien und Mobilkommunikation (IITM). Vol. 9, Mar. 2014.

[77] 3GPP TS 37.320, "Universal Mobile Telecommunications System (UMTS); LTE; Universal Terrestrial Radio Access (UTRA) and Evolved Universal Terrestrial Radio Access (E-UTRA); Radio measurement collection for Minimization of Drive Tests (MDT); Overall description; Stage 2", 2011-04, v10.1.0 Release 10.

[78] Mohamed Y. Selim, A. Alsharoa, A. E. Kamal and M. Abdullah Alnuem, "SURE: A Novel Approach for Self Healing Battery Starved Users Using Energy Harvesting," in IEEE Access, vol. 5, pp. 6110-6120, 2017.

[79] T. Le, K. Mayaram and T. Fiez, "Efficient Far-Field Radio Frequency Energy Harvesting for Passively Powered Sensor Networks," IEEE Journal of Solid-State Circuits, vol. 43, no. 5, pp. 1287-1302, May 2008.

[80] H. H. Yang, J. Lee and T. Q. S. Quek, "Heterogeneous Cellular Network With Energy Harvesting-Based D2D Communication," IEEE Transactions on Wireless Communications, vol. 15, no. 2, pp. 1406-1419, Feb. 2016.

[81] A. Bou Saleh, S. Redana, B. Raaf, T. Riihonen, J. Hamalainen and R. Wichman, "Performance of Amplify-and-Forward and Decode-and-Forward Relays in LTE-Advanced," in Proc. of the 70th IEEE Vehicular Technology Conference (VTC Fall), Anchorage, Alaska, USA Sept. 2009, pp. 1-5.

[82] X. Ji, W. P. Zhu and D. Massicotte, "Transmit Power Minimization for Two-Way Amplify-and-Forward Relaying With Asymmetric Traffic Requirements," IEEE Transactions on Vehicular Technology, vol. 65, no. 12, pp. 9687-9702, Dec. 2016.

[83] S. Hmlnen, H. Sanneck, and C. Sartori, LTE Self-Organising Networks (SON): Network Management Automation for Operational Efciency. Hoboken, NJ, USA: Wiley, 2012.

[84] Basic Open-source Nonlinear Mixed INteger programming (BONMIN), https://projects.coin-or.org/Bonmin.

[85] P. Belotti, J. Lee, L. Liberti, F. Margot and A. Wchter, "Branching and bound tightening techniques for nonconvex MINLPs", Optimization Methods and Software vol. 24, pp. 597-634, 2009.

[86] Stefan Vigerske, Ambros Gleixner, "SCIP: Global Optimization of Mixed-Integer Nonlinear Programs in a Branch-and-Cut Framework", ZIB-Report, Takustr.7, 14195 Berlin, Aug. 2016.

[87] Interior Point OPTimizer (IPOPT), https://www.coin-or.org/Ipopt/documentation/.

[88] Y. Zeng, R. Zhang, and T. J. Lim, "Wireless communications with unmanned aerial vehicles: Opportunities and challenges," IEEE Communications Magazine, vol. 54, no. 5, pp. 3642, May 2016.

[89] S. Rohde, M. Putzke, and C. Wietfeld, "Ad-hoc self-healing of OFDMA networks using UAV-based relays", Ad Hoc Networks, vol. 11, no. 7, pp. 18931906, Sep. 2013

[90] A. Merwaday and I. Guvenc, "UAV assisted heterogeneous networks for public safety communications", in Proc. IEEE Wireless Commun. and Netw. Conf. Workshops (WCNCW), Mar. 2015, pp. 329334.

[91] M. Mozaffari, W. Saad, M. Bennis and M. Debbah, "Drone Small Cells in the Clouds: Design, Deployment and Performance Analysis," 2015 IEEE Global Communications Conference (GLOBECOM), San Diego, CA, 2015, pp. 1-6.

[106] J. Lyu, Y. Zeng, R. Zhang, "UAV-Aided Cellular Offloading: A Potential Solution to Hot-Spot Issue in 5G", available online "https://arxiv.org/abs/1705.09024".

[93] A. Al-Hourani, S. Kandeepan and A. Jamalipour, "Modeling air-to-ground path loss for low altitude platforms in urban environments," 2014 IEEE Global Communications Conference, Austin, TX, 2014, pp. 2898-2904.

[94] Y. Zheng, Y. Wang and F. Meng, "Modeling and Simulation of Pathloss and Fading for Air-Ground Link of HAPs within a Network Simulator," 2013 International Conference on Cyber-Enabled Distributed Computing and Knowledge Discovery, Beijing, 2013, pp. 421-426.

[95] G. Auer, O. Blume, V. Giannini, I. Godor, M. Imran, "Energy efficiency analysis of the reference systems, areas of improvements and target breakdown," Energy Aware Radio and Network Technologies, Dec. 2010.

[96] A. Alsharoa, H. Ghazzai, A. Kadri and A. E. Kamal, "Energy Management in Cellular HetNets Assisted by Solar Powered Drone Small Cells," IEEE Wireless Communications and Networking Conference (WCNC), San Francisco, CA, 2017.

[97] T. Wang and L. Vandendorpe, "Successive convex approximation based methods for dynamic spectrum management", IEEE International Conference on Communications (ICC), Ottawa, ON, 2012.

[98] Q. Wu, Y. Zeng, R. Zhang, "Joint Trajectory and Communication Design for Multi-UAV Enabled Wireless Networks", available online "https://arxiv.org/abs/1705.02723".

[99] S.Boyd and L. Vandenberghe, Convex Optimization. Cambridge University Press, 2004.

[100] E. Vattapparamban, . Gven, A. Yurekli, K. Akkaya, S. Uluaa, "Drones for smart cities: Issues in cybersecurity, privacy, & public safety," International Wireless Communications & Mobile Computing Conference, 2016.

[101] X. Zhu, Z. Guo, Z. Hou, "Solar-powered airplanes: a historical perspective and future challenges", Progress in Aerospace Sciences, vol. 71 (2014).

[102] I. Bucaille, S. Hthuin, A. Munari, R. Hermenier, T. Rasheed, S. Allsopp, "Rapidly Deployable Network for Tactical Applications: Aerial BS with Opportunistic Links for Unattended and Temporary Events ABSOLUTE Example," IEEE Military Communications Conference, CA, 2013.

[103] S. Chandrasekharan, K. Gomez, A. Al-Hourani, S. Kandeepan, T. Rasheed, L. Goratti, L. Reynaud, D. Grace, I. Bucaille, T. Wirth, and S. Allsopp, "Designing and implementing future aerial communication networks," IEEE Communications Magazine, vol. 54, no. 5, pp. 2634, May 2016.

[104] 3GPP, "Telecommunication management: Self-Organizing Networks (SON) concepts and requirements," 3GPP TS 32.500, 2012.

[105] O. G. Aliu, A. Imran, M. A. Imran, B. Evans, "A Survey of Self Organisation in Future Cellular Networks," IEEE Comm. Surveys & Tutorials, vol.15, no.1, pp.336-361, 2013.

[106] J. Lyu, Y. Zeng, R. Zhang, "UAV-aided cellular offloading: A potential solution to hotspot issue in 5G," Arxiv: https://arxiv.org/abs/1705.09024.

[107] M. Y. Selim, A. Alsharoa and A. E. Kamal, "Hybrid Cell Outage Compensation in 5G Networks: Sky-Ground Approach," IEEE International Conference on Communications (ICC), Kansas City, MO, USA, May 2018.

[108] M. Alzenad, M. Z. Shakir, H. Yanikomeroglu and M. S. Alouini, "FSO-Based Vertical Backhaul/Fronthaul Framework for 5G+ Wireless Networks," in IEEE Communications Magazine, vol. 56, no. 1, Jan. 2018.

[109] General Algebraic Modeling System (GAMS) https://www.gams.com/

[110] M. Erdelj and E. Natalizio, "UAV-assisted disaster management: Applications and open issues," 2016 International Conference on Computing, Networking and Communications (ICNC), Kauai, HI, 2016

[111] "Presidential memorandum for the secretary of transportation" Nov. 2017. Available at: https://www.whitehouse.gov/presidential-actions/presidential-memorandum-secretary-transportation/.

[112] "Aerial Base-Stations with Opportunistic Links for Unexpected and Temporary Events: ABSOLUTE" Available at: http://www.absolute-project.eu.

[113] Qingqing Wu, Jie Xu, Rui Zhang, "Capacity Characterization of UAV-Enabled Two-User Broadcast Channel", submitted to IEEE Journal of Selected Areas in communications (JSAC), Jan. 2018. Available at: https://arxiv.org/abs/1801.00443.

[114] Azade Fotouhi, Ming Ding, Mahbub Hassan, "DroneCells: Improving 5G Spectral Efficiency using Drone-mounted Flying Base Stations," submitted to Journal of Transactions on Mobile Computing (JTMC), Jul. 2017. Available at: https://arxiv.org/abs/1707.02041.

[115] S. Naqvi, S. Hassan, H. Pervaiz and Q. Ni, "Drone-Aided Communication as a Key Enabler for 5G and Resilient Public Safety Networks," in IEEE Communications Magazine, vol. 56, no. 1, pp. 36-42, Jan. 2018.

[116] Mohamed Y. Selim, Ahmed E. Kamal, "Post-disaster 4G/5G Network Rehabilitation using Drones: Solving Battery and Backhaul Issues", Accepted at IEEE Global Communications Wi-UAV Workshop 2018. Available online at: https://arxiv.org/abs/1809.07859.

[117] O. Graven, et al., "Managing disasters-rapid deployment of sensor network from drones: Providing first responders with vital information," 2nd International Conference on Control and Robotics Engineering (ICCRE), Bangkok, 2017.

[118] E. Zedini, H. Soury and M. S. Alouini, "On the Performance Analysis of Dual-Hop Mixed FSO/RF Systems," in IEEE Transactions on Wireless Communications, vol. 15, no. 5, pp. 3679-3689, May 2016.

[119] J. V. Dries Hulens and T. Goedeme, "How to choose the best embedded processing platform for onboard UAV image processing", in International Conference Computer Vision, Imaging, Computer Graphics and Application, Berlin, Germany, Mar. 2015.

[120] Mohammad Abu Alsheikh, Dusit Niyato, Shaowei Lin, Hwee-Pink Tan, and Zhu Han. Mobile big data analytics using deep learning and Apache Spark. IEEE network, 2016.

[121] Yann LeCun, Yoshua Bengio, and Geoffrey Hinton. Deep learning. Nature, 521(7553):436444, 2015.

APPENDIX. PUBLICATIONS

Book Chapters

1. **Mohamed Selim**, Ahmed Kamal, Khaled Elsayed, Heba Abd-El-Atty, Mohammed Alnuem, Book Chapter: "Self-Healing in 5G HetNets. Book: 5G Networks: A Research and Development Perspective, April 5, 2016 by CRC Press, ISBN 9781498739542.

Journal Papers

1. **Mohamed Y. Selim**, Ahmed E. Kamal, "Self-backhauling Failure Mitigation Using 5G New Radio", In preparation to be submitted to a Journal (Expected submission date December 2018).

2. **Mohamed Selim**, Ahmad Alsharoa, Ahmed E. Kamal, Mohammed Alnuem, "SURE: A Novel Approach for Self-Healing Battery Starved Users using Energy Harvesting, IEEE Access, vol.PP, no.99, pp.1-1, March 2017.

3. **Mohamed Selim**, Ahmed E. Kamal, Khaled Elsayed, Heba Abdel-Atty and Mohamed Alnuem, "Fronthaul cell outage compensation for 5G networks," in IEEE Communications Magazine, vol. 54, no. 8, pp. 169-175, August 2016.

Conference Papers

1. **Mohamed Y. Selim**, Ahmad Alsharoa, A. E. Kamal, "Short-term and Long-term Cell Outage Compensation using UAVs in 4G/5G Networks", accepted at IEEE Global Communications Conference 2018.

2. A. Almasoud, **Mohamed Y. Selim**, A. Alqasir, T. Shabanam, A. Masadeh, A. Kamal, "Energy Efficient Data Forwarding in Disconnected Networks using Cooperative UAVs", accepted at IEEE Global Communications Conference 2018.

3. **Mohamed Y. Selim**, Ahmad Alsharoa, A. E. Kamal, "Hybrid Cell Outage Compensation in 5G Networks: Sky-Ground Approach", IEEE International Conference on Communications (ICC) 2018.

4. **Mohamed Selim**, Ahmed E. Kamal, Khaled Elsayed, Heba Abd-El-Atty, Mohamed Alnuem, "A Novel Approach for Back-haul Self-Healing in 4G/5G HetNets", IEEE International Conference on Communications (ICC), London, 2015.

Workshop Papers

1. **Mohamed Y. Selim**, A. E. Kamal, "Post-disaster 4G/5G Network Rehabilitation using Drones: Solving Battery and Backhaul Issues", Accepted at IEEE Global Communications Wi-UAV Workshop 2018. Available online at: https://arxiv.org/abs/1809.07859